UNDERSTANDING THE NOVEL ROLE OF CHECKPOINT PROTEIN ROUGH DEAL IN HOMOLOG ORIENTATION AND CENTROMERIC COHESION IN DROSOPHILA MALE MEIOSIS

A Dissertation Presented for the
Doctor of Philosophy
Degree
The University of Tennessee, Knoxville

Qiutao He
August 2021

DEDICATION

To my wife Bai Qu for all the love, trust and understanding; my kids Quinn He and Rico He for your love and support

To my father Zhimin He and my mother Min Zhang. They were the constant source of support and encouragement throughout my Ph.D. stage. I could not have been in a position to pursue the Ph.D. degree without the great opportunity of education and the environment you provided to me.

ACKNOWLEDGEMENTS

First, I would like to express my deep gratitude to my mentor Dr. Bruce D. McKee for his support and advice. During my Ph.D. Stage, I was received comprehensive training, from experimental design to problem-solving, from critical paper review to manuscript preparing. Throughout my Ph.D. training Dr. McKee constantly gave me freedom and trust to think and perform experiments for tackling the problems in my project, but always provided constructive feedback when I need help. All these skills I equipped in this stage will pave the way for my independent research in the future.

I am particularly grateful to my dissertation committee: Dr. Mariano Labrador, Dr. Hong Guo and Dr. Todd Reynolds. You constantly give me constructive feedback and comments on my research and scientific writings during the committee meetings and on other occasions when I sought your help. I am also grateful for the fly stocks used in my study donated by Dr. Roger Karess and Dr. Terry Orr-weaver.

I want to thank past and present members of Dr. Bruce McKee's lab for their help during my Ph.D. stage. I thank Hiro Yamada for his guidance on the FISH technique and fly work in the early stage of my training. I thank previous graduate students Dr. Badri Krishnanand Dr. Avik Mukherjee as well as previous postdoc Dr. Ariane Blattner for their help in protocol optimization and active discussions. I thank current graduate student Elsie Adams for her scientific input, help and friendship.

Finally, I want to express my deepest gratitude for the constant support, understanding and love from my wife Bai Qu and two kids Quinn and Rico.

ABSTRACT

Meiosis is a central mechanism in sexual reproduction, through which the diploid precursor cells in the germline produce haploid gametes. After fertilization, a new set of diploid genome forms in the offspring with the characteristics of mother and father. The faithful transmission of genetic material to next generation relies on the fidelity of chromosome segregation during meiosis. A variety of mechanisms regulate the chromosome segregations in meiosis, including homolog interaction, chromosome cohesion, and sister-chromatid orientation. In most eukaryotic organisms, homolog interactions are built by the formation of chiasmata resulted from crossovers, but it is absent in male *Drosophila* in which an alternative conjunction complex is obligate to stabilize homologous chromosome. In addition, *Drosophila* also deploys a three-member complex, called SOS consisting of SOLO, ORD and SUNN, to establish and maintain the sister-chromatid cohesion in meiosis, while this responsibility is executed by a well-known cohesin complex composed of four subunits (SMC1, SMC3, REC8 and SA) in other eukaryotes. A conserved meiosis-specific sister-chromatid mono-orientation is evident in Drosophila, as in the meiosis I of other eukaryotes, but the regulatory pathway has been elusive until now in both sexes of *Drosophila*.

In this investigation, we used conventional genetic and advanced fluorescence microscopy to investigate the role of checkpoint Rough Deal (ROD) in Drosophila male meiosis by using trans-heterozygous *rod* mutants. Based on our results, ROD protein is required for the maintenance, but not the establishment, of centromere cohesion by prohibiting the redistribution of Shugoshin protein MEI-S332. More importantly, ROD

modulates the orientation of sister chromatid in meiosis I, might through the regulation and coordination of microtubule attachments on kinetochores. Therefore, dysfunction of ROD causes a high frequency of chromosome mis-segregation, which gives rise to premature equational segregation and 4/O chromosome nondisjunction in the first meiotic division. To get more insights into the ROD function in meiosis, we further generate a conditional ROD-depleted line in which we expect to induce the degradation of ROD protein in *Drosophila* spermatocytes, which could help us to fully understand the role of ROD in a null-like background.

TABLE OF CONTENTS

LIST OF TABLES

LIST OF FIGURES

CHAPTER I: GENERAL INTRODUCTION

Meiosis: A specialized cell division in sexual reproduction

Meiosis plays a pivotal role in sexual reproduction and produces haploid gametes from diploid precursors. It serves to provide a long-term survival strategy for generating diversity and mixing genetic material within species. Unlike mitosis in which two daughter cells inherit the identical genome from the mother cell, in meiosis homologous chromosomes segregate randomly and each gamete receives only one member of each homologous chromosome pair. Spermatogonia or oogonia (2N) undergo two consecutive chromosome segregations after the last round of DNA replication, which halves the copy number of chromosomes in gametes (1N). Then, the chromosome copy number is restored in the zygotes (2N) by the conjugation of sperm and eggs. During the two meiotic divisions, reductional segregation takes place in meiosis I in which homologous chromosomes (or homologs) disjoin from each other, whereas two sister chromatids separate and move to opposite spindle pole in meiosis II, termed equational segregation (Figure 1-1) [Ohkura 2015; Page and Hawley 2003].

Accurate chromosome segregation is the top mission in nuclear division of meiosis to ensure the faithful transmission of genetic information in the gametes for the success of fertilization and the development of offspring. Errors in meiotic chromosome segregation are the major source of aneuploid gametes, i.e. cells that lack or carry extra copies of one or more chromosomes. Aneuploidy results in genome unbalance and is the leading source of infertility, spontaneous miscarriage and development disorders in humans. In human studies, it has been shown that

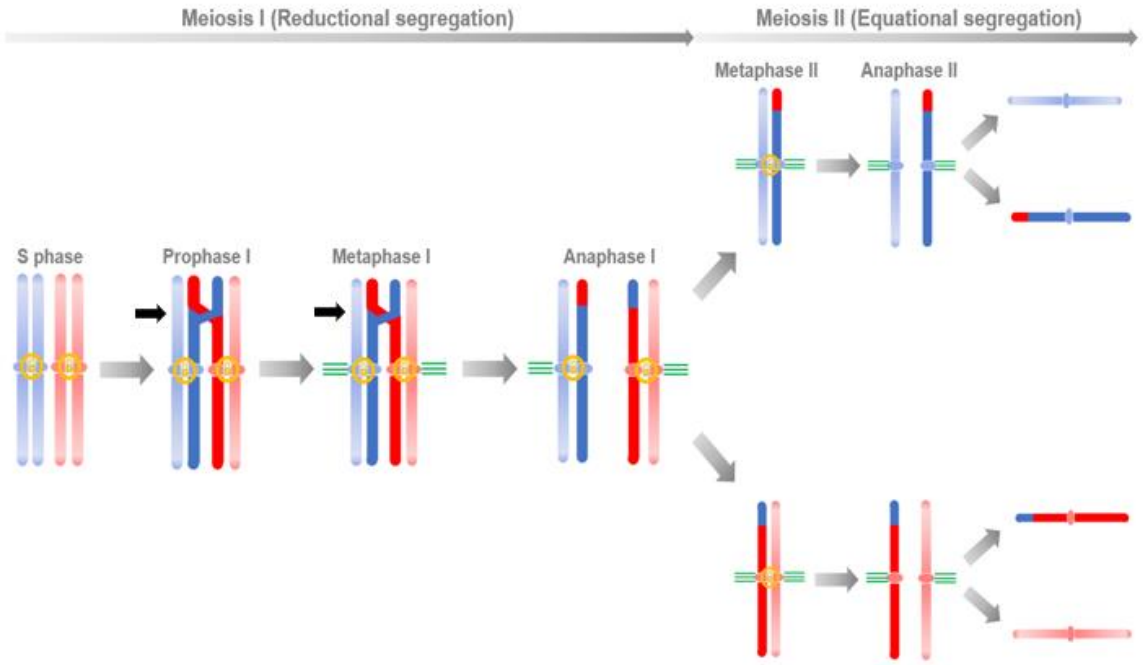

Figure 1-1. Diagram of chromosome segregation in meiosis. Orange circles: centromere cohesion; black arrows: chiasmata; green lines: microtubules.

aneuploidy for chromosome 13, 18, 21 and sex chromosomes usually leads to abortion [Nagaoka et al 2012; Ioannou et al 2018]. Moreover, unbalanced genomic information underlies the disruption of proteins' expression, which affects the intrinsic cellular physiology. For example, an additional copy of chromosome 21 is the basis of human Down syndrome that causes severe impairment in cognition and is related to the increased expression of mutant APP protein, relating the extra chromosome copies to disruption of protein homeostasis. Similarly, Edward's syndrome and Patau syndrome in humans are malignant developmental diseases induced by the trisomy of chromosome 18 and chromosome 13 respectively [Oromendia and Amon 2014]. An investigation of human oocytes in vitro revealed that 26.4% of the total population showed aneuploidy for at least one chromosome and this phenomenon was proposed to be correlated with chromosome mis-segregation, particularly in meiosis I [Pellestor et al 2006]. Even worse, as maternal age is advanced, the frequency of aneuploid eggs increases through a well-known mechanism termed cohesion exhaustion, by which, further increases the risk of infertility and aneuploid embryos [Jessberger 2012; Webster & Schuh 2017].

Each division of meiosis (refer to meiosis I or meiosis II) is subdivided into four stages - prophase, prometaphase, metaphase and anaphase. During DNA replication, duplicated sister-chromatid pairs are stabilized by the cohesion on the arms and centromeres, forming homologs. Homologs in early prophase I come together and pair with each other, and then undergo recombination and crossover ensue. This process generates an interhomolog structure, called chiasmata, which

connects two homologs before anaphase I onset. After nuclear envelop breakdown, chromosomes start to be accessible to and align on the spindle and the attachments are established between microtubules (also known as K-fibers) and a proteinaceous structure, named kinetochores. In early prometaphase, kinetochores tend to bind the lateral surface of microtubules efficiently and move along the spindle, which is referred as to lateral attachments and contributes to chromosome accumulation to spindle equator. Later, lateral attachment-mediated poleward movement bring kinetochores to a microtubule-rich area near the pole where the conversion of lateral to end-on attachment occurs in the late prometaphase I. Then, properly oriented chromosomes congress to and align up on spindle equator in metaphase I followed by the segregation when anaphase I begins. Unlike mitosis and meiosis II in which sister chromatids orient to opposite spindle poles (bi-orientation), kinetochores on each homolog (sister kinetochores) are oriented to the same spindle pole (mono-orientation). Therefore, chromosomes segregate reductionally, in meiosis I in which the segregation occurs between homologs, whereas they adopt equational segregation in mitosis and meiosis II defined as the segregation between sister chromatids [Sakuno et al 2009; Watanabe 2012].

In principle, two essential tasks in prophase I include homolog pairing that aligns the two axes of homologous chromosomes in proximity, referred as homolog pairing, and recombination between non-sister chromatids on different homologs through homologous repair (HR) pathway. Prophase I can be divided into four substages and, within each stage, chromosome organization undergoes profound changes

molecularly and structurally. The first substage is leptotene in which chromosomes become condensed to form chromosome axes and recombination may initiate near the end. After that, the homologous chromosomes begin to pair bring chromosome axes closely to each other in the second substage, called zygotene. Full synapsis between homolog pairs occurs in the pachytene stage, during which, the process of recombination is completed. In the last diplotene stage, homologous chromosomes desynapase but are physically connected by a crossing-over resultant structure, termed chiasmata, until anaphase I onset [Kleckner 1996; Bolcun-Filas and Handel 2018].

Paring and interaction between homologous chromosomes is essential for reductional segregation

Homologous chromosome paring is mediated by the formation of a protein complex, known as the synaptonemal complex (SC). The tripartite proteinaceous structure of SCs bring the axes of the two homologs into proximity and maintains such close association until diplotene substage to promote recombination and crossing-over. The fundamental architecture of SC is constructed by two parallel axial elements(AEs) and central elements (CEs) connected by the overlapping transverse filaments (TFs) [Page and Hawley 2004]. Even though homolog pairing starts before recombination in fruit fly and worm, DNA double-strand breaks occur before paring in mammals, suggesting a complexity between the two mechanisms in functionality and evolution.

Although there are numerous differences among eukaryotes in the details of

how recombination is regulated, the basic meiotic recombination pathway is highly conserved. Recombination events are initiated by programmed double-strand breaks mediated by the conserved topoisomerase-like Spo11 protein. These breaks are then repaired by a modified HR pathway biased toward the use of homologous rather than sister chromatids as repaired templates. After resection of both 5’ strand ends, one end searches throughout the genome and identifies homologous sequences on a homologous chromatid forming a nascent interaction (D-loop). After that, a complicated decision has to be made to determine whether these interhomolog interactions develop into crossovers with the reciprocal exchange of flanking parental DNA sequences or are resolved to form noncrossovers without genetic exchange, but the frequency of crossovers in the genome is highly regulated by a poorly understood underlying mechanism termed crossover interference (COI) [Wang et al 2019].

Besides the exchange of genetic material, another outcome of recombination and crossovers is the formation of chiasmata between homologous chromosomes. Chiasmata result from crossovers between non-sister chromatids and are stabilized by sister chromatid cohesion (Figure 1-2A). They hold two homologs together after the disappearance of synapsis in diplotene and provide the resistance necessary for homolog pairs to align on the meiosis I spindle. Chiasmata are removed in anaphase I when Separase cleaves the stabilizing “arm cohesion” complexes, thereby releasing homologs and assuring reductional segregation in meiosis I [Petronczki et al 2003; Kudo et al 2006].

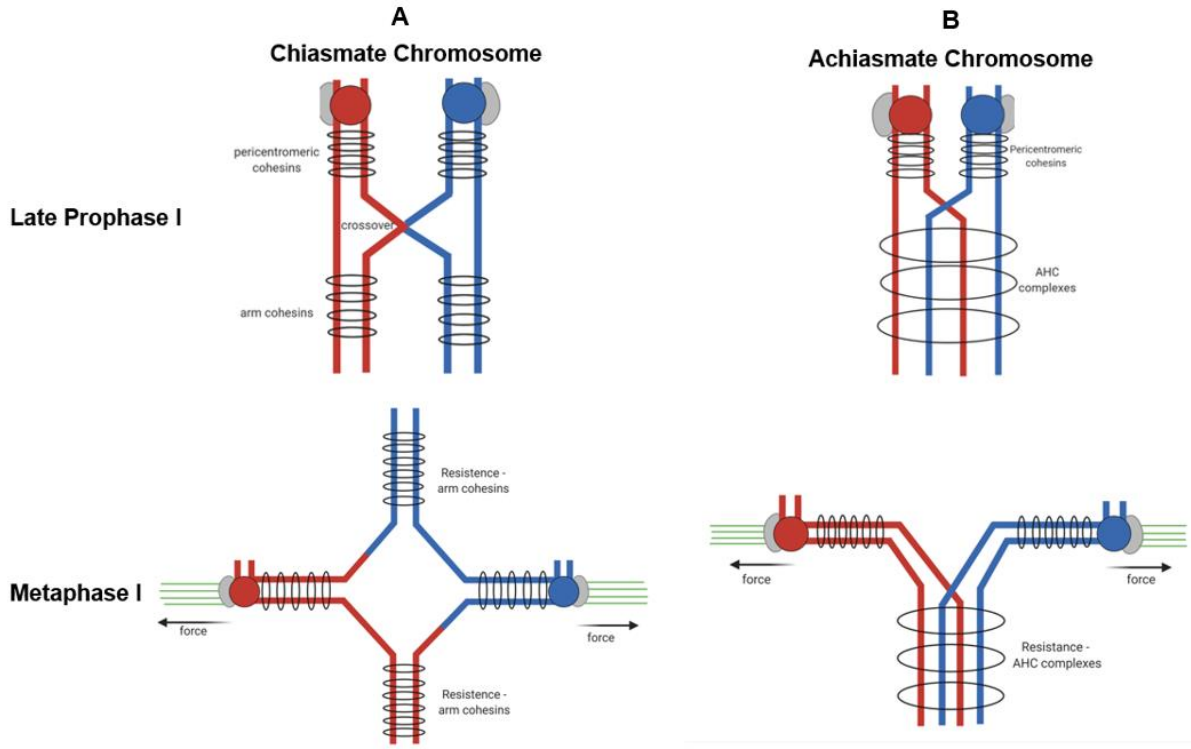

Figure 1-2. Two distinct mechanisms stabilize the interactions between homologs in different eukaryotic organisms. (A) Chiasmata mediate the interactions between homologous chromosomes. (B) Alternative homolog conjunction (AHC) establishes the interactions between achiasmate chromosomes.

In the three decades, male Drosophila has been paid more attention in the field of meiosis due to their unique features to ensure the success of spermatocyte production. First of all, as we know, recombination and crossing over boost the genetic exchange within species and endows the species with more genetic diversity and higher fitness in nature. However, meiotic recombination and synaptonemal complexes are completely absent from *Drosophila* male meiosis (but present in female meiosis). Therefore, it has long been a question, without recombination and resultant chiasmata, how homologous chromosomes realize pairing and reductional segregation in the first meiotic division. Different from most eukaryotic organisms, an alternative strategy in homolog pairing has been found in *Drosophila* males. *Drosophila* sex chromosomes share homology for the ribosomal RNA genes encoding 18S, 5.8S, 2S and 28S rRNAs. These rDNA sequences arrange in the tandem arrays of 200-250 copies in the heterochromatin of X chromosome and the short arm of Y chromosome. Noteworthy, deletion of proximal region on X chromosome, including those rDNAs, led to the perturbation of X-Y pairing and chromosome nondisjunction. Nevertheless, the insertion of rRNA genes on rRNA gene-depleted X chromosome rescued the phenotype of defective X-Y pairing and segregation. Finally, the capacity of paring was found in 240 bp-repeats which reside six to ten copies upstream of each rDNA transcription unit, together serving as the X-Y paring center in male *Drosophila* [McKee and Karpen 1990; McKee et al 1992; McKee 1996].

So far, it has been shown that cis-elements (PCs) act to specify positions of

homolog paring but proper pairing also requires the binding of glue molecules on those sites to build interhomolog association. Subsequently, two meiosis-specific proteins - MNM (Modifier of Mdg4 in Meiosis) and SNM (Stromalin in Meiosis) were identified in *Drosophila* spermatocytes (Figure 1-2B). Cytological data confirmed both MNM and SNM colocalized in the X-Y paring center (240 bp-repeats) from G2 to metaphase I. Subsequent detections showed that, not only on X-Y pair, both SMNM and MNM localize on autosomes with a much lower fluorescence intensity and mutations in either SNM or MNM destabilized interhomolog connections for both sex chromosomes and autosomes, leading to the occurrence of univalent (unpaired homologs) on the spindle from prometaphase I and homolog nondisjunction at anaphase I. Besides SNM and MNM, autosomal conjunction in male *Drosophila* also requires *teflon* (*tef*) gene. Mutations in *tef* destroyed the interhomolog interactions between autosomes, but did not affect the X-Y pair, and ablated autosomal foci of MNM from G2 to Prometaphase I, thereby disrupting bivalent formation in meiosis I [Tomkiel et al 2001; Thomas et al 2005]. Later, the combination of genetic and cytological approaches further demonstrated that both homolog segregation and the dissociation of SNM and MNM from chromosome at anaphase I are mediated by a Separase-dependent proteolytic pathway [Blattner et al 2016], reminiscent of the disassembly of chiasmata in other eukaryotes, which suggests the functional similarity between these two mechanisms, although the composition of these proteinaceous structures is evolutionally divergent. In a recent study, Weber et al identified a novel protein involved in alternative homolog conjunction (AHC) system,

called UNO, which was associated with SNM and MNM in the first meiotic division. More significantly, the authors demonstrated that UNO was the substrate of Separase and the cleavage on UNO released the conjunction complex in anaphase I [Weber et al 2020].

Establishment of sister-chromatid cohesion depends on the assembly of cohesins

Homolog interactions in meiosis are mediated by either establishment of chiasmata or by the alternative conjunction mechanism described above the male *Drosophila*. However, sister chromatid interactions are equally important for chromosome segregation. In both mitosis and meiosis, sister chromatids become aligned and stably connected from end-to-end during DNA replication by a mechanism known as “cohesion”. Since sister-chromatid cohesion is a central mechanism in both mitosis and meiosis, numerous efforts have been focused on this topic in the last several decades. In the initial observations, researchers found that, during DNA replication, sister chromatids tend to intertwine with each other at multiple sites where replication forks collide and such DNA catenations are removed by topoisomerase II prior to sister-chromatid segregation in anaphase [Sundin and Varshavsky 1980; DiNardo et al 1984]. Subsequent studies demonstrated that catenations indeed promote sister chromatid cohesion in the absence of topoisomerase activity under experimental conditions [Toyoda and Yanagida 2006]. But, a study in yeast overrode this preliminary explanation by evidence that circular sister minichromosomes can maintain a cohesive state even in the absence of

catenation [Koshland and Hartwell 1987]. Instead, from genetic screens in yeast, a protein complex, consisting of four components (SMC1, SMC3, SCC1/RAD21 and SCC3/SA), was identified and named cohesin to indicate its function in sister-chromatid cohesion.

In the ensuing studies, it has been shown that the cohesin complex is associated with chromosomes from late G1 phase to metaphase and establishes cohesion from end-to-end during DNA replication. Cohesin complexes not only serve to maintain the cohesion between sister chromatids but are required for establishing cohesion since cohesin mutants fail to form sister chromatid cohesion [Gruber et al 2006]. In mitosis, cohesin has a particularly critical role at pericentromeres which referred as a cohesin-enriched domain surrounding the core centromere sequence. The stable connections in pericentromeric regions are necessary to provide resistance to spindle forces during prometaphase and metaphase to enable the chromosomes to achieve bipolar alignment on the spindle equator. Reflecting this role, cohesin complexes are particularly abundant in the vicinity of centromeres in all eukaryotes. In addition, in metazoans, where most non-centromeric cohesins are removed during chromosome condensation by a non-proteolytic “prophase pathway”, peri-centromeric cohesin complexes are protected and preserved until anaphase onset, when they are removed in a proteolytic cleavage pathway mediated by the conserved protease Separase [Michaelis et al 1997; Gruber et al 2003]. Cohesin complex is largely conserved throughout eukaryotic organisms and shares a similar assembly through its core components [Strunnikov and Jessberger 1999;

Peters et al 2008].

SMC1 and SMC3 are two members of a family of Structural Maintenance of Chromosome proteins whose members are large ATPases. In yeast, SMC1 and SMC3 fold back on themselves around a hinge domain in the central region followed by a long coil-coiled region, while the other end is a globular ATPase (referred to head domain) formed by N-terminal and C-terminal sequences (Figure 1-3A). The two SMC subunits bind to each other tightly by hinge domains and contact with the SCC1/RAD21 subunit through their head (SMC1) or neck (SMC3) domains (Figure 3). SCC1/RAD21 is a member of the kleisin protein family and bridges the head domains of SMC1 and SMC3 by interactions with its C- and N-terminal regions respectively to form a ring-like structure with the diameter of 50 nm [Hearing et al 2002]. Electron microscopy confirmed this ring-like structure of cohesin complex in vertebrate species [Anderson et al 2002], which suggests cohesin complex is highly conserved in composition and structure. The last component SCC3/SA is associated with SCC1 and required for the establishment and maintenance of sister-chromatid cohesion.

Cohesion and cohesins have multiple roles in meiotic chromosome segregation

In meiosis, cohesin complexes are composed of similar subunits, but with paralogous substitutions that vary among species. A nearly universal substitution involves the replacement of the mitotic kleisin subunit SCC1/RAD21 by its paralog – REC8 in most meiotic cohesin complexes. Although REC8 provides the same core

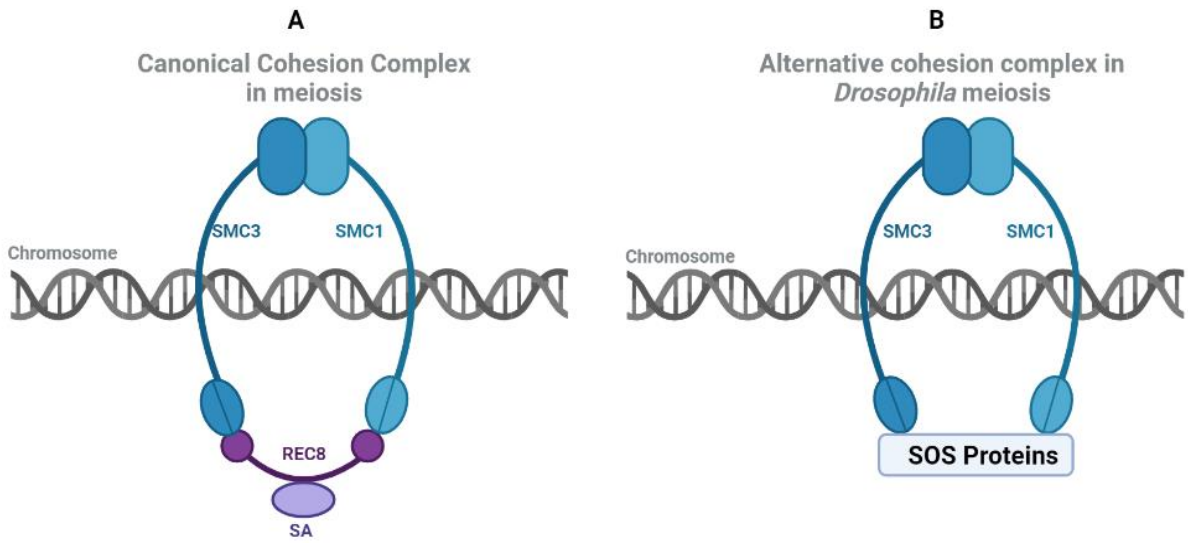

Figure 1-3. Schematic of the composition of meiotic cohesion complex. (A) canonical cohesion complex consisting of SMC1, SMC3, RE and SA in mitosis and composed by SMC1, SMC3, REC8 and SA in meiosis. (B) *Drosophila* meiotic cohesion complex constituted by SOS proteins (SOLO, ORD and SUNN).

functionality as its mitotic counterpart - joining the head domain of SMC1 and SMC3 to form stable rings and providing sites for cleavage and removal of cohesin by Separase, REC8 has additional functions that cannot be replaced by SCC1/RAD21 (discussed below) and has therefore been found essential for proper meiotic chromosome segregation. It is therefore puzzling that no clear REC8 homolog has been identified in *Drosophila*. This raised the question of how the cohesin complex is assembled in *Drosophila* spermatocytes without REC8.

Firstly, a meiotic kleisin in *Drosophila*, named C(2)M, drew the attention, and raised the possibility that this distant kleisin substitutes for the role of REC8 in *Drosophila* meiosis. However, it has been shown that C(2)M only regulates SC formation and crossing over prior to meiotic division in female *Drosophila*. Moreover, mutations in the putative Separase cleavage sites of C(2)M did not affect chromosome segregation [Manheim and McKim 2003; Heidmann et al 2004]. Alternatively, another possibility tested was whether the mitotic kleisin subunit RAD21 functions to assemble meiotic cohesin complexes, but this hypothesis was rejected by a genetic study by using a RAD21 variant in *Drosophila* female meiosis in which RAD21 only showed a role in SC maintenance by interacting with C(2)M, irrelevant to sister chromatid cohesion [Urban et al 2014].

Albeit no known kleisin subunit is functional in sister chromatid cohesion, three meiosis-specific proteins - SOLO, ORD and SUNN (SOS) were identified in *Drosophila* and found to be responsible for sister chromatid cohesion (Figure 1-3B). Mutations in *solo*, *ord* and *sunn* cause precocious sister chromatid separation and

the premature dissociation of SMC subunits from chromosomes including centromeres and arms. Moreover, cytological evidence has shown that SOS proteins colocalize with SMC cohesin on centromeres at least from prophase I to metaphase II in *Drosophila* spermatocytes. Mutations in *ord* completely abolished the centromere localization of SOLO and null mutation of SOLO prevented the binding of SUNN and SMC1 on chromosomes, which indicates an inner co-dependency among SOS proteins and the formation of SMC-involved cohesin complex in *Drosophila*. Subsequent structural comparison suggested that SUNN is a distant member in HEAT-repeat protein family and a possible structural homolog of the cohesin subunit SA, but the structure of the *Drosophila* meiotic cohesin complex is still not understood without a functional kleisin subunit [Webber et al 2004; Yan et al 2010; Krishnan et al 2014].

The release of cohesin complex depends on the proteolytic activity of Separase when cells enter anaphase, leading to the dissociation of sister chromatids. Unlike mitosis, meiosis adopts a stepwise dissociation of cohesin complexes in the two divisions. Reductional segregation in meiosis I requires the cleavage of cohesin complex on chromosome arms to release the connections between homologs, while equational segregation in meiosis II relies on the liberation of sister chromatids by the resolution of cohesin complexes in the vicinity of centromeres. The protection of centromeric cohesion in meiosis I depends on a widely conserved cohesion guardian protein, called Shugoshin. Studies have revealed that SGOs colocalize with pericentromeric cohesin complexes where they collaborate with phosphatase PP2A

to counteract the phosphorylation of REC8 which is necessary for its cleavage by Separase. This is one of REC8's essential functions; SCC1 can (and in some species does) contribute to arm cohesion, but it cannot be protected by SGO-PP2A complexes, so is fully removed at anaphase I [Kitajima et al 2006; Riedel et al 2006; Rivera and Losada 2006].

The *Drosophila* shugoshin gene, mei-s332, was identified by Orr-weaver et al in 1992; mutations in this gene caused precocious sister-chromatid separation in *Drosophila* spermatocytes at late anaphase I, suggesting a role of MEI-S332 in maintaining sister chromatid cohesion. In the subsequent studies, it has been shown that MEI-S332 localizes on centromeres from prophase to anaphase in both meiotic division and mutations of MEI-S332 result in the premature removal of *Drosophila* cohesins - ORD and SOLO from centromeres after anaphase I onset [Tang et al 1998; Nogueira et al 2014; Bickel et al 1998; Yan et al 2010]. The latest study in *Drosophila* male meiosis revealed that MEI-S332 can directly bind to B subunit of PP2A and they are mutually dependent for the centromere localization and the protection of centromeric cohesion [Pinto and Orr-Weaver 2017]. Given the absence of an apparent REC8 homolog, the identity of the protein(s) that is/are protected by MEI-S332-PP2A is a mystery. That there must be a kleisin-like subunit in the cohesion complex is implied by the observation that inhibition of Separase prevents anaphase II segregation and causes the SOS protein SOLO to persist at centromeres well beyond anaphase II [Blattner et al 2016]. This subunit is not UNO, the recently discovered Separase target in the conjunction complex; UNO is

removed at anaphase I and mutations in *uno* do not disrupt sister centromere cohesion. The implication is that the *Drosophila* genome contains another kleisin-like protein that functions specifically in meiosis II and serves as the target of MEI-S332-PP2A.

Sister-chromatid mono-orientation in meiosis I promotes reductional segregation in meiosis I

In mitosis, all the chromosomes congress to the middle of the cell from where the two sister chromatids are pulled to the opposite poles. During this process, the movement of chromosomes depends on the interaction between a microtubule-based spindle and a centromeric protein complex called the kinetochore. Accurate chromosome segregation in mitosis requires two kinetochores on sister chromatid pairs to attach to microtubules emanating from the opposite spindle poles and achieve bi-orientation (amphitelic attachment, Figure 1-4A). Sister bi-orientation is essential both for chromosome alignment at the spindle equator during metaphase and for the bipolar movement of sister chromatids in anaphase. Erroneous microtubule attachment can lead to aberrant chromosome orientations. For example, monotely refers to only one of the two sister kinetochores attached by microtubules from one single pole, syntely refers to attachment of both sister kinetochores to the same spindle pole and merotely refers to attachment of one sister kinetochore to microtubules emanating from the opposite poles. Improper chromosome orientation is a common cause of chromosome mis-segregation unless it can be resolved prior to chromosome move off spindle equator [Tanaka 2005; Compton 2007]. However,

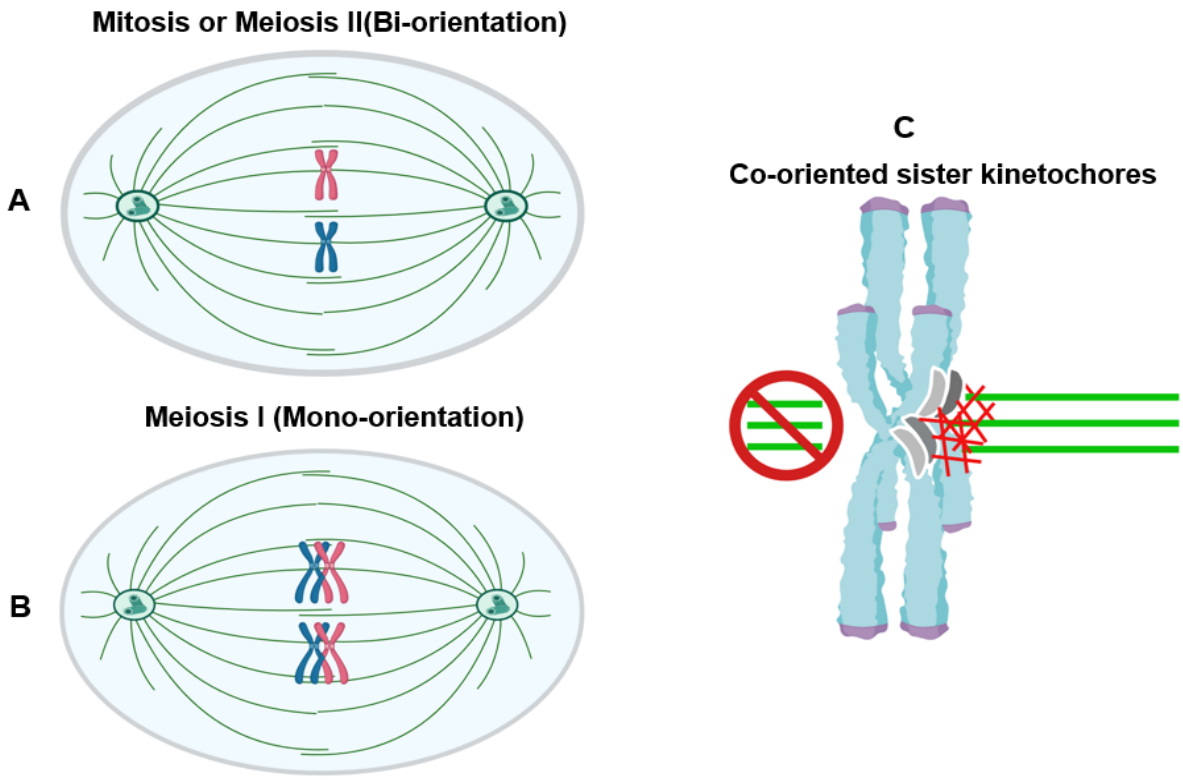

Figure 1-4. Sister-chromatid orientation in mitosis and meiosis. (A) Two sister chromatids adopt bi-orientation in mitosis and meiosis II. (B) Sister chromatids on each homolog are mono-oriented in meiosis I. (C) Model of coordinated sister kinetochores attached by microtubules from one pole. Gray crescent disc: inner plate of kinetochore; Dark crescent disc: outer plate of kinetochore; Red-crossing network: fibrous corona.

in contrast, chromosomes in meiosis I adopt a unique orientation pattern distinct to the traditional bi-orientation in mitosis and meiosis II. Reductional segregation in meiosis dictates the segregation between homologous chromosomes, so two sister chromatids on each homolog move side-by-side to the same pole (Figure 1-4B). To achieve this goal, two sister kinetochores have to be attached by microtubule bundles emanating from the same pole, termed mono-orientation or co-orientation.

Two fundamental questions are how the two sister kinetochores become capable of connecting with microtubules from one pole but become resistant to the other pole and whether the kinetochores share the same composition or assembly between mitosis and meiosis (Figure 1-4C). Such special kinetochore geometry was first attributed to the meiotic (REC8-containing) cohesin complex. In fission yeast, cohesin complexes are loaded on both peri-centromeric and centromeric core (kinetochore-forming domain) regions during meiotic S phase, while they are only preserved at pericentromeric regions after anaphase I and held on chromosomes until anaphase II. The meiosis I-specific cohesins at core centromeres function to clamp the sister centromeres on which sister kinetochores are established. Therefore, deletion of REC8 in fission yeast disrupts reduction segregation in meiosis I, which implicates a perturbed sister-chromatid mono-orientation due to the loss of cohesin-dependent cohesion. Similar observations have been reported in various eukaryotic species [Watanabe and Nurse 1999; Severson et al 2009; Yan et al 2010]. Nevertheless, an obvious flaw for such cohesin-based theory is that the cohesin complex only appears to connect the inner centromeres and show up on

chromosome arms, both are distant to outer kinetochore where actually contacts with microtubules. Also, since REC8 cohesin is responsible for sister centromere/pericentromere cohesion in both meiosis I and meiosis II in most eukaryotes, other factors must contribute to meiosis I mono-orientation. Recently, another protein complex consisting of four proteins (MAM1, CSM1, LRS4 and HRR25) was identified in budding yeast, named Monopolin. Genetic and cytological evidence showed that Monopolin complex localizes on centromere in meiosis I and promotes the centromere co-orientation in a cohesin-independent manner [Tóth et al 2000; Rabitsch et al 2003]. Crystallographic study uncovered that Monopolin complex exhibits a V-shape structure composed by the dimerization of scaffolding protein CSM1 with coiled-coil domains and globular domains in the N- and C-terminal regions, respectively. Two copies of LRS4 binds to the coiled-coil domain of CSM1 whose globular domain is associated with one copy of MAM1 and HRR25. The following studies revealed that CSM1 binds to kinetochores through the interaction between its globular domain and two constitutive kinetochore proteins - DSN1 (MIS12 subunit) and MIF2 (CENP-C homolog) [Corbett et al 2010; Corbett and Harrison 2012]. It raised the possibility that Monopolin might be able to crosslink sister kinetochores using the two globular domains at opposite ends of the anti-parallel CSM1 dimer. This idea was supported by an experiment of laser trap and quantitative fluorescent microscopy in yeast, by which kinetochore particles were isolated from mitosis and meiosis. Stronger microtubule attachments were achieved on meiosis-I kinetochores compared to those in mitosis or meiosis II. Moreover, the

strength on kinetochore can be enforced by ectopic expression of Monopolin [Sarangapani et al 2014]. Taken together, budding yeast Monopolin complex promotes the fusion between sister kinetochores, by which two sister kinetochores form one functional unit and only accessible for the microtubules from one spindle pole.

Although the discovery of Monopolin shed light on orientation regulation in meiosis I, it was soon found that, although Monopolin components are also expressed in fission yeast, the mutations of Monopolins do not affect reductional segregation in meiosis I [Rabitsch et al 2003]. This observation implies that Monopolin might not be the only functional complex to ensure sister-chromatid mono-orientation even in yeast species. Recently, a group of meiosis-specific proteins have been identified in a range of organisms, from yeast to mammals, named meiosis-I kinase regulator (MOKIRs). The remarkable features of MOKIRs are that all of them act to promote sister-chromatid mono-orientation in different species by protecting sister cohesion depending on the interaction with POLO kinase, but they share poor sequence homology between each other. The first two MOKIRs members were identified in yeast, SPO13 in budding yeast and MOA1 in fission yeast, and other functional homologs were found in fruit fly and mouse - MTRM and MEIKIN. Initial phenotypic studies showed that the dysfunction of MOKIRs dramatically increased chromosome mis-segregation in the first meiotic division. Subsequent studies have attributed the orientation regulation of MOKIRs to their capacity of protecting sister-chromatid cohesion [Galander and Marston 2020].

For instance, a reduced Shugoshin localization was reported in MOA1 and MEIKIN deleted cells indicating a role of MOKIR proteins in cohesion protection at pericentromere, whereas SPO13 preserved the sister chromatid cohesion by preventing the phosphorylation of cohesin [Kiburz et al 2005; Kim et al 2015; Miyazaki et al 2017].

In *Drosophila* meiosis, the understanding of mono-orientation regulation has drawn more attention but how sister chromatids become co-oriented is still not clear. However, a previous study of kinetochore structure by electron microscopy revealed that, after loading on centromeres, kinetochores underwent structural changes from early prometaphase I to anaphase I in *Drosophila* spermatocytes. The hemispheric structure in early prometaphase I was proposed to facilitate microtubule capturing and it was soon converted a single-disc structure which was suggested to promote sister mono-orientation. Finally, double-disc structure observed in anaphase I endowed the sister kinetochore with the ability of bi-orientation [Goldstein 1981]. An RNAi-induced disruption of SPC105R (KNL homolog in *Drosophila*) destroyed the sister chromatid co-orientation depending on Separase activity, which was correlated to the premature loss of sister-chromatid cohesion. However, *Drosophila* seems to employ another mechanism to regulate mono-orientation through the interaction between kinetochore and microtubule, independent of the cohesion-related pathway, since phosphatase PP1-87B RNAi can trigger sister centromere separation by antagonizing the POLO kinase and BubR1, suggesting the inhibitory regulation of PP1-87B in stable microtubule attachment [Wang et al 2019]. Another intriguing

finding of the sister-orientation alternation has been reported, in which two-thirds of univalents liberated from homolog conjunction in *mnm* mutants showed a stretched/split centromeres in metaphase I and delayed poleward movement after anaphase I onset, suggesting a disrupted sister-chromatid orientation in absence of interhomolog connections [Chaurasia and Lehner 2018] . These observations in *Drosophila* meiosis elicit the questions that whether other kinetochore components or kinetochore-associated proteins are involved in these two pathways and whether the cohesion-related or -independent pathways are completely insulated between each other or conjoined in any point molecularly and timely.

Spindle assembly checkpoint (SAC): A Cell cycle regulator in M-Phase

Checkpoints in Cell Cycle

Cell division is a tightly regulated biological process in which mediates the transmission of the whole genome from parental cells to their descendants, and its regulation relies on an accurate cell cycle. Eukaryotic cell cycle is divided into four stages: G1, S, G2 and M. G1 (Gap 1) phase is a growth phase and metabolically active. DNA replication occurs in S (synthesis) phase and the whole genome is duplicated. G2 (Gap2) phase contributes to protein synthesis for the subsequent M (Mitosis) phase where DNA and cytoplasm are equally distributed in daughter cells [Schafer 1998 and Johnson and Walker 1999]. Several regulatory mechanisms functioning in different cell cycle phases underlies the progression of cell division and proliferation (Figure 1-5). On the other hand, cells are sensitive to extracellular signals that coordinate the progression of the cell cycle with nutrient availability and

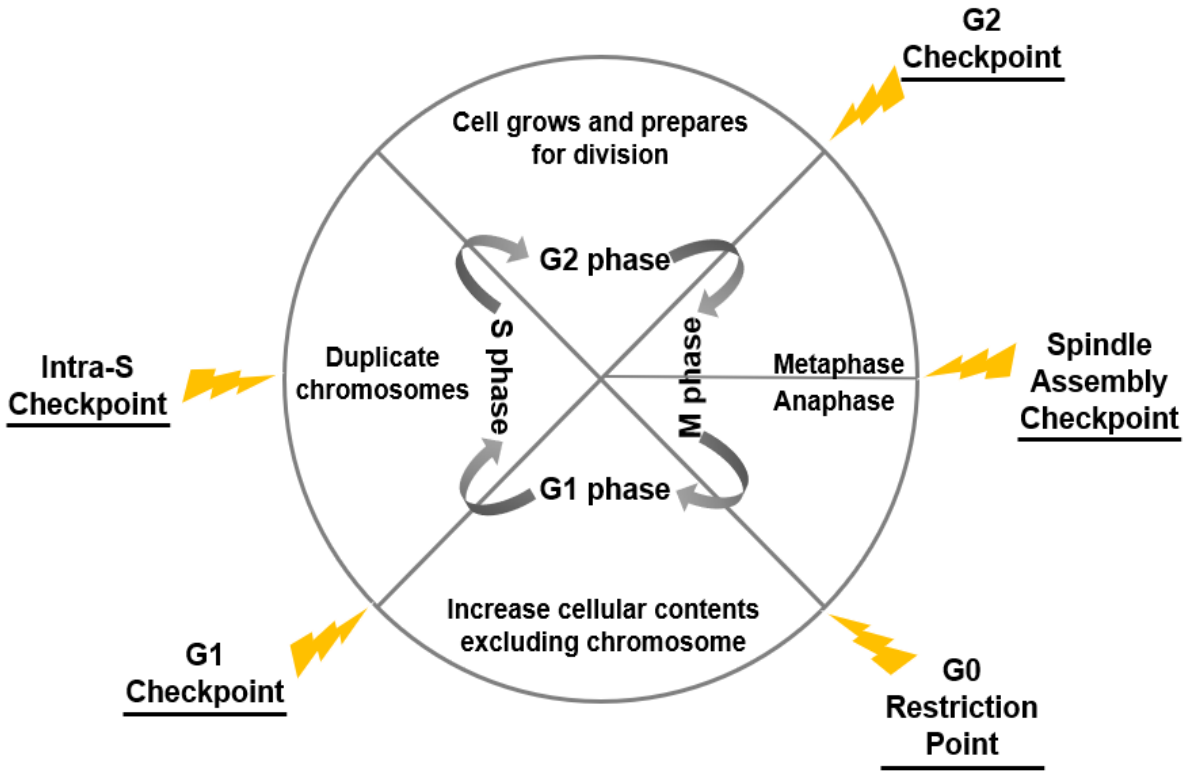

Figure 1-5. Schematic of major checkpoints during the cell cycle.

growth factors, reflecting by START in yeast and restriction point in animal cells respectively [Charvin 2010; Pardee 1974; Blagosklonny and Pardee 2002]. In G1, cell size is tightly controlled in order to maintain an appropriate amount distribution of genetic and biosynthetic material in progeny cells [Barnum et al. 2014].

DNA damage checkpoints act to prevent the transmission of aberrant genetic material to daughter cells when DNA damage or other stresses occur. It takes place in G1, S and G2 phases and, through which, cell cycle is ceased to allow time for the process of DNA repair. In principle, DNA lesions trigger the activation of checkpoint pathways that maintain CDKs (CYCLIN Dependent Kinases) to be inactive preventing cells from entering the next stage [Barnum et al. 2014; Kastan and Bartek 2004]. Although checkpoint mechanism is critical for the progression from G1 to G2 to monitor cell growth and genome fidelity, it is also essential in M phase in which chromosomes segregate and distribute in daughter cells accurately.

Discovery and composition of Spindle Assembly Checkpoint

Spindle assembly checkpoint (SAC), also known as M-phase cell cycle checkpoint, maintains genome integration and stability by regulating the progression of the cell cycle when cells are dividing. The history of M-phase checkpoint research was dated to 1930s at which initial observations in vertebrates found that microtubule depolymerization drugs, such as sodium cacodylate and colchicine, are able to inhibit mitosis and cause cell arrest in mitosis [Brues and Cohen 1936; Brues and Jackson 1937]. After that, the concept of a checkpoint in metaphase was proposed to be associated with unpaired chromosomes derived from chromosome

mis-congression on metaphase spindle and block anaphase onset [Nicklas & Arana 1992]. In the following several years, three studies in different eukaryotic organisms tethered the activation of metaphase checkpoint to the function of centromeres and kinetochores where microtubule attach to during cell division, from where people started to correlate metaphase checkpoint and spindle attachment [Spencer & Hieter 1992; Rieder et al. 1994; Rieder et al. 1995].

However, a thorough understanding of this checkpoint requires the decoding of the entire molecular pathway and the first attempt was reported in yeast. Two parallel studies published back-to-back identified two protein families – MADs (MAD1, MAD2, MAD3 or BUBR1 in higher eukaryotes) and BUBs (BUB1 & BUB3) in *S. cerevisiae*. Their results first demonstrate that MADs & BUBs are required for mitotic cell arrest and MAD/BUB mutations allow cells exit mitosis in presence of a disrupted spindle leading to chromosome mis-segregation and cell death [Li and Murray 1991; Hoyt et al. 1991]. On evolutionary course, MADs and BUBs maintain high conservation among eukaryotes, but the exception is that BUBR1 in multicellular organisms only shows homology with the N-terminal of MAD3 in yeast and an exclusive kinase-like domain (Table 1-1) [Malmanche and Sunkel 2006]. In various organisms, cytological evidence has demonstrated a similar localization pattern that MAD and BUB proteins are recruited on kinetochores in a timely manner from prometaphase to anaphase [Taylor et al. 1998; Chen et al. 1998; Logarinho et al. 2004].

Except for MADs and BUBs, mitotic kinases also play pivotal roles in SAC

Table 1-1. The profile of conserved SAC proteins in eukaryotic organisms.

SAC components	S. cerevisiae	S. pombe	C. elegans	D. melanogaster	X. tropicalis	M. musculus	H. sapiens
MAD1	MAD1	MAD1	MDF-1	MAD1	MAD1	MAD1	MAD1
MAD2	MAD2	MAD2	MDF-2	MAD2	MAD2	MAD2	MAD2
MAD3	MAD3	MAD3	SAN-1	BUBR1	BUB1B	BUB1B	BUB1B
BUB1	BUB1	BUB1	BUB-1	BUB1	BUB1	BUB1	BUB1
BUB3	BUB3	BUB3	BUB-3	BUB3	BUB3	BUB3	BUB3
MPS1	MPS1	MPH1	-	MPS1	MPS1/TTK	TTK	TTK
AURORA B	IPL1	ARK1	AIR-2	AURB	AURKB	AURKB	AURKB

signaling cascade. MPS1 is an essential protein kinase and required for spindle pole body duplication, but genetic evidence in yeast showed that microtubule depolymerization fails to activate SAC checkpoint in *mps1* mutants and overexpression of MPS1 causes arrest in mitosis [Weiss and Winey 1996; Hardwick et al 1996]. Later, Abrieu et al found that MPS1 acts upstream in SAC signaling and is necessary for kinetochore-localization of MAD1 and MAD2 in vertebrate [Abrieu et al 2001]. But, the exact role of MPS1 has been hazy until intensive studies in yeast and human uncovered that recruitment of BUB1 on kinetochore depends on MPS1-mediated phosphorylation [London et al 2012; Shepperd et al 2012; Yamagishi et al 2012]. Another SAC-associated kinase is Aurora B which is also a subunit of chromosome passenger complex. Early observations reported that Aurora B inactivation abolishes the SAC function in Xenopus and rats [Kallio et al 2002 and Murata-Hori et al 2002]. Subsequent study in human cell culture showed that the treatments of Aurora B inhibitors disrupt kinetochore-localization of SAC proteins, like BUB1, BUBR1 and MAD2 [Ditchfield et al 2003 and Hauf et al 2003], therefore the function of Aurora B is critical for SAC signaling pathway.

After the identification of major players involved in SAC cascade, the remaining questions are that how these SAC components generate “Wait-anaphase” signal and what the downstream effectors associated with cell cycle and chromosome segregation. Logically, cell cycle is tightly regulated by CYCLIN/CDK complexes and transition from G2 to M demands the activation of CYCLIN B/CDK1 [Johnson and Walker 1999]. Subsequent studies revealed that SAC proteins target CDC20 to

inactivate a cullin-Ring finger E3 ubiquitin ligase - APC/C (Anaphase Promotion Complex/ Cyclosome),by which CYCLIN B, a substrate of APC/C, fails to undergo polyubiquitination arresting cell in metaphase-to-anaphase transition with high CDK1 activity (Figure 1-6). In the meantime, segregation of sister chromatids is prohibited because the APC/C activation is also required for the release of a protease Separase which mediates the resolution of sister-chromatid association [Hwang et al. 1998; Kim et al. 1998; Peters 2006].

SAC signaling in mitosis versus in meiosis

The cell cycle is a highly coordinated event to determine cell growth and proliferation, which is critical for the development of living organisms and the regeneration of adult tissues. Chromosome segregation error is the basis of chromosome imbalance and instability (CIN) that has been attributed to aging and tumorigenesis [Aguilera and Gómez-González 2008]. SAC signaling pathway serves to tightly monitor M-phase and ensure faithful chromosome segregation, but mutations in SAC genes have been shown to be highly associated with the production of aneuploidy and CIN in mitosis, leading to cell death in the early developmental stage and various types of cancer in human. The null mutation of MAD2 causes massive chromosome mis-segregation and embryonic lethality in mouse and Bub1 deletion in *Drosophila* is also embryonic lethal [Dobles et al 2000; Basu et al 1999]. However, this is not the case in *Drosophila* neuroblasts since *mad2*-null *Drosophila* are viable and fertile. More importantly, deletion of *mad2* gives rise to a defective checkpoint and an accelerated mitotic “clock”, but no defect in

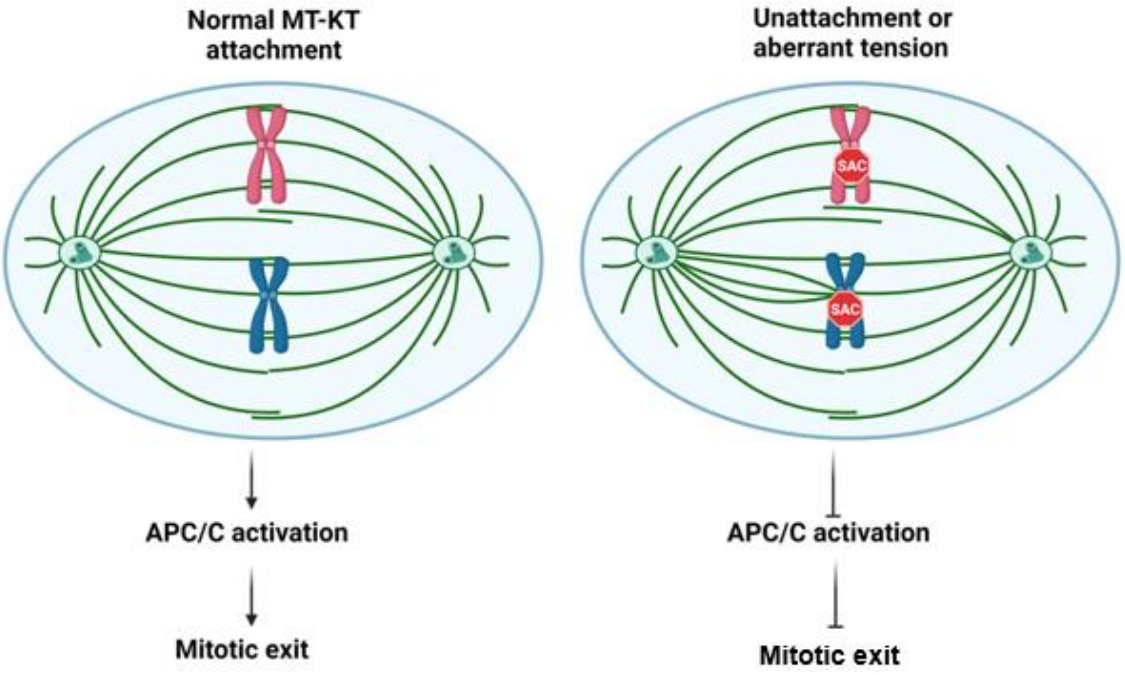

Figure 1-6. Schematic of the activation of SAC signaling pathway.

chromosome segregation [Buffin et al 2007]. In recent years, growing evidence has been demonstrated that the mutations or altered expression of SAC genes are associated with human cancer. Mutations in *mad1*, *mad2* and *bub1* lead to lung, colon and breast cancer lines [Cahill et al 1999; Myrie et al 2000; Michel et al 2001]. Knockdown of BUBR1 in murine induces polyploidy in fibroblast cells and megakaryogenesis in bone marrow progenitors aggravating rapid tumor development [Scannevin et al 2004; Dai et al 2004].

Genomic imbalance in mitotic cells causes developmental deficiencies and tumorigenesis, but its outcome in meiosis is usually the production of aneuploidy during gametogenesis leading to infertility, spontaneous abortion and birth defects. Although the defining features make meiosis unique, many studies have been shown that mutations or depletion of SAC proteins are associated with chromosome mis-segregation and the production of aneuploidy. The absence of MAD2 in budding yeast caused a high frequency of chromosome nondisjunction and produced nonviable spores [Shonn et al 2000; 2003]. Similar result observed in meiosis I of female mice in which either reduced or overexpressed MAD2 leads to chromosome segregation error in meiosis I, resulting the generation of aneuploid oocytes in meiosis II [Niault et al 2007].

However, there has been, so far, a debate involving SAC function in meiosis: whether the regular metaphase arrest in meiotic cell cycle is somehow dependent on checkpoint function of SAC in eukaryotic organisms. Several lines of evidence have demonstrated a function of meiotic arrest or delay through the SAC pathway in

yeast, worms, fruit fly and mammals [Homer et al 2005; Stein et al 2007; Rebollo and González 2000; Wassmann et al 2003; Niault et al 2007]. In contrast, the inhibition of APC/C in the oocytes of Xenopus did not induce metaphase-to-anaphase arrest and it was also the case when meiotic spindle was disrupted [Peter et al 2001; Taieb et al 2001; Shao et al 2013]. In addition, Tsurumi et al also pointed out that SAC proteins were dispensable for metaphase II arrest in mouse oocytes [Tsurumi et al 2004]. Therefore, such evidence clearly shows that SAC regulation in meiosis shows species-based and stage-based variations.

Besides, growing studies have demonstrated that some of SAC components exhibited multiple roles during meiosis and regulated meiosis-specific events independent of their checkpoint function. Firstly, BUB1 kinase activity is required for sister-chromatid cohesion through localizing cohesion protector (Shugoshin) to kinetochores in yeast and *C. elegans* [Bernard et al 2001; Kawashima et al 2010; Borja et al 2020]. Yeast MAD3 lacking the C-terminal kinase domain delays prophase progression in both divisions in presence of an error-prone chromosome pair [Cheslock et al 2005]. MAD3 homolog BUBR1 not only accelerates cell cycle in mouse oocytes but is required for sister-chromatid cohesion in *Drosophila*. [Touati et al 2015; Malmanche et al 2007]. Except for the effect on the maintenance of sister-chromatid cohesion, SAC proteins are also responsible for proper microtubule attachment, particularly in meiosis I. In budding yeast and mouse, MPS1 kinase facilitates the formation of a force-bearing connection between microtubule and kinetochore to establish a correct attachment [Meyer et al 2013; Hached et al 2011].

Another SAC-associated kinase involved in kinetochore-microtubule attachment is Aurora B that is responsible for the correction of microtubule attachment [Tanaka et al 2002; Lampson et al 2004]. In meiosis, it has been shown homologous chromosomes failed to segregate in Aurora B-depleted oocytes in *C. elegans* suggesting its role in the dissociation of homologs [Kaitna et al 2002]. Later, studies in budding and fission yeast found that yeast Aurora B is required for centromere cohesion and co-orientation in meiosis I by protecting Shugoshin-PP2A on centromeres and correcting merotelic attachment on sister kinetochores [Monje-Casas et al 2007; Hauf et al 2007; Sakuno et al 2011]. Thus, SAC proteins adapt the meiosis-specific events and ensure accurate chromosome segregation independent of their checkpoint function.

SAC activation: the formation of MCC

SAC cascade is of great significance in both mitosis and mitosis to ensure the faithful transmission of genetic information in progeny, but how the “wait-anaphase” signaling is created in the cells is still not fully characterized. The first and widely recognized model regarding the communication between SAC and CDC20 is the formation of MCC (mitotic checkpoint complex). A biochemical study in HeLa cells isolated the MCCs, APC/C inhibitory factors, consisting of four SAC components - MAD2, BUBR1 (MAD3 in yeast), BUB3 and CDC20, and further demonstrated the physical association between MCC and APC/C. Even though the unattached kinetochore is thought to be the triggering condition of SAC, the formation of MCC is not dependent on the kinetochore's assembly as it can be detected in interphase

[Sudakin et al 2001; Poddar et al 2005]. The following studies involving these MCC subunits further verified that the binding of MCC to APC/C extinguish the ubiquitin-ligase activity and delay the cell cycle [Fraschini et al 2001; Shannon et al 2002; Millband and Hardwick 2002]. However, BUB3 later has been shown to be dispensable for MCC formation which could be normally established in BUB3-depleted yeast cells [Sczaniecka et al 2008]. Moreover, BUB3 was not required for MCC-dependent suppression of APC/C [Tang et al 2001; Fang 2002; Malureanu et al 2009]. Thus, MAD2 and BUBR1, serve as core SAC effector, gained increasing attention in order to fully understand the interaction between MCC and APC/C.

The molecular basis of MCC-mediated APC/C inhibition has been unfolded in a crystallographic experiment by using MCC subunits in fission yeast, in which the authors identified that the critical interaction interfaces in MCC trimer. Specifically, MAD3 binds to MAD2 and CDC20 through a helix-loop-helix (HLH) domain in its N-terminus, named KEN box, and scaffolding TRP domain, while MAD2, an α/β-HORMA-class protein, interacts with HLH domain in MAD3 by its α-C helix and β8′–β8″ hairpin regions. CDC20 recognizes KEN box on MAD3 and MAD2 through N-terminal WD40 domain and MAD2-binding motif, and two disordered APC/C interacting motifs reside in N- and C-terminus, respectively [Chao 2012].

A key question is how MCC is recruited on kinetochore and triggers the downstream APC/C inhibition. In the last two decades, two models have been proposed to explain how the MCC assemble in response to the activation signal from kinetochore. The “MAD2 template model” underlies a conformational change of

MAD2 after interacting with its partners. In brief, MAD2 has two different conformations: open conformation (O-MAD2) and closed conformation (C-MAD2). Upon binding to MAD1 or CDC20, O-MAD2 can be converted to C-MAD2conformer through the motion of two β-sheet across the face of the protein. In cytosol, the majority of MAD1 is maintained in C-MAD2 bound stat serving as the template of the C-MAD2-CDC20 inhibitory complex. Although CDC20 also carries MAD2 binding motif and binds O-MAD2 spontaneously, the forward rate constant is much lower than normal protein interaction rate, so it implicates a large catalytic barrier to prevent the binding between O-MAD2 and CDC20 in normal condition. But, C-MAD2-MAD1 is constantly recruited on kinetochore when aberrant microtubule attachment appears, by which the catalytic barriers are overridden and the formation of MCC is intensified [Luo et al 2002; Sironi et al 2002; Musacchio and Salmon 2007].

However, one remaining question in the “MAD2 template” model is why the C-MAD2-MAD1 in cytosol pool cannot induce the efficient conversion of O-MAD2 before the kinetochore signal fires. Another model proposed that the restriction of cytosolic MAD2 conversion is implemented by a SAC negative regulator, called $p31^{comet}$. In principle, $p31^{comet}$ completes the dimerization interface on C-MAD2 to constrain the catalytic effect of C-MAD2-MAD1 in cytosol, leading to the restriction in the conversion of MAD2 from open state to closed state and to block the downstream of SAC [Xia et al 2004; Yang et al 2007].

The assembly of SAC machinery on kinetochore

Temporospatial assembly of SAC apparatus on kinetochore activates the inhibition of APC/C and functions to block the mitotic entry when erroneous microtubule attachment occurs. Next important question is what condition triggers the activation and silencing of SAC signaling cascade. In cell division, the foremost mission is dividing the genetic material equally to the daughter cells for the sake of genome stability between generations. Therefore, chromosomes composed by DNA and nucleosome undergo replication in S phase and segregation in M phase, which ensures the production of euploid progeny. To achieve accurate chromosome segregation, it comes down to two fundamental questions: i) where the regions on chromosome that mediate the attachment on the mitotic spindle; ii) what machinery is required for this chromosome-spindle connection.

Centromeres are highly specialized regions on chromosomes recognized by segregation machinery when cells are dividing. In most eukaryotic organisms, centromere resides in a restricted region on each chromosome (termed mono-centric) and the absence or abnormal formation of centromere causes chromosome mis-segregation or fragmentation, so the positioning of centromeres is a critical and tightly regulated process. Although short centromere-associated DNA sequences have been identified in budding yeast (125 bp) and human (171 bp), the centromere specification in other eukaryotes only depends on the installation of histone H3 variant CENP-A to form centromere-specific nucleosome [Biggins 2003; Masumoto et al 1989; Palmer et al 1987].

Building on CENP-A heterochromatin, a proteinaceous structure kinetochore is assembled dynamically by more than 100 proteins with a defining three-layer architecture (inner kinetochore, outer kinetochore and newly identified fibrous corona). The inner kinetochore is constructed by a conserved CCAN subcomplex and two CENPs (CENP-B and CENP-C) that are constitutively associated with CENP-A chromatin, while the outer layer is largely assembled by three protein complexes called KNL1, MIS12 and NDC80 (together known as the KMN protein network) to form a platform and conduct the signal between chromosome and mitotic apparatus. Unlike constitutive kinetochore components, KMN network binds chromosomes prior to M-phase and persists after anaphase onset. Recruitment of SAC components on kinetochores starts right after the assembly of kinetochore core, among which the scaffold KNL1 is phosphorylated by MPS1 within its MELT motifs. Then, the phosphorylated KNL1 can interact with BUB1/BUB3 to activate the downstream SAC assembly and promote the checkpoint function [Kops et al 2020]. When a proper microtubule-kinetochore attachment is achieved, the extinction of SAC signaling depends on a minus-end-directed motor called Dynein that strips SAC proteins away from kinetochores, like MAD1 and MAD2, allowing cells to enter anaphase. However, recent studies have shown that phosphatase activity of PP1 is required for SAC inactivation through the interaction with KNL1 in budding yeast and perturbation of this interaction leads to the failure of SAC silencing and lethality [Rosenberg et al 2011]. Subsequent studies have confirmed that SAC inactivation depends on the interaction of KNL1 and PP1 in fission yeast and *C. elegans*

[Meadows et al 2011; Espeut et al 2012].

The characterization of RZZ complex

Besides MAD and BUB protein, RZZ complex is also considered as an essential component in SAC signaling pathway, and its name derives from the three constitutive subunits - Rough Deal (ROD), Zeste-white 10 (ZW10) and Zwilch. rod and zw10 genes were first identified in *Drosophila* encoding two proteins with the mass of 200kDa and 84kDa, respectively. Null mutations in these two genes caused similar abnormal phenotypes in nuclei including chromosome laggards and the production of aneuploids. In addition, treatment of cells with the microtubule depolymerizer - colchicine in *rod* and *zw10* mutants triggered precocious sister chromatid separation (PSCS) in metaphase suggesting an abrogated SAC function. Subsequent antibody-based studies have exhibited that both ROD and ZW10 are first visible on kinetochores in the transition between prophase and prometaphase, and then they distribute on both chromosome and spindle as all chromosome aligns to the cellular plate. After anaphase onset, they are exclusively associated with kinetochores in the leading ends to the spindle poles until the late telophase [Karess and Glover 1989; Williams et al 1992; Scaërou et al 1999]. Later, Goldberg et al showed that ROD and ZW10 shared the same localization pattern in *Drosophila* larval brains and co-immunoprecipitated them in embryo extracts, which implicates that ROD and ZW10 function together as a soluble complex within the same pathway. Protein sequence analysis revealed that ROD and ZW10, even though are highly diverged, exist throughout higher eukaryotic organisms, from *Drosophila* to

human. Double-strand RNA injection (RNAi) induced the abnormalities in *C. elegans*, like lagging chromosome and sister chromatid segregation defect, and cytological evidence confirmed a similar dynamic of ZW10 and ROD in human HeLa cells [Starr et al 1997; Scaërou et al 2001]. Taken together, ROD and ZW10 are assembled as a functional unit during in M phase and conserved among multicellular organisms serving the same pathway. The last RZZ component - ZWILCH (75 kDa) was isolated in immunoaffinity chromatography by using *Drosophila* embryo extracts, which was co-immunoprecipitated with ZW10 and mutations in *zwilch* gene caused the same defects in chromosome segregation and checkpoint function [Williams et al 2003]. In *Drosophila* mitotic cells, mutations in either of the three RZZ subunits, ROD, ZW10 and Zwilch, cause high frequency of chromosome mis-segregation and lagging chromosomes at anaphase. Similarly, RZZ function is also indispensable for chromosome segregation in *Drosophila* meiosis since mutations in *rod* results in aneuploid meiosis II spermatocytes following by a disrupted chromosome segregation at anaphase II and mutations in *zw10* give rise to chromosome nondisjunction and laggards in both meiotic divisions [Karess and Glover 1989; Williams et al 1992; 1996; 2003].

The dynamic of subcellular localization has been revealed by immunostaining in *Drosophila* neuroblasts and spermatocytes. Before prometaphase onset, RZZ subunits remain in the cytoplasm, but it is unclear if they are in a monomer state or assembled as complex already. After nuclear envelope breakdown, RZZ complex is rapidly recruited on kinetochores and persists until late anaphase, and this behavior

is conserved in invertebrate and vertebrate species [Williams et al 1992; Scaërou et al 1999; 2001; Basto et al 2004]. Notably, once sister kinetochores are attached to microtubule bundles and bi-oriented, the RZZ complex undergoes a “redistribution” along the microtubules toward spindle poles accompanying a reduced localization on kinetochores. Once anaphase begins, RZZ returned to the kinetochores, suggesting that the redistribution from kinetochores to the spindle is driven by the tension between sister kinetochores. In the following studies, people have attributed this highly dynamic RZZ distribution to the association with Dynein/Dynactin complex by which regulates the dynamic of kinetochore peripheral proteins and mediates the minus-end-directed cargo transportation. The profile of Dynein’s cargo includes not only the RZZ complex but also the other major SAC proteins, like MADs and BUBs, which explains the role of Dynein in SAC inactivation [Silva et al 2014].

The next questions are how RZZ complex interacts with dynein motor and how it regulates SAC signaling. High throughput RNAi applied in *Drosophila* S2 cells uncovered a conserved dynein regulator on kinetochore, named Spindly, whose kinetochore targeting relies on RZZ complex. Depletion of Spindly abolished kinetochore function of dynein and caused the accumulation of SAC protein, leading to cell arrest [Griffis et al 2007]. In human cell culture, a strong interaction between Spindly and ROD/ZW10 has been confirmed by co-IP experiment and subsequent data further demonstrated that farnesylation sites in C-terminal region of Spindly are critical for RZZ-mediated Spindly localization on kinetochores but these farnesylation sites are dispensable for RZZ localization on kinetochore, which suggests an RZZ-

Spindly-Dynein axis functioning in SAC silencing [Barisic et al 2010; Moudgil et al 2015]. The role of RZZ complex in conduction of SAC signaling have been elucidated in two genetic studies with depletion of ROD and ZW10 in three different organisms - *Drosophila*, *Xenopus* and human, from which the authors reached a consensus that ROD and ZW10 are required for the recruitment of MAD1-MAD2 complex on unattached kinetochores to execute checkpoint function [Buffin et al 2005; Kops et al 2005]. Subsequently, reciprocal co-IP confirmed a direct interaction between ROD and MAD1 in *Drosophila* embryo[Défachelles et al 2015]. Recently, one study in *C. elegans* pointed out that the kinetochore accumulation of RZZ depends on the N-terminal of KNL1, a constitutive kinetochore component. Moreover, RZZ complex together with BUB1 promotes the recruitment of MAD1-MAD2 on kinetochores in *C. elegans* and human. However, in cultured *Drosophila* S2 cells, KNL ortholog SPC105R is not required for the kinetochore localization of RZZ complex. Interestingly, one study in *Drosophila* oocytes showed that the kinetochore localization of ROD was abolished in the knockdown of SPC105R, this result implies that the localization of RZZ complex on kinetochores might be different between mitosis and meiosis. In addition, multiple lines of evidence by biochemical analysis reveals that the loading of RZZ complex on *Drosophila* kinetochore depends on the interaction between ZW10 and centromeric protein CAL1 [Caldas et al 2015; Radford et al 2015; Rodriguez-Rodriguez et al 2018; Pauleau et al 2019; Zhang et al 2019].

Molecular structure of RZZ complex and its assembly in subcellular compartments

The remaining questions are how the RZZ complex is assembled and whether the three RZZ components (ROD, ZW10 and ZWILCH) always form a complex in a temporospatial manner. Previous studies by using gel extrusion chromatography showed the purified RZZ complex with the mass of 800 kDa [Williams et al 2003]. Considering the molecular weight of individual constituents (ROD: 240kDa, ZW10: 85kDa and ZWILCH: 75kDa), the overall mass of RZZ is exactly equal to double value of RZZ molecular weight, implicating a dimerized assembly of RZZ in vivo. Subsequently, recombinant reconstitution of human RZZ subunits co-expressed in insect cells shed light on the fundamental assembly of RZZ complex and the presence of noncrystallograhic two-fold axis and crystallographic three-fold axis implied the two RZZ complex in asymmetric units [Altenfeld et al 2015]. However, the structure of RZZ complex has been elusive until applying the combination of single-particle cryo-EM and structure modeling [Mosalaganti et al 2017]. In this study, advanced microscopy and structural modeling revealed the 3D structure of RZZ complex at the resolution of 10.4 Å and confirmed that two copies of each subunit build up the entire RZZ complex. In detail, two anti-parallel ROD proteins establish the scaffold and span the entire length of the complex with β-propeller at opposite ends. ZWILCH binds to ROD β-propeller regions at the two ends, while ZW10 is positioned in the mild zone on each copy of ROD. In terms of temporospatial distribution, some evidence supports the idea that the three RZZ subunits may work

as individual to implement their responsibilities differently than SAC.

In fly and human culture cells, it was reported that a small fraction of ZW10, but not ROD, binds on the central spindle and midbody, suggesting a role of ZW10 in cytokinesis. On the contrary, ROD, but not ZW10, can linger at the spindle poles in HeLa cells [Scaërou et al 2001; Williams et al 1996]. In mammals, ZW10, not only form the RZZ complex, is also a component of the NZR complex together with RINT1 and NAG, which is essential for the vesicle trafficking from ER to Golgi. In *Drosophila* spermatogenesis, the three RZZ subunits show distinct subcellular localization and functions on different organelles. ROD is enriched at the Golgi stack and the acroblast, but, except for these two places, ZW10 can be found at the ER and ZWILCH never bind any membrane structure. Therefore, both ROD and ZW10 are required for Golgi integrity and acroblast assembly, but only ZW10 is required for cytokinesis to promote membrane fusion [Wainman et al 2012]. In conclusion, forming RZZ complex is not a prerequisite for ROD, ZW10 and ZWILCH to implement their functions and, more importantly, their roles may vary depending on the subcellular localization and potential partners that they bind to.

REFERENCES

Abrieu, A., Magnaghi-Jaulin, L., Kahana, J. A., Peter, M., Castro, A., Vigneron, S., and Labbé, J. C. et al. (2001). Mps1 is a kinetochore-associated kinase essential for the vertebrate mitotic checkpoint. *Cell*, *106*, 83-93.

Aguilera, A., and Gómez-González, B. (2008). Genome instability: a mechanistic view of its causes and consequences. *Nature Reviews Genetics*, *9*, 204-217.

Altenfeld, A., Wohlgemuth, S., Wehenkel, A., Vetter, I. R., and Musacchio, A. (2015). Complex assembly, crystallization and preliminary X-ray crystallographic analysis of the human Rod–Zwilch–ZW10 (RZZ) complex. *Acta Crystallographica Section F: Structural Biology Communications*, *71*, 438-442.

Anderson, D. E., Losada, A., Erickson, H. P., and Hirano, T. (2002). Condensin and cohesin display different arm conformations with characteristic hinge angles. *The Journal of Cell Biology*, *156*, 419-424.

Barisic, M., Sohm, B., Mikolcevic, P., Wandke, C., Rauch, V., Ringer, T., and Geley, S. et al. (2010). Spindly/CCDC99 is required for efficient chromosome congression and mitotic checkpoint regulation. *Molecular Biology of the Cell*, *21*, 1968-1981.

Barnum, K. J., and O'Connell, M. J. (2014). Cell cycle regulation by checkpoints. In *Cell Cycle Control*, pp. 29-40. Humana Press, New York, NY.

Basto, R., Scaerou, F., Mische, S., Wojcik, E., Lefebvre, C., Gomes, R., and Karess, R. et al. (2004). In vivo dynamics of the rough deal checkpoint protein during Drosophila mitosis. *Current Biology*, *14*, 56-61.

Basu, J., Bousbaa, H., Logarinho, E., Li, Z., Williams, B. C., Lopes, C., and Goldberg, M. L. et al. (1999). Mutations in the essential spindle checkpoint gene bub1 cause chromosome missegregation and fail to block apoptosis in Drosophila. *The Journal of Cell Biology*, *146*, 13-28.

Bernard, P., Maure, J. F., and Javerzat, J. P. (2001). Fission yeast Bub1 is essential in setting up the meiotic pattern of chromosome segregation. *Nature Cell Biology*, *3*, 522-526.

Bickel, S. E., Moore, D. P., Lai, C., and Orr-Weaver, T. L. (1998). Genetic interactions between mei-S332 and ord in the control of sister-chromatid cohesion. *Genetics*, *150*, 1467-1476.

Biggins, S. (2013). The composition, functions, and regulation of the budding yeast kinetochore. *Genetics*, *194*, 817-846.

Blagosklonny, M. V., and Pardee, A. B. (2002). The restriction point of the cell cycle. *Cell Cycle*, *1*, 102-109.

Blattner, A. C., Chaurasia, S., McKee, B. D., and Lehner, C. F. (2016). Separase is required for homolog and sister disjunction during Drosophila melanogaster male meiosis, but not for biorientation of sister centromeres. *PLoS Genetics*, *12*, e1005996.

Bolcun-Filas, E., and Handel, M. A. (2018). Meiosis: the chromosomal foundation of reproduction. *Biology of Reproduction*, *99*, 112-126.

Borja, L. B., Soubigou, F., Taylor, S. J., Bringas, C. F., Budrewicz, J., Lara-Gonzalez, P., and Pelisch, F. et al. (2020). BUB-1 targets PP2A: B56 to regulate chromosome congression during meiosis I in C. elegans oocytes. *Elife*, *9*, e65307.

Brues, A. M., and Cohen, A. (1936). Effects of colchicine and related substances on

cell division. *Biochemical Journal*, *30*, 1363.
Brues, A. M., and Jackson, E. B. (1937). Nuclear abnormalities resulting from inhibition of mitosis by colchicine and other substances. *The American Journal of Cancer*, *30*, 504-511.
Buffin, E., Lefebvre, C., Huang, J., Gagou, M. E., and Karess, R. E. (2005). Recruitment of Mad2 to the kinetochore requires the Rod/Zw10 complex. *Current Biology*, *15*, 856-861.
Buffin, E., Emre, D., and Karess, R. E. (2007). Flies without a spindle checkpoint. *Nature cell biology*, *9*, 565-572.
Cahill, D. P., Da Costa, L. T., Carson-Walter, E. B., Kinzler, K. W., Vogelstein, B., and Lengauer, C. (1999). Characterization of MAD2B and other mitotic spindle checkpoint genes. *Genomics*, *58*, 181-187.
Caldas, G. V., Lynch, T. R., Anderson, R., Afreen, S., Varma, D., and DeLuca, J. G. (2015). The RZZ complex requires the N-terminus of KNL1 to mediate optimal Mad1 kinetochore localization in human cells. *Open Biology*, *5*, 150160.
Chao, W. C., Kulkarni, K., Zhang, Z., Kong, E. H., and Barford, D. (2012). Structure of the mitotic checkpoint complex. *Nature*, *484*, 208-213.
Charvin, G., Oikonomou, C., Siggia, E. D., and Cross, F. R. (2010). Origin of irreversibility of cell cycle start in budding yeast. *PLoS Biology*, *8*, e1000284.
Chaurasia, S., and Lehner, C. F. (2018). Dynamics and control of sister kinetochore behavior during the meiotic divisions in Drosophila spermatocytes. *PLoS genetics*, *14*, e1007372.
Chen, R. H., Shevchenko, A., Mann, M., and Murray, A. W. (1998). Spindle checkpoint protein Xmad1 recruits Xmad2 to unattached kinetochores. *The Journal of Cell Biology*, *143*, 283-295.
Cheslock, P. S., Kemp, B. J., Boumil, R. M., and Dawson, D. S. (2005). The roles of MAD1, MAD2 and MAD3 in meiotic progression and the segregation of nonexchange chromosomes. *Nature Genetics*, *37*, 756-760.
Compton, D. A. (2007). Chromosome orientation. *The Journal of Cell Biology*, *179*, 179-181.
Corbett, K. D., Yip, C. K., Ee, L. S., Walz, T., Amon, A., and Harrison, S. C. (2010). The monopolin complex crosslinks kinetochore components to regulate chromosome-microtubule attachments. *Cell*, *142*, 556-567.
Corbett, K. D., and Harrison, S. C. (2012). Molecular architecture of the yeast monopolin complex. *Cell Reports*, *1*, 583-589.
Dai, W., Wang, Q., Liu, T., Swamy, M., Fang, Y., Xie, S., and Rao, C. V. et al. (2004). Slippage of mitotic arrest and enhanced tumor development in mice with BubR1 haploinsufficiency. *Cancer Research*, *64*, 440-445.
Défachelles, L., Raich, N., Terracol, R., Baudin, X., Williams, B., Goldberg, M., and Karess, R. E. (2015). RZZ and Mad1 dynamics in Drosophila mitosis. *Chromosome Research*, *23*, 333-342.
DiNardo, S., Voelkel, K., and Sternglanz, R. (1984). DNA topoisomerase II mutant of Saccharomyces cerevisiae: topoisomerase II is required for segregation of daughter molecules at the termination of DNA replication. *Proceedings of the National Academy of Sciences*, *81*, 2616-2620.
Ditchfield, C., Johnson, V. L., Tighe, A., Ellston, R., Haworth, C., Johnson, T., and Taylor, S. S. et al. (2003). Aurora B couples chromosome alignment with anaphase by targeting BubR1, Mad2, and Cenp-E to kinetochores. *The Journal of Cell Biology*, *161*, 267-280.

Dobles, M., Liberal, V., Scott, M. L., Benezra, R., and Sorger, P. K. (2000). Chromosome missegregation and apoptosis in mice lacking the mitotic checkpoint protein Mad2. *Cell*, *101*, 635-645.

Espeut, J., Cheerambathur, D. K., Krenning, L., Oegema, K., and Desai, A. (2012). Microtubule binding by KNL-1 contributes to spindle checkpoint silencing at the kinetochore. The *Journal of Cell Biology*, *196*, 469-482.

Fang, G. (2002). Checkpoint protein BubR1 acts synergistically with Mad2 to inhibit anaphase-promoting complex. *Molecular Biology of the Cell*, *13*, 755-766.

Fraschini, R., Beretta, A., Sironi, L., Musacchio, A., Lucchini, G., and Piatti, S. (2001). Bub3 interaction with Mad2, Mad3 and Cdc20 is mediated by WD40 repeats and does not require intact kinetochores. *The EMBO Journal*, *20*, 6648-6659.

Galander, S., and Marston, A. L. (2020). Meiosis I kinase regulators: conserved orchestrators of reductional chromosome segregation. *BioEssays*, *42*, 2000018.

Goldstein, L. S. (1981). Kinetochore structure and its role in chromosome orientation during the first meiotic division in male D. melanogaster. *Cell*, *25*, 591-602.

Griffis, E. R., Stuurman, N., and Vale, R. D. (2007). Spindly, a novel protein essential for silencing the spindle assembly checkpoint, recruits dynein to the kinetochore. *The Journal of Cell Biology*, *177*, 1005-1015.

Gruber, S., Haering, C. H., and Nasmyth, K. (2003). Chromosomal cohesin forms a ring. *Cell*, *112*, 765-777.

Gruber, S., Arumugam, P., Katou, Y., Kuglitsch, D., Helmhart, W., Shirahige, K., and Nasmyth, K. (2006). Evidence that loading of cohesin onto chromosomes involves opening of its SMC hinge. *Cell*, *127*, 523-537.

Hached, K., Xie, S. Z., Buffin, E., Cladière, D., Rachez, C., Sacras, M., and Wassmann, K. et al. (2011). Mps1 at kinetochores is essential for female mouse meiosis I. *Development*, *138*, 2261-2271.

Haering, C. H., Löwe, J., Hochwagen, A., and Nasmyth, K. (2002). Molecular architecture of SMC proteins and the yeast cohesin complex. *Molecular Cell*, *9*, 773-788.

Hardwick, K. G., Weiss, E., Luca, F. C., Winey, M., and Murray, A. W. (1996). Activation of the budding yeast spindle assembly checkpoint without mitotic spindle disruption. *Science*, *273*, 953-956.

Hauf, S., Cole, R. W., LaTerra, S., Zimmer, C., Schnapp, G., Walter, R., and Peters, J. M. et al. (2003). The small molecule Hesperadin reveals a role for Aurora B in correcting kinetochore–microtubule attachment and in maintaining the spindle assembly checkpoint. *The Journal of Cell Biology*, *161*, 281-294.

Hauf, S., Biswas, A., Langegger, M., Kawashima, S. A., Tsukahara, T., and Watanabe, Y. (2007). Aurora controls sister kinetochore mono-orientation and homolog bi-orientation in meiosis-I. *The EMBO Journal*, *26*, 4475-4486.

Heidmann, D., Horn, S., Heidmann, S., Schleiffer, A., Nasmyth, K., and Lehner, C. F. (2004). The Drosophila meiotic kleisin C (2) M functions before the meiotic divisions. *Chromosoma*, *113*, 177-187.

Homer, H. A., McDougall, A., Levasseur, M., Yallop, K., Murdoch, A. P., and Herbert, M. (2005). Mad2 prevents aneuploidy and premature proteolysis of cyclin B and securin during meiosis I in mouse oocytes. *Genes & Development*, *19*, 202-207.

Hoyt, M. A., Totis, L., and Roberts, B. T. (1991). S. cerevisiae genes required for cell cycle arrest in response to loss of microtubule function. *Cell*, *66*, 507-517.

Hwang, L. H., Lau, L. F., Smith, D. L., Mistrot, C. A., Hardwick, K. G., Hwang, E. S., and Murray, A. W. et al. (1998). Budding yeast Cdc20: a target of the spindle checkpoint. *Science*, *279*, 1041-1044.

Ioannou, D., Fortun, J., and Tempest, H. (2018). Meiotic nondisjunction and sperm aneuploidy in humans. *Reproduction*, *1*.

Jessberger, R. (2012). Age‐related aneuploidy through cohesion exhaustion: 'Exploring aneuploidy: the significance of chromosomal imbalance'review series. *EMBO reports*, *13*(6), 539-546.

Kaitna, S., Pasierbek, P., Jantsch, M., Loidl, J., and Glotzer, M. (2002). The aurora B kinase AIR-2 regulates kinetochores during mitosis and is required for separation of homologous chromosomes during meiosis. *Current Biology*, *12*, 798-812.

Kallio, M. J., McCleland, M. L., Stukenberg, P. T., and Gorbsky, G. J. (2002). Inhibition of aurora B kinase blocks chromosome segregation, overrides the spindle checkpoint, and perturbs microtubule dynamics in mitosis. *Current Biology*, *12*, 900-905.

Karess, R. E., and Glover, D. M. (1989). rough deal: a gene required for proper mitotic segregation in Drosophila. *The Journal of cell biology*, *109*, 2951-2961.

Kastan, M. B., and Bartek, J. (2004). Cell-cycle checkpoints and cancer. *Nature*, *432*, 316-323.

Kawashima, S. A., Yamagishi, Y., Honda, T., Ishiguro, K. I., and Watanabe, Y. (2010). Phosphorylation of H2A by Bub1 prevents chromosomal instability through localizing shugoshin. *Science*, *327*, 172-177.

Kiburz, B. M., Reynolds, D. B., Megee, P. C., Marston, A. L., Lee, B. H., Lee, T. I., and Amon, A. et al. (2005). The core centromere and Sgo1 establish a 50-kb cohesin-protected domain around centromeres during meiosis I. *Genes and Development*, *19*, 3017-3030.

Kim, J., Ishiguro, K. I., Nambu, A., Akiyoshi, B., Yokobayashi, S., Kagami, A., and Watanabe, Y. (2015). Meikin is a conserved regulator of meiosis-I-specific kinetochore function. *Nature*, *517*, 466-471.

Kim, S. H., Lin, D. P., Matsumoto, S., Kitazono, A., and Matsumoto, T. (1998). Fission yeast Slp1: an effector of the Mad2-dependent spindle checkpoint. *Science*, *279*, 1045-1047.

Kitajima, T. S., Sakuno, T., Ishiguro, K. I., Iemura, S. I., Natsume, T., Kawashima, S. A., and Watanabe, Y. (2006). Shugoshin collaborates with protein phosphatase 2A to protect cohesin. *Nature*, *441*, 46-52.

Kleckner, N. (1996). Meiosis: how could it work?. *Proceedings of the National Academy of Sciences*, *93*, 8167-8174.

Kops, G. J., Kim, Y., Weaver, B. A., Mao, Y., McLeod, I., Yates III, J. R., and Cleveland, D. W. et al. (2005). ZW10 links mitotic checkpoint signaling to the structural kinetochore. *The Journal of Cell Biology*, *169*, 49-60.

Kops, G. J., Snel, B., and Tromer, E. C. (2020). Evolutionary dynamics of the spindle assembly checkpoint in eukaryotes. *Current Biology*, *30*, R589-R602.

Koshland, D., and Hartwell, L. H. (1987). The structure of sister minichromosome DNA before anaphase in Saccharomyces cerevisiae. *Science*, *238*, 1713-1716.

Krishnan, B., Thomas, S. E., Yan, R., Yamada, H., Zhulin, I. B., and McKee, B. D.

(2014). Sisters unbound is required for meiotic centromeric cohesion in Drosophila melanogaster. *Genetics*, *198*, 947-965.

Kudo, N. R., Wassmann, K., Anger, M., Schuh, M., Wirth, K. G., Xu, H., and Nasmyth, K. et al. (2006). Resolution of chiasmata in oocytes requires separase-mediated proteolysis. *Cell*, *126*, 135-146.

Lampson, M. A., Renduchitala, K., Khodjakov, A., and Kapoor, T. M. (2004). Correcting improper chromosome–spindle attachments during cell division. *Nature Cell Biology*, *6*, 232-237.

Ioannou, D., Fortun, J., and Tempest, H. (2018). Meiotic nondisjunction and sperm aneuploidy in humans. *Reproduction*, *1*.

Logarinho, E., Bousbaa, H., Dias, J. M., Lopes, C., Amorim, I., Antunes-Martins, A., and Sunkel, C. E. (2004). Different spindle checkpoint proteins monitor microtubule attachment and tension at kinetochores in Drosophila cells. *The Journal of Cell Science*, *117*, 1757-1771.

London, N., Ceto, S., Ranish, J. A., and Biggins, S. (2012). Phosphoregulation of Spc105 by Mps1 and PP1 regulates Bub1 localization to kinetochores. *Current Biology*, *22*, 900-906.

Luo, X., Tang, Z., Rizo, J., and Yu, H. (2002). The Mad2 spindle checkpoint protein undergoes similar major conformational changes upon binding to either Mad1 or Cdc20. *Molecular Cell*, *9*, 59-71.

Malmanche, N., Maia, A., and Sunkel, C. E. (2006). The spindle assembly checkpoint: preventing chromosome mis-segregation during mitosis and meiosis. *FEBS Letters*, *580*, 2888-2895.

Malmanche, N., Owen, S., Gegick, S., Steffensen, S., Tomkiel, J. E., and Sunkel, C. E. (2007). Drosophila BubR1 is essential for meiotic sister-chromatid cohesion and maintenance of synaptonemal complex. *Current Biology*, *17*, 1489-1497.

Malureanu, L. A., Jeganathan, K. B., Hamada, M., Wasilewski, L., Davenport, J., and van Deursen, J. M. (2009). BubR1 N terminus acts as a soluble inhibitor of cyclin B degradation by APC/CCdc20 in interphase. *Developmental Cell*, *16*, 118-131.

Manheim, E. A., and McKim, K. S. (2003). The synaptonemal complex component C (2) M regulates meiotic crossing over in Drosophila. *Current Biology*, *13*, 276-285.

Masumoto, H., Masukata, H., Muro, Y., Nozaki, N., and Okazaki, T. (1989). A human centromere antigen (CENP-B) interacts with a short specific sequence in alphoid DNA, a human centromeric satellite. *The Journal of Cell Biology*, *109*, 1963-1973.

McKee, B. D., and Karpen, G. H. (1990). Drosophila ribosomal RNA genes function as an XY pairing site during male meiosis. *Cell*, *61*, 61-72.

McKee, B. D., Habera, L., and Vrana, J. A. (1992). Evidence that intergenic spacer repeats of Drosophila melanogaster rRNA genes function as XY pairing sites in male meiosis, and a general model for achiasmatic pairing. *Genetics*, *132*, 529-544.

McKee, B. D. (1996). The license to pair: Identification of meiotic pairing sites in Drosophila. *Chromosoma*, *105*, 135.

Meadows, J. C., Shepperd, L. A., Vanoosthuyse, V., Lancaster, T. C., Sochaj, A. M., Buttrick, G. J., and Millar, J. B. et al. (2011). Spindle checkpoint silencing requires association of PP1 to both Spc7 and kinesin-8 motors. *Developmental Cell*, *20*, 739-750.

Meyer, R. E., Kim, S., Obeso, D., Straight, P. D., Winey, M., and Dawson, D. S.

(2013). Mps1 and Ipl1/Aurora B act sequentially to correctly orient chromosomes on the meiotic spindle of budding yeast. *Science*, *339*, 1071-1074.

Michaelis, C., Ciosk, R., and Nasmyth, K. (1997). Cohesins: chromosomal proteins that prevent premature separation of sister chromatids. *Cell*, *91*, 35-45.

Michel, L. S., Liberal, V., Chatterjee, A., Kirchwegger, R., Pasche, B., Gerald, W., and Benezra, R. et al. (2001). MAD2 haplo-insufficiency causes premature anaphase and chromosome instability in mammalian cells. *Nature*, *409*, 355-359.

Millband, D. N., and Hardwick, K. G. (2002). Fission yeast Mad3p is required for Mad2p to inhibit the anaphase-promoting complex and localizes to kinetochores in a Bub1p-, Bub3p-, and Mph1p-dependent manner. *Molecular and Cellular Biology*, *22*, 2728.

Miyazaki, S., Kim, J., Yamagishi, Y., Ishiguro, T., Okada, Y., Tanno, Y., and Watanabe, Y. et al. (2017). Meikin-associated polo-like kinase specifies Bub1 distribution in meiosis I. *Genes to Cells*, *22*, 552-567.

Monje-Casas, F., Prabhu, V. R., Lee, B. H., Boselli, M., and Amon, A. (2007). Kinetochore orientation during meiosis is controlled by Aurora B and the monopolin complex. *Cell*, *128*, 477-490.

Mosalaganti, S., Keller, J., Altenfeld, A., Winzker, M., Rombaut, P., Saur, M., and Musacchio, A. (2017). Structure of the RZZ complex and molecular basis of its interaction with Spindly. *The Journal of Cell Biology*, *216*, 961-981.

Moudgil, D. K., Westcott, N., Famulski, J. K., Patel, K., Macdonald, D., Hang, H., and Chan, G. K. (2015). A novel role of farnesylation in targeting a mitotic checkpoint protein, human Spindly, to kinetochoresFarnesylation of the kinetochore protein hSpindly. *The Journal of Cell Biology*, *208*, 881-896

Murata-Hori, M., Tatsuka, M., and Wang, Y. L. (2002). Probing the dynamics and functions of aurora B kinase in living cells during mitosis and cytokinesis. *Molecular Biology of the Cell*, *13*, 1099-1108.

Musacchio, A., and Salmon, E. D. (2007). The spindle-assembly checkpoint in space and time. *Nature Reviews Molecular Cell Biology*, *8*, 379-393.

Myrie, K. A., Percy, M. J., Azim, J. N., Neeley, C. K., and Petty, E. M. (2000). Mutation and expression analysis of human BUB1 and BUB1B in aneuploid breast cancer cell lines. *Cancer Letters*, *152*, 193-199.

Nagaoka, S. I., Hassold, T. J., and Hunt, P. A. (2012). Human aneuploidy: mechanisms and new insights into an age-old problem. *Nature Reviews Genetics*, *13*, 493-504.

Niault, T., Hached, K., Sotillo, R., Sorger, P. K., Maro, B., Benezra, R., and Wassmann, K. (2007). Changing Mad2 levels affects chromosome segregation and spindle assembly checkpoint control in female mouse meiosis I. *PloS one*, *2*, e1165.

Nicklas, R. B., and Arana, P. (1992). Evolution and the meaning of metaphase. *Journal of Cell Science*, *102*, 681-690.

Nogueira, C., Kashevsky, H., Pinto, B., Clarke, A., and Orr-Weaver, T. L. (2014). Regulation of centromere localization of the Drosophila Shugoshin MEI-S332 and sister-chromatid cohesion in meiosis. *G3: Genes, Genomes, Genetics*, *4*, 1849-1858.

Ohkura, H. (2015). Meiosis: an overview of key differences from mitosis. *Cold Spring*

Harbor Perspectives in Biology, *7*, a015859.
Oromendia, A. B., and Amon, A. (2014). Aneuploidy: implications for protein homeostasis and disease. *Disease models and mechanisms*, *7*, 15-20.
Page, S. L., and Hawley, R. S. (2003). Chromosome choreography: the meiotic ballet. *Science*, *301*, 785-789.
Page, S. L., and Hawley, R. S. (2004). The genetics and molecular biology of the synaptonemal complex. *Annual Review of Cell and Developmental Biology*, *20*, 525-558.
Palmer, D. K., O'Day, K., Wener, M. H., Andrews, B. S., and Margolis, R. L. (1987). A 17-kD centromere protein (CENP-A) copurifies with nucleosome core particles and with histones. *The Journal of Cell Biology*, *104*, 805-815.
Pardee, A. B. (1974). A restriction point for control of normal animal cell proliferation. *Proceedings of the National Academy of Sciences*, *71*, 1286-1290.
Pauleau, A. L., Bergner, A., Kajtez, J., and Erhardt, S. (2019). The checkpoint protein Zw10 connects CAL1-dependent CENP-A centromeric loading and mitosis duration in Drosophila cells. *PLoS genetics*, *15*, e1008380.
Pellestor, F., Andréo, B., Anahory, T., and Hamamah, S. (2006). The occurrence of aneuploidy in human: lessons from the cytogenetic studies of human oocytes. *European Journal of Medical Genetics*, *49*, 103-116.
Peter, M., Castro, A., Lorca, T., Le Peuch, C., Magnaghi-Jaulin, L., Dorée, M., and Labbé, J. C. (2001). The APC is dispensable for first meiotic anaphase in Xenopus oocytes. *Nature Cell Biology*, *3*, 83-87.
Peters, J. M. (2006). The anaphase promoting complex/cyclosome: a machine designed to destroy. *Nature Reviews Molecular Cell Biology*, *7*, 644-656.
Peters, J. M., Tedeschi, A., and Schmitz, J. (2008). The cohesin complex and its roles in chromosome biology. *Genes & development*, *22*(22), 3089-3114.
Petronczki, M., Siomos, M. F., and Nasmyth, K. (2003). Un menage a quatre: the molecular biology of chromosome segregation in meiosis. *Cell*, *112*, 423-440.
Pinto, B. S., and Orr-Weaver, T. L. (2017). Drosophila protein phosphatases 2A B′ Wdb and Wrd regulate meiotic centromere localization and function of the MEI-S332 Shugoshin. *Proceedings of the National Academy of Sciences*, *114*, 12988-12993.
Poddar, A., Stukenberg, P. T., and Burke, D. J. (2005). Two complexes of spindle checkpoint proteins containing Cdc20 and Mad2 assemble during mitosis independently of the kinetochore in Saccharomyces cerevisiae. *Eukaryotic Cell*, *4*, 867.
Rabitsch, K. P., Petronczki, M., Javerzat, J. P., Genier, S., Chwalla, B., Schleiffer, A., and Nasmyth, K. et al. (2003). Kinetochore recruitment of two nucleolar proteins is required for homolog segregation in meiosis I. *Developmental Cell*, *4*, 535-548.
Radford, S. J., Hoang, T. L., Głuszek, A. A., Ohkura, H., and McKim, K. S. (2015). Lateral and end-on kinetochore attachments are coordinated to achieve bi-orientation in Drosophila oocytes. *PLoS genetics*, *11*, e1005605.
Rebollo, E., and González, C. (2000). Visualizing the spindle checkpoint in Drosophila spermatocytes. *EMBO Reports*, *1*, 65-70.
Riedel, C. G., Katis, V. L., Katou, Y., Mori, S., Itoh, T., Helmhart, W., and Nasmyth, K. et al. (2006). Protein phosphatase 2A protects centromeric sister chromatid cohesion during meiosis I. *Nature*, *441*, 53-61.
Rieder, C. L., Schultz, A., Cole, R., and Sluder, G. (1994). Anaphase onset in

vertebrate somatic cells is controlled by a checkpoint that monitors sister kinetochore attachment to the spindle. *Journal of Cell Biology*, *127*, 1301-1310.

Rieder, C. L., Cole, R. W., Khodjakov, A., and Sluder, G. (1995). The checkpoint delaying anaphase in response to chromosome monoorientation is mediated by an inhibitory signal produced by unattached kinetochores. *The Journal of Cell Biology*, *130*, 941-948.

Rivera, T., and Losada, A. (2006). Shugoshin and PP2A, shared duties at the centromere. *Bioessays*, *28*, 775-779.

Rodriguez-Rodriguez, J. A., Lewis, C., McKinley, K. L., Sikirzhytski, V., Corona, J., Maciejowski, J., and Jallepalli, P. V. et al. (2018). Distinct roles of RZZ and Bub1-KNL1 in mitotic checkpoint signaling and kinetochore expansion. *Current Biology*, *28*, 3422-3429.

Rosenberg, J. S., Cross, F. R., and Funabiki, H. (2011). KNL1/Spc105 recruits PP1 to silence the spindle assembly checkpoint. *Current Biology*, *21*, 942-947.

Sakuno, T., Tada, K., and Watanabe, Y. (2009). Kinetochore geometry defined by cohesion within the centromere. *Nature*, *458*, 852-858.

Sakuno, T., Tanaka, K., Hauf, S., and Watanabe, Y. (2011). Repositioning of aurora B promoted by chiasmata ensures sister chromatid mono-orientation in meiosis I. *Developmental Cell*, *21*, 534-545.

Sarangapani, K. K., Duro, E., Deng, Y., de Lima Alves, F., Ye, Q., Opoku, K. N., and Asbury, C. L. et al. (2014). Sister kinetochores are mechanically fused during meiosis I in yeast. *Science*, *346*, 248-251.

Scaërou, F., Aguilera, I., Saunders, R., Kane, N., Blottière, L., and Karess, R. (1999). The rough deal protein is a new kinetochore component required for accurate chromosome segregation in Drosophila. *Journal of Cell Science*, *112*, 3757-3768.

Scaërou, F., Starr, D. A., Piano, F., Papoulas, O., Karess, R. E., and Goldberg, M. L. (2001). The ZW10 and Rough Deal checkpoint proteins function together in a large, evolutionarily conserved complex targeted to the kinetochore. *Journal of Cell Science*, *114*, 3103-3114.

Scannevin, R. H., Wang, K., Jow, F., Megules, J., Kopsco, D. C., Edris, W., and Rhodes, K. J. et al. (2004). Two N-terminal domains of Kv4 K+ channels regulate binding to and modulation by KChIP1. *Neuron*, *41*, 587-598.

Schafer, K. A. (1998). The cell cycle: a review. *Veterinary Pathology*, *35*, 461-478.

Severson, A. F., Ling, L., van Zuylen, V., and Meyer, B. J. (2009). The axial element protein HTP-3 promotes cohesin loading and meiotic axis assembly in C. elegans to implement the meiotic program of chromosome segregation. *Genes and Development*, *23*, 1763-1778.

Sczaniecka, M., Feoktistova, A., May, K. M., Chen, J. S., Blyth, J., Gould, K. L., and Hardwick, K. G. (2008). The spindle checkpoint functions of Mad3 and Mad2 depend on a Mad3 KEN box-mediated interaction with Cdc20-anaphase-promoting complex (APC/C). *Journal of Biological Chemistry*, *283*, 23039-23047.

Shannon, K. B., Canman, J. C., and Salmon, E. D. (2002). Mad2 and BubR1 function in a single checkpoint pathway that responds to a loss of tension. *Molecular Biology of the Cell*, *13*, 3706-3719.

Shao, H., Li, R., Ma, C., Chen, E., and Liu, X. J. (2013). Xenopus oocyte meiosis lacks spindle assembly checkpoint control. *The Journal of Cell Biology*, *201*, 191-200.

Shepperd, L. A., Meadows, J. C., Sochaj, A. M., Lancaster, T. C., Zou, J., Buttrick, G. J., and Millar, J. B. et al. (2012). Phosphodependent recruitment of Bub1 and Bub3 to Spc7/KNL1 by Mph1 kinase maintains the spindle checkpoint. *Current Biology*, *22*, 891-899.

Shonn, M. A., McCarroll, R., and Murray, A. W. (2000). Requirement of the spindle checkpoint for proper chromosome segregation in budding yeast meiosis. *Science*, *289*, 300-303.

Shonn, M. A., Murray, A. L., and Murray, A. W. (2003). Spindle checkpoint component Mad2 contributes to biorientation of homologous chromosomes. *Current Biology*, *13*, 1979-1984.

Silva, P. M., Reis, R. M., Bolanos-Garcia, V. M., Florindo, C., Tavares, Á. A., and Bousbaa, H. (2014). Dynein-dependent transport of spindle assembly checkpoint proteins off kinetochores toward spindle poles. *FEBS Letters*, *588*, 3265-3273.

Sironi, L., Mapelli, M., Knapp, S., De Antoni, A., Jeang, K. T., and Musacchio, A. (2002). Crystal structure of the tetrameric Mad1–Mad2 core complex: implications of a 'safety belt'binding mechanism for the spindle checkpoint. *The EMBO Journal*, *21*, 2496-2506.

Spencer, F., and Hieter, P. H. I. L. I. P. (1992). Centromere DNA mutations induce a mitotic delay in Saccharomyces cerevisiae. *Proceedings of the National Academy of Sciences*, *89*, 8908-8912.

Starr, D. A., Williams, B. C., Li, Z., Etemad-Moghadam, B., Dawe, R. K., and Goldberg, M. L. (1997). Conservation of the centromere/kinetochore protein ZW10. *The Journal of Cell Biology*, *138*, 1289-1301.

Stein, K. K., Davis, E. S., Hays, T., and Golden, A. (2007). Components of the spindle assembly checkpoint regulate the anaphase-promoting complex during meiosis in Caenorhabditis elegans. *Genetics*, *175*, 107-123.

Strunnikov, A. V., and Jessberger, R. (1999). Structural maintenance of chromosomes (SMC) proteins: conserved molecular properties for multiple biological functions. *European journal of biochemistry*, *263*(1), 6-13.

Sudakin, V., Chan, G. K., and Yen, T. J. (2001). Checkpoint inhibition of the APC/C in HeLa cells is mediated by a complex of BUBR1, BUB3, CDC20, and MAD2. *The Journal of Cell Biology*, *154*, 925-936.

Sundin, O., and Varshavsky, A. (1980). Terminal stages of SV40 DNA replication proceed via multiply intertwined catenated dimers. *Cell*, *21*, 103-114.

Taieb, F. E., Gross, S. D., Lewellyn, A. L., and Maller, J. L. (2001). Activation of the anaphase-promoting complex and degradation of cyclin B is not required for progression from Meiosis I to II in Xenopus oocytes. *Current Biology*, *11*, 508-513.

Tanaka, T. U., Rachidi, N., Janke, C., Pereira, G., Galova, M., Schiebel, E., and Nasmyth, K. et al. (2002). Evidence that the Ipl1-Sli15 (Aurora kinase-INCENP) complex promotes chromosome bi-orientation by altering kinetochore-spindle pole connections. *Cell*, *108*, 317-329.

Tanaka, T. U. (2005). Chromosome bi-orientation on the mitotic spindle. *Philosophical Transactions of the Royal Society B: Biological Sciences*, *360*, 581-589.

Tang, T. T. L., Bickel, S. E., Young, L. M., and Orr-Weaver, T. L. (1998). Maintenance of sister-chromatid cohesion at the centromere by the Drosophila MEI-S332 protein. *Genes and Development*, *12*, 3843-3856.

Tang, Z., Bharadwaj, R., Li, B., and Yu, H. (2001). Mad2-Independent inhibition of

APCCdc20 by the mitotic checkpoint protein BubR1. *Developmental Cell*, *1*, 227-237.

Taylor, S. S., Ha, E., and McKeon, F. (1998). The human homologue of Bub3 is required for kinetochore localization of Bub1 and a Mad3/Bub1-related protein kinase. *The Journal of Cell Biology*, *142*, 1-11.

Thomas, S. E., Soltani-Bejnood, M., Roth, P., Dorn, R., Logsdon Jr, J. M., and McKee, B. D. (2005). Identification of two proteins required for conjunction and regular segregation of achiasmate homologs in Drosophila male meiosis. *Cell*, *123*, 555-568.

Tomkiel, J. E., Wakimoto, B. T., and Briscoe Jr, A. (2001). The teflon gene is required for maintenance of autosomal homolog pairing at meiosis I in male Drosophila melanogaster. *Genetics*, *157*, 273-281.

Tóth, A., Rabitsch, K. P., Gálová, M., Schleiffer, A., Buonomo, S. B., and Nasmyth, K. (2000). Functional genomics identifies monopolin: a kinetochore protein required for segregation of homologs during meiosis I. *Cell*, *103*, 1155-1168.

Touati, S. A., Buffin, E., Cladière, D., Hached, K., Rachez, C., Van Deursen, J. M., and Wassmann, K. (2015). Mouse oocytes depend on BubR1 for proper chromosome segregation but not for prophase I arrest. *Nature Communications*, *6*, 1-13.

Toyoda, Y., and Yanagida, M. (2006). Coordinated requirements of human topo II and cohesin for metaphase centromere alignment under Mad2-dependent spindle checkpoint surveillance. *Molecular Biology of the Cell*, *17*, 2287-2302.

Tsurumi, C., Hoffmann, S., Geley, S., Graeser, R., and Polanski, Z. (2004). The spindle assembly checkpoint is not essential for CSF arrest of mouse oocytes. *The Journal of Cell Biology*, *167*, 1037-1050.

Urban, E., Nagarkar-Jaiswal, S., Lehner, C. F., and Heidmann, S. K. (2014). The cohesin subunit Rad21 is required for synaptonemal complex maintenance, but not sister chromatid cohesion, during Drosophila female meiosis. *PLoS Genetics*, *10*, e1004540.

Wainman, A., Giansanti, M. G., Goldberg, M. L., and Gatti, M. (2012). The Drosophila RZZ complex–roles in membrane trafficking and cytokinesis. *The Journal of Cell Scienc*e, *125*, 4014-4025.

Wang, L. I., Das, A., and McKim, K. S. (2019). Sister centromere fusion during meiosis I depends on maintaining cohesins and destabilizing microtubule attachments. *PLoS Genetics*, *15*, e1008072.

Wang, S., Liu, Y., Shang, Y., Zhai, B., Yang, X., Kleckner, N., and Zhang, L. (2019). Crossover interference, crossover maturation, and human aneuploidy. *BioEssays*, *41*, 1800221.

Wassmann, K., Niault, T., and Maro, B. (2003). Metaphase I arrest upon activation of the Mad2-dependent spindle checkpoint in mouse oocytes. *Current Biology*, *13*, 1596-1608.

Watanabe, Y., and Nurse, P. (1999). Cohesin Rec8 is required for reductional chromosome segregation at meiosis. *Nature*, *400*, 461-464.

Watanabe, Y. (2012). Geometry and force behind kinetochore orientation: lessons from meiosis. *Nature reviews Molecular cell biology*, *13*, 370-382.

Webber, H. A., Howard, L., and Bickel, S. E. (2004). The cohesion protein ORD is

required for homologue bias during meiotic recombination. *The Journal of Cell Biology*, *164*, 819-829.

Weber, J., Kabakci, Z., Chaurasia, S., Brunner, E., and Lehner, C. F. (2020). Chromosome separation during Drosophila male meiosis I requires separase-mediated cleavage of the homolog conjunction protein UNO. *PLoS Genetics*, *16*, e1008928.

Webster, A., and Schuh, M. (2017). Mechanisms of aneuploidy in human eggs. *Trends in Cell Biology*, *27*, 55-68.

Weiss, E., and Winey, M. (1996). The Saccharomyces cerevisiae spindle pole body duplication gene MPS1 is part of a mitotic checkpoint. *The Journal of cell biology*, *132*, 111-123.

Williams, B. C., Karr, T. L., Montgomery, J. M., and Goldberg, M. L. (1992). The Drosophila l (1) zw10 gene product, required for accurate mitotic chromosome segregation, is redistributed at anaphase onset. *The Journal of Cell Biology*, *118*, 759-773.

Williams, B. C., Gatti, M., and Goldberg, M. L. (1996). Bipolar spindle attachments affect redistributions of ZW10, a Drosophila centromere/kinetochore component required for accurate chromosome segregation. *The Journal of Cell Biology*, *134*, 1127-1140.

Williams, B. C., Li, Z., Liu, S., Williams, E. V., Leung, G., Yen, T. J., and Goldberg, M. L. (2003). Zwilch, a new component of the ZW10/ROD complex required for kinetochore functions. *Molecular biology of the cell*, *14*, 1379-1391.

Xia, G., Luo, X., Habu, T., Rizo, J., Matsumoto, T., and Yu, H. (2004). Conformation-specific binding of p31comet antagonizes the function of Mad2 in the spindle checkpoint. *The EMBO journal*, *23*, 3133-3143.

Yamagishi, Y., Yang, C. H., Tanno, Y., and Watanabe, Y. (2012). MPS1/Mph1 phosphorylates the kinetochore protein KNL1/Spc7 to recruit SAC components. *Nature cell biology*, *14*, 746-752.

Yan, R., Thomas, S. E., Tsai, J. H., Yamada, Y., and McKee, B. D. (2010). SOLO: a meiotic protein required for centromere cohesion, coorientation, and SMC1 localization in Drosophila melanogaster. *Journal of Cell Biology*, *188*, 335-349.

Yang, M., Li, B., Tomchick, D. R., Machius, M., Rizo, J., Yu, H., and Luo, X. (2007). p31comet blocks Mad2 activation through structural mimicry. *Cell*, *131*, 744-755.

Zhang, G., Kruse, T., Guasch Boldú, C., Garvanska, D. H., Coscia, F., Mann, M., and Nilsson, J. (2019). Efficient mitotic checkpoint signaling depends on integrated activities of Bub1 and the RZZ complex. *The EMBO journal*, *38*, e100977.

CHAPTER II: Checkpoint Protein Rough Deal Promotes Reductional Segregation by Regulating Mono-orientation and Centromere Cohesion in *Drosophila* male meiosis

This chapter is a modified version of a manuscript for my investigation of the meiotic role of Rough Deal and will be submitted to the Journal of Current Biology (following the format of the journal).

Qiutao He's primary contribution: the investigations of the phenotype of the trans-heterozygous rod mutants, which includes both genetic and cytological studies. Specifically, I examined the nondisjunction rate for all four *Drosophila* chromosomes, detection of chromosome lagging and mis-segregation patterns for sex chromosome and autosome in anaphase I, investigation of homolog conjunction & centromere cohesion, the identified a perturbed sister-chromatid orientation prior to anaphase I onset in *rod* mutants. I have contributed to experiment design, data collection, figure plotting, manuscript writing and revision.

ABSTRACT

Chromosome segregation is mediated by bipolar microtubule (MT)-based spindles to which chromosomes attach via centromeric complexes called kinetochores. In mitosis and meiosis II, the kinetochores of sister chromatids connect to microtubules from opposite spindle poles (bi-orientation), but in meiosis I, sister kinetochores orient to the same pole (mono-orientation) so that homologous sister pairs can bi-orient and homologs can segregate [Hauf and Watanabe 2004; Watanabe 2006]. Hitherto, the mechanism of mono-orientation, however, is still not fully understood. In early prometaphase I (PM I) of *Drosophila* male meiosis, before stable microtubule attachments are achieved, sister kinetochores are visibly fused into dense hemispheric structures that resolve into double-disc structures once stable microtubule attachments form [Goldstein 1981]. Hemisphere structures were proposed to underlie mono-orientation, but the molecular basis for such structures and direct evidence for a role in centromere orientation has been elusive. Here, we report that Rough Deal (ROD), a component of the fibrous corona [Basto et al 2004; Kops and Gassmann 2020], that drives transient kinetochore expansion in early prometaphase, then delocalizes once kinetochores achieve stable microtubule attachments, plays an essential role in sister kinetochore mono-orientation in *Drosophila*. A point mutation in *rod* leads to lagging chromosomes, equational segregation and homolog nondisjunction (NDJ) at meiosis I. We provide evidence that, despite normal pairing of homologs, mutations of ROD disrupt sister kinetochore orientation by metaphase I (M I) and result in the chromosome laggards after

anaphase I (A I) onset. In addition, some sisters lose pericentromeric cohesion due to redistribution of MEI-S332, the *Drosophila* Shugoshin (SGO) homolog, from the inner centromere to peripheral sites on both sister kinetochores, and segregate equationally. In conclusion, we propose that kinetochore remodeling upon the recruitment of ROD is a conserved aspect of a mechanism to enable sister kinetochore fusion and mono-orientation during meiosis.

INTRODUCTION

Meiosis plays a pivotal role in sexual reproduction, reducing the chromosome number by half to produce haploid gametes from diploid precursors. Chromosomes undergo two consecutive segregations following one single round of DNA replication [Marston and Amon 2005; Hochwagen 2008; McKee et al 2012; Orr-Weaver 1995]: a reductional division in which homologous chromosomes pair and segregate, known as meiosis I, followed by an equational division, meiosis II, in which sister chromatids segregate. Errors in meiotic chromosome segregation produce aneuploid progeny and are a major source of infertility, spontaneous abortion and birth defects in humans [Harton and Tempest 2012; MacLennan et al 2015; Potapova and Gorbsky 2017]. Accurate chromosome segregation relies on carefully programmed changes in sister-chromatid cohesion and centromere orientation to enable the disjunction of homologs in meiosis I and sister chromatids in meiosis II.

Proper chromosome segregation in mitosis and both meiotic divisions relies on the cohesion between sister chromatids. Cohesion is established during DNA replication and fully removed at anaphase only once all chromosome pairs have achieved bi-polar orientation, in which the kinetochores of the segregating chromosomes (sister chromatids in mitosis and meiosis II; homologous chromosomes in meiosis I) have formed stable end-on attachments to microtubule bundles from opposite spindle poles. Cohesion, between sister pericentromeric domains in mitosis and meiosis II or between sister chromatid arms distal to sites of crossovers in meiosis I, keeps the segregating chromosomes from separating prematurely and provides

resistance to spindle forces during prometaphase that is essential for the achievement of bipolarity. Cohesion is mediated by conserved cohesin complexes consisting of SMC1, SMC3, the alpha-kleisin SCC1/RAD21 (or its meiosis-specific paralog REC8) and SCC3/SA. Cohesin complexes are large rings that topologically entrap sister chromatids. Release of cohesion at anaphase of mitosis and both meiotic divisions entails cleavage of the alpha-kleisin subunit of cohesin (SCC1/RAD21 or REC8) by Separase. Activation of Separase occurs by Anaphase Promoting Complex/Cyclosome (APC/C)-mediated proteolytic degradation of the Separase inhibitor Securin and is regulated by a conserved checkpoint pathway, known as the Spindle Assembly Checkpoint (SAC). The SAC monitors progress toward spindle bipolarity and generates a diffusible “wait-anaphase” signal as long as one or more chromosomes are not properly attached to the spindle. SAC activation is mediated by the recruitment of multiple proteins including BUB proteins (BUB1, BUB3 and BUBR1), MAD proteins (MAD1 and MAD2) and the RZZ complex (ROD-ZW10-ZWILCH) to unattached or improperly attached kinetochores. The wait-anaphase signal is a complex (Mitotic Checkpoint Complex (MCC)) of BUB3, BUBR1, MAD2 and CDC20, a key activating cofactor of the APC/C [Zhou et al 2002; Musacchio and Salmon 2007; Lara-Gonzalez et al 2012]. The MCC functions to sequester CDC20 and inhibit the APC/C activity as long as one or more chromosomes are improperly attached to the spindle. The establishment of a fully bipolar spindle with all sister kinetochore pairs properly attached to microtubule bundles from opposite poles triggers dynein mediated shedding of SAC proteins from kinetochores along kinetochore microtubules and

dissolution of the MCC [Chan and Yen 2003; Izawa and Pines 2015].

The correct sequence of reductional and equational segregations in meiosis requires stepwise release of cohesion, first from chromosome arms at anaphase I to release the chiasmata that hold homologs together and then in anaphase II in peri-centromeric domains to enable sister chromatids to segregate [Peters et al 2008; Onn et al 2008]. Preservation of peri-centromeric cohesion in meiosis I requires the meiosis-specific cohesin subunit REC8 (the target of Separase cleavage) and centromeric Shugoshin (SGO) proteins which recruit the phosphatase PP2A to dephosphorylate REC8 and protect it from Separase cleavage at anaphase I [Watanabe 2005]. Distinct from other eukaryotes, the *Drosophila* genome appears to lack a REC8 ortholog. Instead, three meiosis-specific proteins (SOLO, ORD and SUNN, also known as SOS) interact with the SMC subunits to establish and maintain sister-chromatid cohesion; dysfunction of any SOS protein causes precocious sister chromatid separation (PSCS) in prophase I and chromosome mis-segregation in both meiosis I and meiosis II [Bickel et al 1996; Yan et al 2010; Krishnan et al 2014]. Besides SOS proteins, the persistence of sister-chromatid cohesion past anaphase I depends on MEI-S332, the *Drosophila* SGO homolog. Mutations in *mei-S332* result in premature removal of SOS cohesin from centromere regions, leading to PSCS beginning in anaphase I (A I) and perturbs sister chromatid segregation in anaphase II (A II) [Kerrebrock et al 1992].

In contrast to equational chromosome segregation in mitosis and meiosis II, in which sister chromatids segregate by attaching, through their centromeric

kinetochores, to microtubule bundles from opposite spindle poles, reductional segregation in meiosis I requires sister chromatids on each homolog to attach to MTs emanating from the same spindle pole (known as mono-orientation or co-orientation) [Hauf and Watanabe 2004; Watanabe 2012]. This enables homologous kinetochores to bi-orient and to segregate to opposite poles at anaphase I. Sometime after the onset of anaphase I and before metaphase II, sister kinetochores re-orient and attach to opposite poles, enabling sister chromatids to segregate at anaphase II. The underlying mechanisms are poorly understood and may differ among eukaryotes. Cytological studies have reported fusion of sister kinetochores in prometaphase I in several organisms, including in *Drosophila*, where prometaphase I kinetochores in spermatocytes are mostly single large hemispheric structures (HS) that occupy one face of the paired sister DNA strands. During later stages of meiosis I, these structures shrink and evolve into flat discs that initially appear as single and elliptical but eventually, by sometime in anaphase I, resolve into side-by-side (SS) double-discs thought to represent individualized sister kinetochores. The HS kinetochore structures are thought to be responsible for mono-orientation but their detailed structure and function remain a mystery. The only well-characterized sister kinetochore linker is the MONOPOLIN complex in budding yeast, which is required for mono-orientation in meiosis I. MONOPOLIN is a dimeric V-shaped complex with identical ends which bind to kinetochore proteins to cross-link sister kinetochores [Corbett and Harrison 2012]. However, MONOPOLIN is not conserved and there are few clues about the identity of kinetochore cross-linkers in other eukaryotes. A recent live-imaging study in

Drosophila spermatocytes showed that sister centromeres undergo transient separations throughout meiosis I, casting doubt on the idea that kinetochore fusion is mediated by rigid mechanical linkers [Chaurasia and Lehner 2018]. An entirely different mechanism involving meiosis I-specific cohesion between sister centromeres (as opposed to peri-centromeres) has been well-documented in *S. pombe* and to a lesser extent in a variety of eukaryotes. This mechanism involves occupancy of core centromeres by REC8 cohesin during meiosis I but not meiosis II and depends on "MOKIR" proteins such as MOAI in *S. pombe* and MEIKIN in mice that function to support centromere cohesion and mono-orientation, at least in part by recruiting Polo-like kinase to meiosis I centromeres [Yokobayashi and Watanabe 2005; Kim et al 2005; Galander and Marston 2020].

The present study grew out of a genetic screen for EMS-induced mutations with defects in chromosome segregation in *Drosophila* male meiosis. One of the recovered mutations ($rod^{Z3\text{-}1641}$) is a point mutation that generates a non-conservative substitution (M1922 to K) in the C-terminus of the conserved SAC protein ROD. Unlike most *rod* alleles, which are late larval-pupal lethal because of defects in mitotic chromosome segregation leading to aneuploidy, $rod^{Z3\text{-}1641}$ is fully viable and fertile and affects mainly meiotic chromosome segregation. This specificity is surprising because RZZ exhibits very similar localization patterns in mitosis and both meiotic divisions: recruitment to kinetochores at the onset of prometaphase and removal by dynein-mediated shedding in late prometaphase and metaphase. ROD has two important roles in SAC signaling, to help activate it by recruiting the MAD1-MAD2 complex to

kinetochores and to help silence it by recruiting dynein. However, SAC function is not required for mitotic segregation or viability in *Drosophila*, so the deleterious effects of null *rod* mutations on mitosis likely result from non-SAC functions of ROD, of which two have been identified, both important for the achievement of spindle bipolarity during prometaphase. One is a remodeling of kinetochore geometry at the onset of prometaphase known as kinetochore expansion in which kinetochores dramatically increase their volume and change from relatively flat structures on the surface of centromeres to much larger hemispheric structures. This modification comes about from the recruitment of a transient outer kinetochore layer known as the fibrous corona which contains multiple microtubule motor proteins that enhance the ability of kinetochores to bind to microtubules. Kinetochore expansion is driven by the recruitment of RZZ and may depend on the ability of RZZ complexes to self-assemble into large polymers [Pereira et al 2018]. The second non-SAC role of ROD is inhibition of stable end-on KT-MT attachments during early prometaphase by blocking the outer kinetochore protein NDC80 from end-on binding to the plus ends of microtubules. This activity of ROD allows transient lateral attachments to predominate during early prometaphase when erroneous attachments are common and stable end-on attachments would lead to mis-segregation [Cheerambathur et al 2013; Barbosa et al 2020].

In this study, we use the new meiosis-specific $rod^{Z3\text{-}1641}$ allele to investigate the meiotic functions of ROD. We describe evidence that ROD is required specifically for the mono-orientation of centromeres during meiosis I. In trans-heterozygotes for $rod^{Z3\text{-}}$

^{1641} and the null deletion allele rod^{X-5} [Scaërou et al 1999] (a genotype referred as rod^{MEI}) substantial fractions of sister chromatid pairs bi-orient during prometaphase I, leading to both equational segregation and homolog nondisjunction (NDJ) during meiosis I.

MATERIALS AND METHODS

Chromosome NDJ assays

In NDJ tests, two females from corresponding compound stock were crossed with one single male from either of the six stocks tested in a shell vial containing molasses food with yeast paste and kept at 25 °C. After 10 days, the parental flies were discarded and the offspring hatching out from each vial were scored in the following 10 days based on the genetic markers on progeny. The compound stocks used in this assay were *C(4)RM*, *ci* ey^R for 4th chromosome NDJ; *C(2)EN*, *b pr* for 2nd chromosome NDJ; *C(3)EN*, *th st* for 3rd chromosome NDJ; and *C(1)RM*, y^2 w^a *su*(w^a)*/O* for sex chromosome NDJ.

Fluorescent in situ hybridization (FISH)

FISH experiments were conducted according to the procedure detailed in [Balicky et al 2002] with modifications [Thomas et al 2005]. Testes were dissected from young adult males within 48 hours after eclosion. Four FISH probes, 359 bp repeats, AATAC repeats, Dodeca repeats and 1.686 g/cm^3 satellite repeats were synthesized and labeled with ATTO 488, Alexa Fluor 546, Rhodamine Red and ATTO 488 respectively (Integrated DNA Technologies). Samples were mounted in an antifade mounting medium (Vectashield).

Testis immunostaining

Immunostaining was performed according to the procedure described in [Bonaccorsi et al 2000] with modifications [White-Cooper 2004]. Testis squash preparations were conducted by using adult males younger than 48-hour-old. For

immunolabeling, mouse monoclonal anti-α-Tubulin DM1A antibody (Sigma) was used at 1:10,000 and secondary antibodies used was Alexa Fluor 488 donkey anti-mouse IgG (H+L, Life Technologies). DNA was stained by DAPI (Sigma) at concentration of 1 μg/ml. Samples were mounted in an antifade mounting medium (Vectashield).

Colchicine treatment and recovery

Whole testes were dissected from adult males younger than 48-hour-old and incubated in Schneider's *Drosophila* medium (Gibco) containing 50 μg/ml colchicine (Acros Organics) for 15 minutes. Recovery was performed by immediately transferring colchicine-treated testes to the fresh culture medium without colchicine and incubating for 15 minutes. X chromosome FISH and DAPI staining for GrM1 detection were conducted by using colchicine-treated and recovered testes as described above.

Fluorescence microscopy and image processing

FISH images were collected by using Axioplan microscope equipped with a 100-W HBO mercury lamp (Zeiss), Plan Neofluar 100×/1.4 oil immersion lenses (Zeiss) and a high-resolution charge-coupled device camera (Roper Industries) at room temperature. Immunostaining images were acquired with a 100×/1.5 oil immersion objective on Axio Observer microscope (Zeiss) at room temperature. Image processing was performed by MetaMorph (MDS Analytical Technologies), AxioVision (Zeiss) and Fiji (NIH).

QUANTIFICATION AND STATISTICAL ANALYSIS

Fly scoring in NDJ tests

For 4th chromosome NDJ test, the number of offspring was recorded in two classes, *ci ey^{R}* (derived from nullo-4 sperm) and ++ (all other sperm types). In NDJ analysis for 2nd and 3rd chromosomes, the total progeny yield was scored for each male. In sister NDJ detection on 2nd chromosome, we scored the number of flies derived from three sperm categories - *b pr/b pr*, *cn bw/cn bw* and *cn bw/+* (or +/+). For the sex chromosome NDJ test, the males carried an X chromosome with y^{+} (dark body) and w^{+} (red eyes) alleles and the dominantly marked Y chromosome *BsYy^{+}* which causes Bar (narrow) eyes. *C(1)RM* carries the recessive marker *y^{2}* (yellow body), *w^{a}* and *su(w^{a})* (light brown eyes), enabling progeny carrying one or two paternal X chromosomes to be readily distinguished from progeny carrying the maternal compound-X, This cross permits discrimination of progeny derived from regular sperm (X-bearing or Y-bearing), and four classes of nondisjunctional sperm – XY (diagnostic of meiosis I NDJ), XX sperm (diagnostic of meiosis II NDJ), XXY sperm (derived from NDJ in both division) and nullo XY sperm (O) sperm, which can arise from nondisjunction in either meiosis I or meiosis II, as well as from chromosome loss. The number of viable progeny was scored based on the genotypes of sperm in different classes: haplo-XY (X or Y), diplo-XY (XY or XX), triplo-XY (XXY) and nullo-XY (O).

Quantification of cytological data

Staging of meiotic cells was achieved by discriminations of DNA content, chromosome territories as well as cohesion state of sister chromatids. Besides, the

number of spermatocytes in a cyst served as an excellent indicator for meiosis I (containing 16 primary spermatocytes) and meiosis II (consisting of 32 secondary spermatocytes). Additionally, the morphology of the spindle stained by DM1A antibody **and FISH probes provided additional information to assist staging.**

In sex chromosome FISH, 359 bp repeat (green) binds to the pericentromeric region of the X chromosome and AATAC repeat (red) resides in the Y chromosome arm distal to the centromere. Therefore, the cohesion or segregation between XY-pair and even between sister chromatids during meiosis I and meiosis II were determined based on the combination and number of green and red spots on DAPI-stained chromosomes in each spermatocyte. Similarly, the Dodeca repeats reside in the pericentromeric region on the 3rd chromosome. Scoring the number and distribution of Dodeca signals during the meiosis I division provided information about homolog segregation and sister chromatid cohesion. Fortuitously, a significant difference in Dodeca repeat copy number between the maternal and paternal homologs in both the *rod*^{MEI} and control males led to substantially different signal intensities. This enabled us to distinguish spots from the two homologs and thereby discriminate between equational and reductional segregation patterns. So, the signal intensity and spot number of Dodeca were indicative of the cohesion state between homologs and sister chromatids. In our cytological data, we distinguished the fluorescent foci based on the outline or the distance between them. One focus (or one spot) referred to the dot with a regular circle outline with strong intensity. Separated two fluorescent foci referred as more than one pronounced round outlines overlapped with each other or split with a

gap between each other.

For the quantification of cohesion-associated proteins, UASp-SUNN::Venus allele regulated by a Nanos (*nos*-Gal4) driver was used to track the sister chromatid cohesion on all eight chromosomes. The GrM1 transgene expresses a mei-S332::GFP protein that was associated with the centromeres on each chromosome. The number of GrM1 signals (sometimes fused as one single spot in centromere spanning space; sometimes separated as two spots at the sides of each centromere) was documented to understand the status of centromeric protection which was highly associated with sister chromatid cohesion.

Statistics

Statistical analysis was performed by one-way *analysis* of variance (ANOVA) using SPSS Statistics v27 (IBM) and significance levels (*P* value) were determined by Tukey's *post hoc* test. In box and whisker plots, thick lines represent the median, boxes represent the 25% and 75% quartiles, and whiskers represent the 5% and 95% quartiles. t test was used to detect significance levels between groups in colchicine-treatment experiments and significant level was set to 0.05. All statistical figures showed in this study were plotted by using OriginPro (OriginLab).

RESULTS AND DISCUSSION

A new trans-heterozygous *rod* mutant is a desired model for functional study of ROD in *Drosophila* male meiosis and causes a reduced male fertility

To preliminarily evaluate the new rod^{MEI} genotype in male *Drosophila* reproduction, we carried out male fertility tests by crossing males from the following stocks singly to two *yw* females and counting embryos produced by the females: 1) $rod^{X\text{-}5}$/+ (control 1); 2) $rod^{Z3\text{-}1641}$/+ (control 2); 3) rod^{MEI} (*rod* mutant); 4) RFP::ROD; rod^{MEI} (rescue stock); 5) *bubR1-KEN* (a substitution mutation in the CDC20-binding site of bubR1); and 6) Bam-GAL4>UAS-*mad1*-RNAi; rod^{MEI} (a spermatocyte-specific knockdown of the key SAC gene MAD1). Both *bubR1-KEN* and *mad1* null mutations specifically ablate the SAC but have only minor effects on mitotic chromosome segregation [Rahmani et al 2009; Ni et al 2011]. The average yield of embryos produced by rod^{MEI} was reduced by 36% compared to $rod^{X\text{-}5}$/+ and $rod^{Z3\text{-}164}$/+ controls (Figure 2-1A). Along with this finding, we observed shrunken seminal vesicles (where mature sperm are stored) in rod^{MEI} ; their size was reduced by 29% compared to the sperm-saturated seminal vesicles in $rod^{X\text{-}5}$/+ and $rod^{Z3\text{-}164}$/+ males (Figure 2-1B and C). A complete rescue was observed in RFP::ROD; rod^{MEI} for both embryo production and seminal vesicle size, indicating that RFP::ROD allele fully complemented the functional loss in male reproduction caused by rod^{MEI} mutation. This observation is consistent with previous studies which correlate chromosome aneuploidy with apoptosis during spermatogenesis in *C. elegans* and human [Carrell et al 2003; Hamer et al 2008;

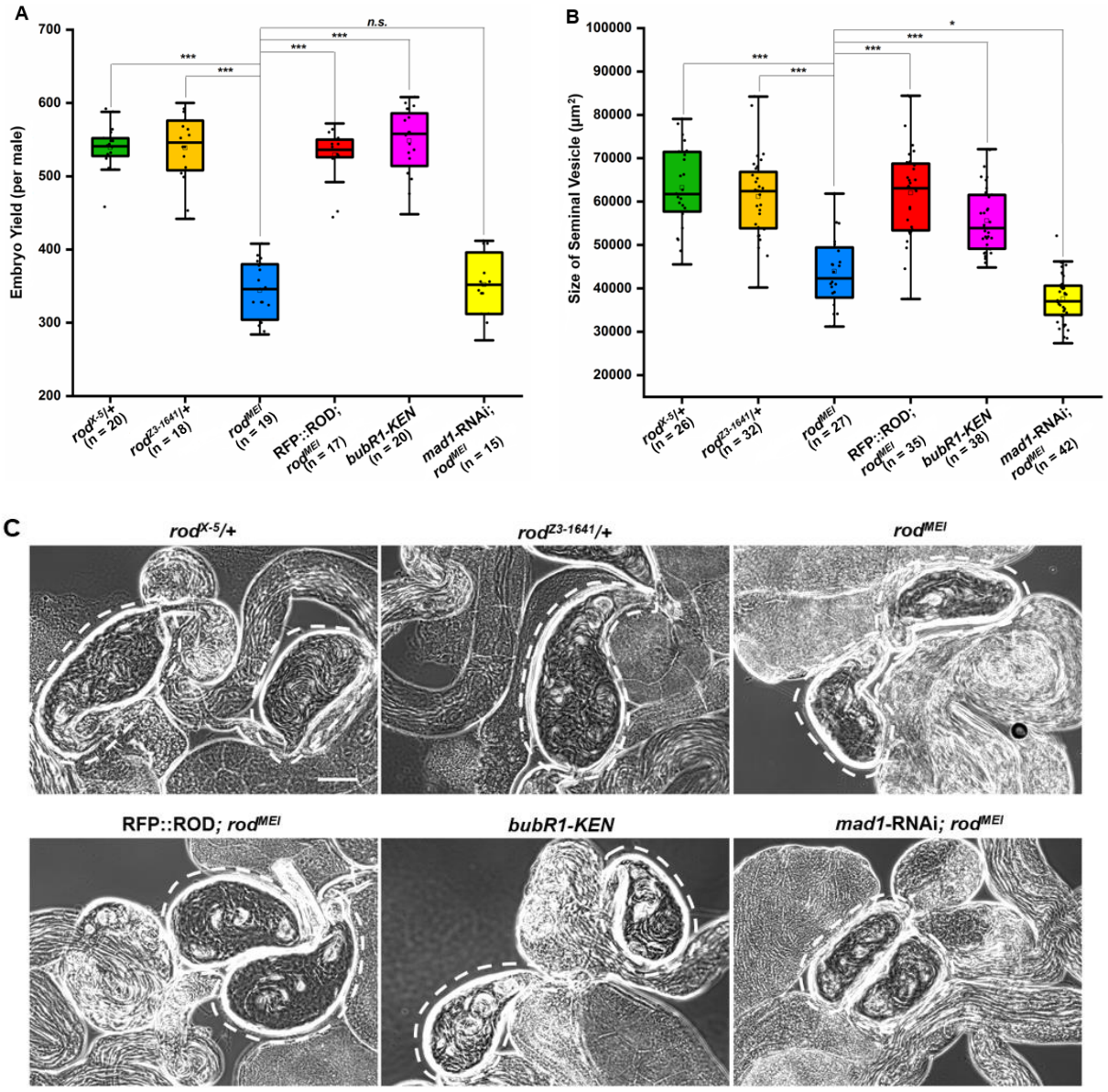

Figure 2-1. Mutations of ROD cause reduced male fertility in *Drosophila*. (A) Embryo production (B) The size of seminal vesicles (C) Morphology of seminal vesicle. White dash lines highlight the seminal vesicles in the reproductive system of male *Drosophila*. The size was measured outside the outline of the dark area of each seminal vesicle.

Vendrell et al 2014]. Thus, we reasoned that the mutations of *rod*^{MEI} imposed detrimental effects in *Drosophila* spermatogenesis, by which the population of mature sperm was reduced in seminal vesicles that eventually caused compromised male fertility. Average embryo yield and seminal vesicle size were similar to the controls in *bubR1-KEN* males and similar to *rod*^{MEI} males in the *mad1-RNAi; rod*^{MEI} double mutants. These results indicate that specifically disrupting the SAC in male meiosis has little if any effect on sperm production.

Mutations of ROD cause equational segregation and homolog NDJ in the first meiotic division

ROD has been shown to localize onto kinetochores during *Drosophila* mitosis and meiosis; *rod* mutations gave rise to aneuploids in both neuroblasts and post-meiotic spermatids, but how ROD affects meiotic chromosome segregation remains unclear [Karess and Glover 1989; Scaërou et al 1999]. Therefore, we employed nondisjunction assays that were carried out using the same six fly stocks as mentioned above.

The assay for mis-segregation of chromosome 4 detects production of nullo-4 sperm using a maternally contributed compound-4 chromosome carrying two recessive mutations (Figure 2-2). Although this assay does not detect diplo-4 sperm, a rough estimate of the NDJ frequency can be obtained by doubling the frequency of 4th chromosome loss. We found an elevated frequency of 4th chromosome NDJ in *rod*^{MEI} (17.1%) compared to two controls (1.9% for *rod*$^{X-5}$/+ and 0.7% for *rod*$^{Z3-1641}$/+)

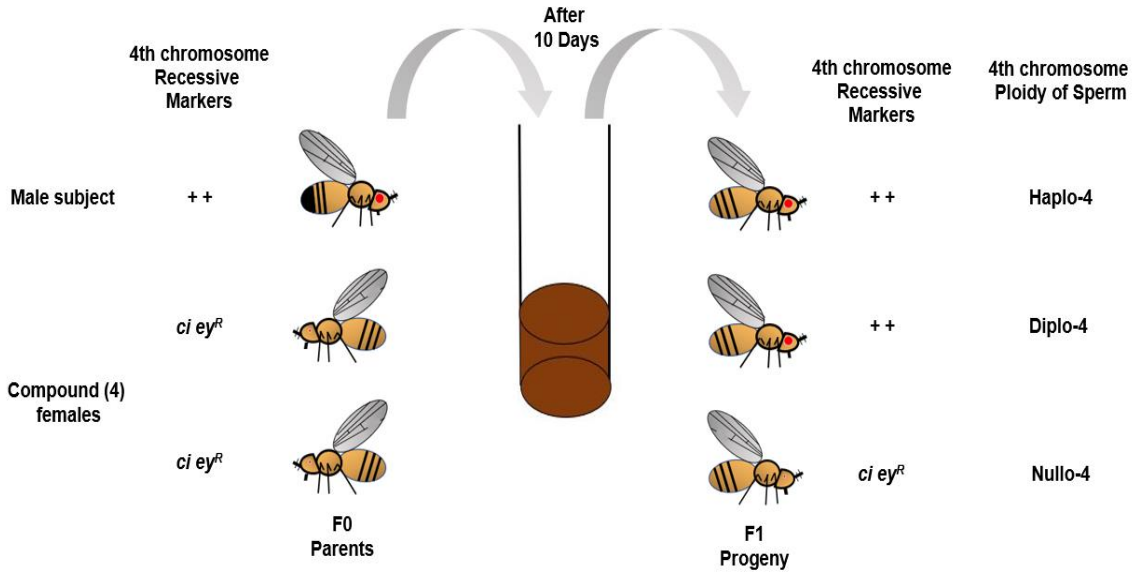

Figure 2-2. Diagram of 4th chromosome NDJ test.

and to the rescue flies (4%). Even though NDJ was 15.3% in *mad1*-RNAi; rod^{MEI}, it was no higher than in rod^{MEI}, and the NDJ rate was at control levels in *bubR1-KEN* mutants (1.3%) (Table 2-1). These results suggest that the rod^{MEI} genotype causes male meiotic mis-segregation of 4th chromosomes but that disrupting the SAC has no effect on 4th chromosome segregation.

To assess whether large autosomal bivalents (chromosome 2 and 3) also undergo mis-segregation, we crossed individual males from the six stocks to females that carried either attached 2nd chromosomes (*C(2)EN*) or attached 3rd chromosomes (*C(3)EN*). *C(2)EN/O* females produce only nullo-2 and diplo-2 eggs and *C(3)EN/O* females produce only nullo-3 and diplo-3 eggs. Aneuploidy for either chromosome 2 or chromosome 3 results in early lethality, so crosses of these females to normal males are usually sterile. However, in crosses to males that undergo NDJ for chromosome 2 or chromosome 3, viable progeny can result from fertilization of disomic eggs by nullo-sperm or vice versa and the number of progeny per male is a rough indicator of the frequency of male NDJ for the tested chromosome. The average progeny yield was 22.47 and 8.2 per male in rod^{MEI} when crossed to *C(2)EN* and *C(3)EN* respectively, consistent with high levels of both chromosome 2 and chromosome 3 NDJ, whereas progeny yields in crosses involving $rod^{X\text{-}5}$/+, $rod^{Z3\text{-}1641}$/+, the rescue flies and *bubR1-KEN* males were negligible (less than 0.5 per male in all crosses). The progeny yields in crosses involving *mad1*-RNAi; rod^{MEI} males were equivalent to those in rod^{MEI} (Table 2-2). Thus, the rod^{MEI} genotype results in high rates of NDJ of the two large bivalents as well as the small 4th chromosome pairs. Notably, average progeny per male was

Table 2-1. Result of 4th chromosome NDJ test.

Male genotype	++	*ci ey*	N_P	%4th NDJ
rod^{X-5}/+	1129	11	1140	1.9
rod$^{Z3-1641}$/+	905	3	908	0.7
rod^{MEI}	1906	178	2084	17.1
RFP::ROD; *rod*^{MEI}	735	15	750	4.0
bubR1-KEN	591	4	595	1.3
mad1-RNAi; *rod*^{MEI}	422	35	457	15.3

Males with indicated genotypes were crossed singly to two *C(4)RM/O*, *ci ey* females. N_P, total number of progeny scored; %4th NDJ (4th chromosome NDJ rate) = 100 x (2 x *ci ey*/ N_p).

Table 2-2. Result of 2nd and 3rd chromosome NDJ tests.

	2nd Chromosome NDJ			3rd Chromosome NDJ		
Male genotype	Progeny number	N_M	Progeny yield per male	Progeny number	N_M	Progeny yield per male
rod^{X-5}/+	3	32	0.09	5	44	0.11
rod$^{Z3-1641}$/+	7	52	0.13	1	36	0.03
rod^{MEI}	2382	106	22.47	443	54	8.20
RFP::ROD; *rod*^{MEI}	17	39	0.44	2	40	0.05
bubR1-KEN	2	38	0.05	5	23	0.22
mad1-RNAi; *rod*^{MEI}	489	27	18.11	188	26	7.23

Males with indicated genotypes were crossed singly to two *C(2)EN/O* females in 2nd chromosome NDJ test or two *C(3)EN/O* females in 3rd chromosome NDJ test. N_M, total number of males tested.

considerably lower (by 61.8%) in crosses of *rod*^{MEI} males to *C(3)EN* females than to *C(2)EN* females. To investigate this discrepancy, we conducted a sequential NDJ test by crossing one-day-old *rod*^{MEI} males to young *C(3)EN* virgins and, after 9 days, transferring males to new vials with young *C(2)EN* virgins were maintained, and assaying progeny yield exactly as in the previous NDJ test. Although the discrepancy between progeny yields in the *C(2)EN* and *C(3)EN* crosses was somewhat reduced (as expected due to generally reduced fertility of older males), a substantial discrepancy was still observed (Figure 2-3A). Thus, we ruled out the possibility that we used males at different ages in *C(2)* and *C(3)* crosses and more older males used in *C(3)* crosses somehow resulted in poor progeny yield. Moreover, progeny yields in NDJ crosses of single *rod*^{MEI} males to *C(2)EN* or to *C(3)EN* females exhibited the same discrepancy (Figure 2-3B), therefore the discrepancy between *C(2)* and *C(3)* crosses is not caused by individual crosses with extremely low fertility. Finally, we measured progeny yields per female in crosses of males and females from the same compound stocks (i.e., three *C(2)EN* males by single *C(2)EN* females and three *C(3)EN* males by single *C(3)EN* females). These crosses remove male NDJ as a factor, allowing a direct comparison of the fertility of *C(2)EN* and *C(3)EN* females. The result was a discrepancy in progeny yields in the *C(2)EN* and *C(3)EN* crosses very similar in direction and magnitude to the discrepancy when *rod*^{MEI} males were used (Figure 2-3C). Therefore, we infer that the difference in progeny yields in the *rod*^{MEI} crosses is due to intrinsic differences in female fertility, perhaps due to the chromosome rearrangements on the compound chromosomes 2 and 3, rather than to a difference

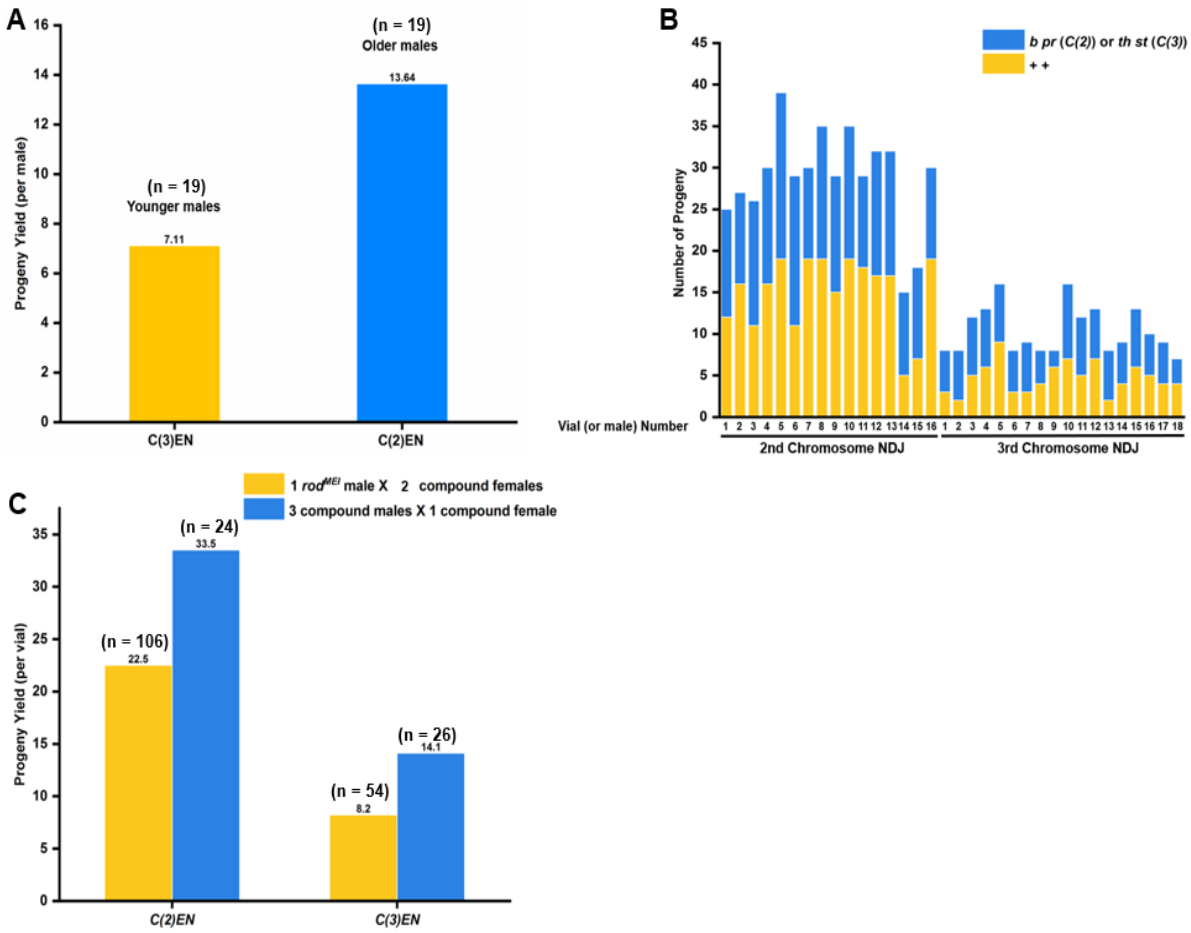

Figure 2-3. Additional autosome NDJ analysis. (A) Test of male's age effect on NDJ (B) Progeny yield of different individuals in 2nd and 3rd chromosome NDJ (C) Test of male's fertility effect on NDJ. n, the number of males tested.

in the NDJ rates of chromosomes 2 and 3 in the *rod*^{MEI} mutant. The *rod* mutant appears to cause similar rates of chromosome 2 and chromosome 3 NDJ.

Next, we asked at what stage NDJ events took place in *rod* mutant flies. *rod* mutants have been shown to cause mis-segregation in mitosis, suggesting that at least some of the aneuploid sperm might result from mitotic NDJ in spermatogonia [Karess and Glover 1989]. Trisomy (but not monosomy) for chromosome 2 or 3 is tolerated in spermatocytes and causes a diagnostic segregation pattern in crosses to *C(2)EN* or *C(3)EN* females in which nearly 100% of the progeny result from fertilization of nullosomic eggs by disomic sperm (because the three homologs form trivalents which nearly always segregate 2:1 at meiosis I). This contrasts with meiotic NDJ of chromosome 2 or 3 bivalents which result in both diplo and nullo sperm, and usually yields fewer progeny from diplo sperm than from nullo sperm. This difference is readily seen in single male crosses. In our single-male crosses to *C(2)EN* and *C(3)EN* females, none of the *rod*^{MEI} males exhibited the segregation pattern diagnostic of trisomy for chromosome 2 or 3 (Figure 2-3B). This result indicates that spermatogonial NDJ is not a major source of the aneuploid sperm in these crosses; therefore, spermatogonial NDJ must be much less frequent than meiotic NDJ in *rod*^{MEI} germ cells.

To determine whether meiotic NDJ occurs at meiosis I or II (or both), *rod*^{MEI} males heterozygous for two recessive 2nd chromosome markers (*cn bw*/+ +; *rod*^{MEI}) were crossed to *C(2)EN* females. Since there is no crossing-over in male meiosis, heterozygous *cn bw*/+ progeny (red-eyed) carry two non-sister paternal chromatids and must result from mis-segregation in meiosis I (either homolog NDJ or equational

segregation) whereas homozygous *cn bw*/*cn bw* (white-eyed) progeny and homozygous + +/+ + progeny (red-eyed) carry two sister chromatids and must result from sister chromatid NDJ at meiosis II. The + +/+ + progeny cannot be readily distinguished from the *cn bw*/+ + progeny, so were estimated from the *cn bw* homozygous progeny. In the rod^{MEI} crosses, progeny with two non-sister paternal chromosomes (7.85 per male) outnumbered progeny with two sister chromatids (1.80 per male), which indicated that the majority of NDJ events occurred at meiosis I (Table 2-3). Progeny derived from nullo-2 sperm were the most numerous (15.60 per male) but are uninformative because they can result from mis-segregation at either meiosis I or meiosis II. In conclusion, all autosomal pairs undergo frequent meiotic mis-segregation and, at least for chromosome 2, meiosis I mis-segregation is considerably more frequent than meiosis II mis-segregation.

To test for sex chromosome mis-segregation, from the six stocks males carrying a dominantly marked Y chromosome were crossed to females carrying an attached-X chromosome (*C(1)RM*) with unique recessive markers. These crosses allow recovery and discrimination of progeny derived from sperm classes diagnostic both of meiosis I mis-segregation (XY sperm), meiosis II NDJ (XX sperm) and both meiosis I and meiosis II NDJ (XXY sperm) as well as nullo-XY sperm (which can result from mis-segregation at either meiotic stage) and from regular X and Y sperm. The overall rate of sex chromosome NDJ (Table 2-4) in rod^{MEI} was 27.84% compared to 0.49% and 0.15% in $rod^{X\text{-}5}$/+ and $rod^{Z3\text{-}1641}$/+, respectively (Table 2-4). As expected, a low overall NDJ rate (0.41%) for sex chromosomes was detected in *bubR1-KEN* while the NDJ

Table 2-3. Detection of the timing of 2nd chromosome NDJ.

Male genotype	Progeny Genotype	Progeny number	N_M	Progeny yield per male
	b pr*/*b pr **(derived from nullo-2 sperm)**	**312**		**15.60**
***cn bw*/+ +; *rod*^{MEI}**	***cn bw*/+ +** **(derived from diplo-2 sperm (sister NDJ + homo NDJ))**	**175**	**20**	**8.75**
	cn bw*/*cn bw **(derived from diplo-2 sperm (sister NDJ only))**	**18**		**0.90**

Males from *cn bw*/+ +; *rod*^{MEI} stock were crossed singly to two *C(2)EN/O* females. N_M, total number of males tested.

Table 2-4. Result of sex chromosome NDJ test.

Male genotype	Sperm class					N_P	%NDJ	%homo
	X	Y	XY	XX	O			
***rod*$^{X\text{-}5}$/+**	577	439	1	0	4	1021	0.49	ND
***rod*$^{Z3\text{-}1641}$/+**	728	633	0	0	2	1361	0.15	ND
***rod*^{MEI}**	671	583	164	7	303	1728	27.84	92.13
RFP::ROD; *rod*^{MEI}	740	578	32	0	157	1507	12.54	ND
bubR1-KEN	602	373	0	1	2	978	0.41	ND
***mad1-RNAi*; *rod*^{MEI}**	477	383	80	4	137	1081	20.81	90.90

Males with indicated genotypes were crossed singly to two *C(1)RM/O, y*^{2} *su(w*^{a}*) w*^{a} females. N_p, total number of progeny scored. %NDJ (overall sex chromosome NDJ rate) = 100 x ((2 x XX) + XY + O)/NP. %homo (homolog NDJ rate) = 100 x (XY/(2 x XX+ XY)).

rate in *mad1*-RNAi; *rod*^{MEI} was identical to that in *rod*^{MEI} single mutants. NDJ was partially rescued by RFP::ROD, declining to 12.54%, a sharp contrast with the complete rescue of autosomal NDJ by RFP::ROD. The difference in the recovery of progeny from XY-sperm and XX-sperm in this cross is an indicator of the timing of NDJ incidence. In both *rod*^{MEI} and *mad1-RNAi; rod*^{MEI} mutants, the recovery of XY-sperm was at least 20-fold higher than that of XX-sperm which occurred at a very low rate, indicating that the great majority of NDJ events occurred in meiosis I between homologous chromosomes rather than meiosis II between sister chromatids, recapitulating the results from the chromosome 2 NDJ test. Taken together, the cross experiments show that *rod*^{MEI} causes substantial NDJ of all four chromosome pairs during male meiosis I but has negligible effects on chromosome segregation in spermatogonial mitosis and meiosis II. This points to an unexpected meiosis I-specific role of ROD despite evidence that its localization sites and dynamics are very similar in mitosis and both meiotic divisions. In addition, the results indicate that mutations in or knockdowns of the SAC genes bubR1 and mad1 that specifically disrupt SAC signaling do not perturb either fertility or meiotic chromosome segregation. Thus, we conclude that mutations in *rod* result in NDJ of meiosis I chromosomes independent of the SAC signaling pathway.

Analysis of meiosis I segregation patterns by FISH

To further characterize the role of ROD in chromosome segregation during meiosis I, we adopted Fluorescence In Situ Hybridization (FISH) to visualize the distribution of homologs and sister chromatids in *rod*^{MEI} mutants and controls during

the meiosis I division stages. To visualize sex chromosome segregation, we hybridized testis squashes with sex chromosome FISH probes against the X-chromosome-specific 359 bp repeats (green) and the Y-chromosome-specific AATAC repeats (red) (as illustrated in Figure 2-4) and also stained with DAPI to visualize the DNA. Our results revealed that all primary spermatocytes at anaphase I (A I) or telophase I (T I) in *rod*$^{Z3\text{-}1641}$/+ controls had undergone reductional segregation (XX/YY), whereas equational (XY/XY) and 4/O (XXYY/O) segregations were observed in 7.4% and 18.1% of A I *rod*^{MEI} spermatocytes (Figure 2-5A and B). Similar frequencies of abnormal meiosis I division products were observed in secondary spermatocytes at prometaphase II/metaphase II (PM II/M II) (Figure 2-5C). A noteworthy feature of these results is the complete absence of 3:1 (i.e. XXY/Y or X/XYY) segregation. This result points to a tight coupling between the X and Y homologs with respect to segregation behavior: either both the X and Y segregate equationally (sister chromatids to opposite poles) or both segregate reductionally (sister chromatids to the same pole).

To analyze the segregation of a major autosome pair, we made use of a probe for a pericentromeric repeat (Dodeca) on the 3rd chromosome that exhibits significant variation of copy number [Abad et al 1992; Carmena et al 1993]. As a consequence, the Dodeca loci of the paternal and maternal chromosome 3 homologs in spermatocytes of *rod*^{ME} and *rod*$^{Z3\text{-}1641}$/+ males exhibited unequal fluorescence intensity that enabled us to reproducibly distinguish the two homologs and to discriminate between reductional and equational segregations. As the sister Dodeca foci in these experiments were sometimes cohesive (fused spots) and sometimes

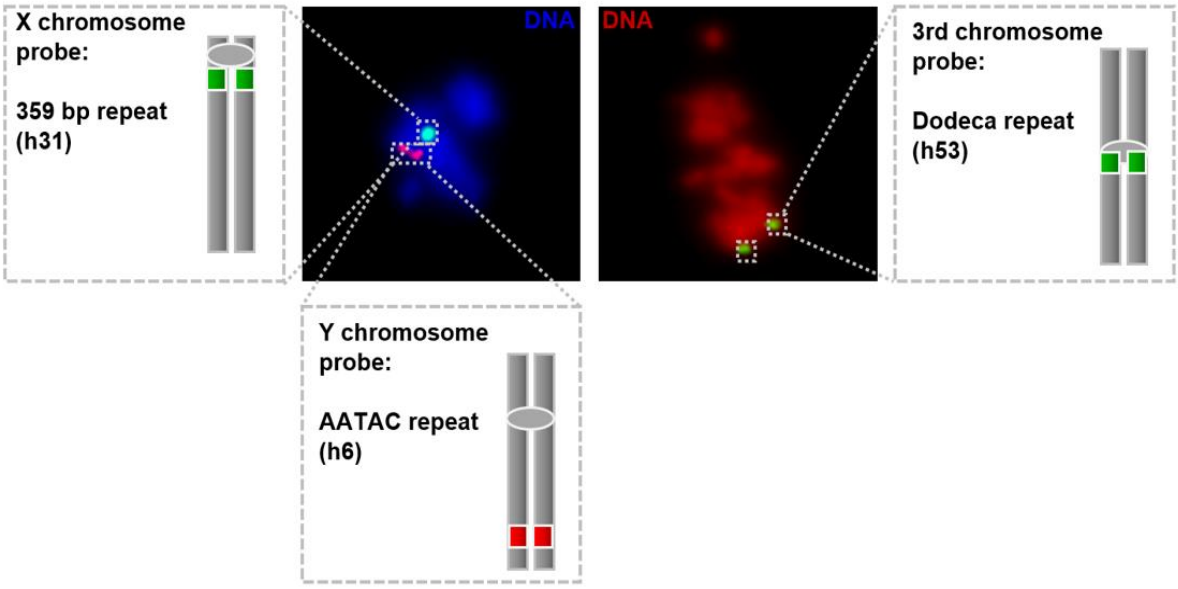

Figure 2-4. Three FISH probes targeted heterochromatic regions on chromosomes.

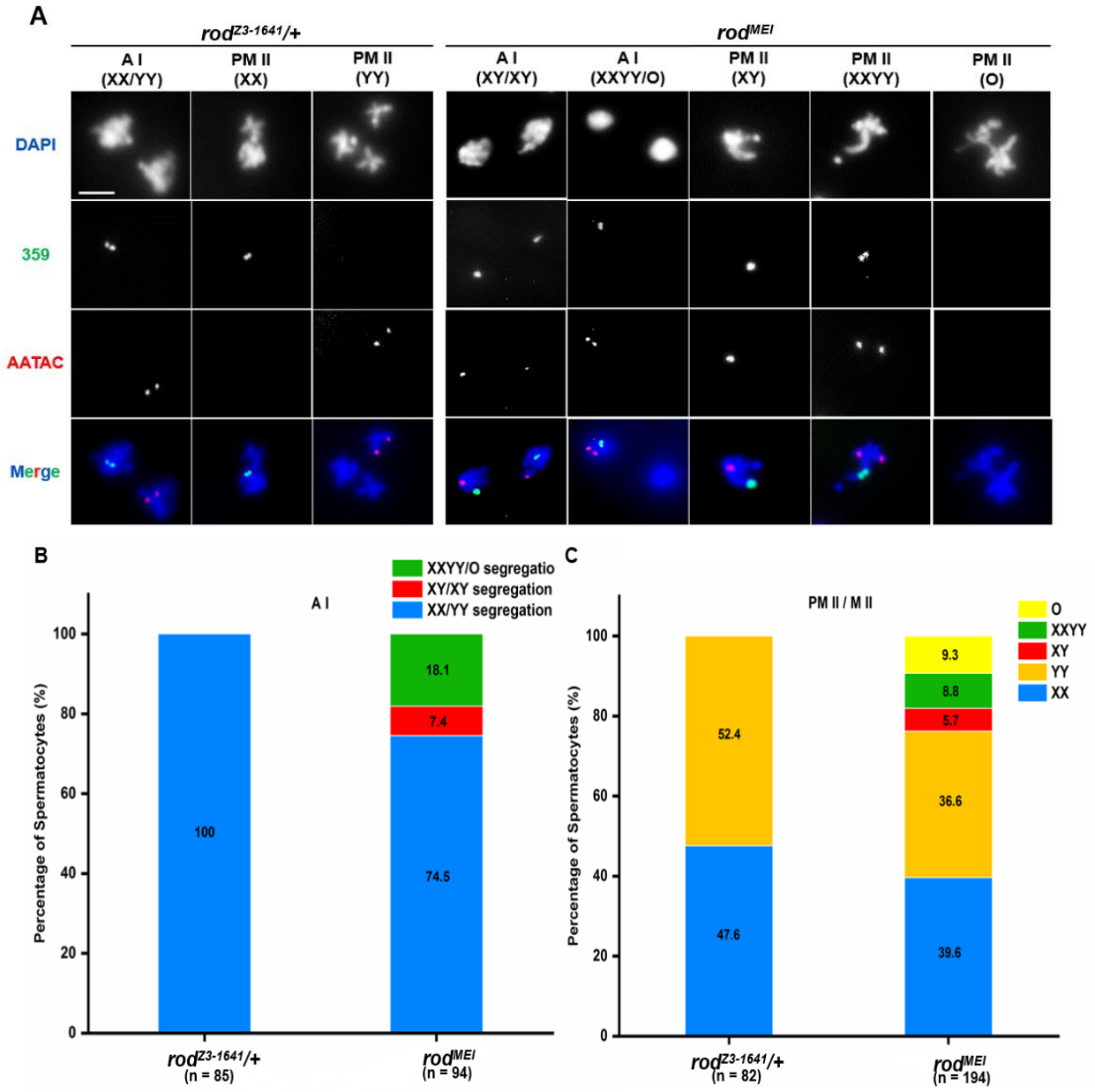

Figure 2-5. Detection of sex chromosome segregation and distribution. (A) Representative images of sex chromosome FISH at A I and PM II (B) Quantification of sex chromosome segregations in A I and T I (C) Quantification of sex chromosome distribution at PM II /M II.

uncohesive (separated spots) for clarity we will refer to fused sister Dodeca spots as either S (strongly fluorescent) or W (weakly fluorescent) and unfused Dodeca spots as S1, S2, W1, W2. In *rod*$^{Z3\text{-}1641}$/+ males, sister Dodeca foci of both homologs remained cohesive throughout meiosis I in 91.7% of spermatocytes (Figure 2-6A and B), and the two fused homologous S and W foci always segregated to opposite poles (S/W, representing reductional segregation). In the remaining 8.3% of spermatocytes, one or both of the Dodeca loci underwent premature sister separation followed by segregation of the separated sisters to opposite poles. S/W reductional segregations were also observed in 68.9% of A I spermatocytes in *rod*^{ME} males but the other 31.1% of A I spermatocytes segregated anomalously. In 16.3% of *rod*^{MEI} spermatocytes, the Dodeca foci fromor both homologs segregated to the same pole, equivalent to the XXYY/O segregations in the sex chromosome FISH experiment. In the remaining 14.8% of *rod*^{MEI} spermatocytes, either one (8.2%) or both (6.6%) pairs of sister foci separated prematurely and moved to opposite A I poles, representing equational segregation of one or both 3rd chromosomes.

Overall, the types and frequencies of mis-segregation were similar between the sex chromosome and 3rd chromosome experiments. The one notable difference was the lack of strong coupling between the 3rd chromosome homologs, leading to significant recovery of 3:1 segregations (either WS1/S2 or SW1/W2), a type of segregation that was not observed among the sex chromosomes. We do not currently have an explanation for this interesting difference, but believe that sister chromatid

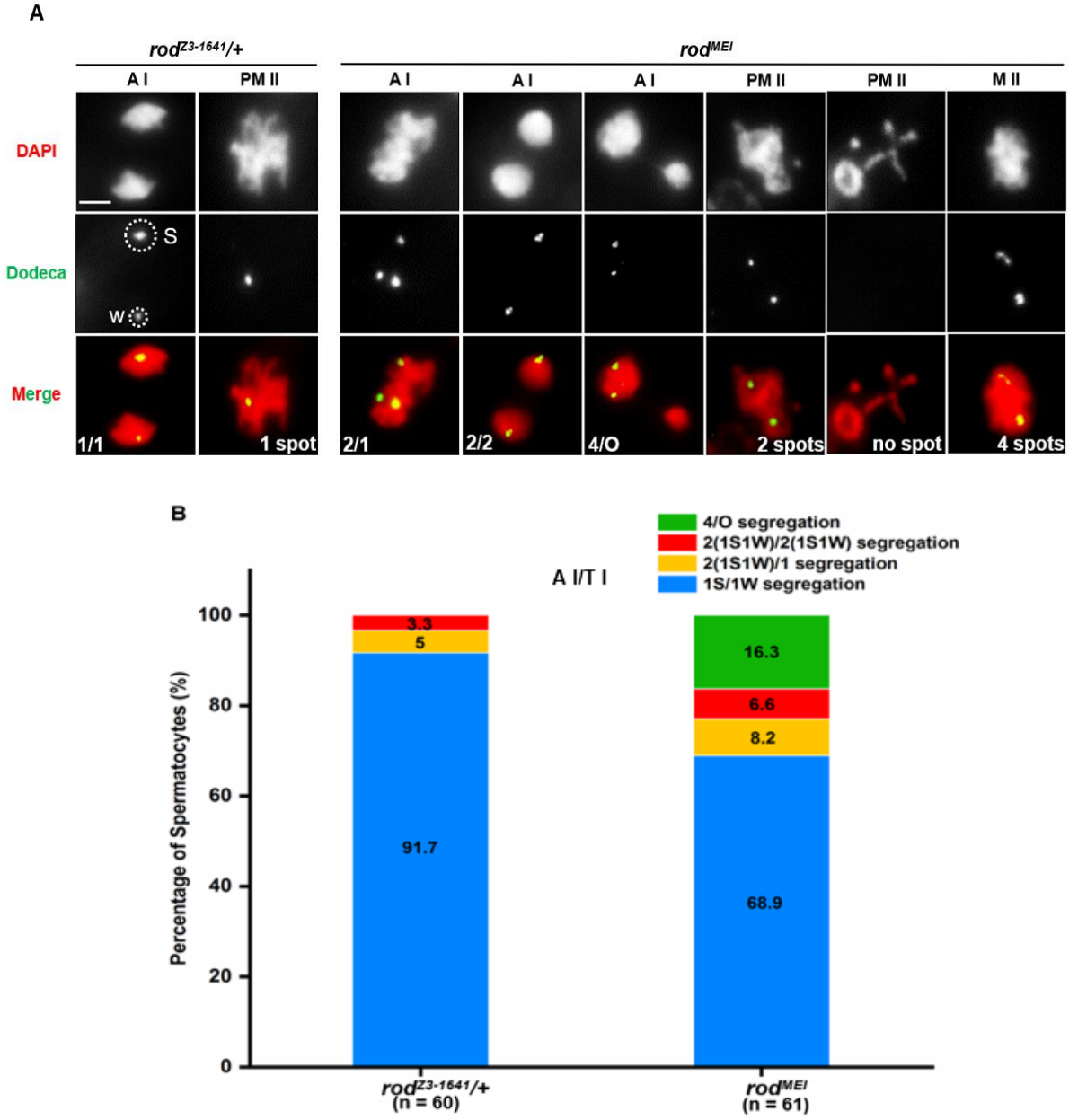

Figure 2-6. FISH detection on 3rd chromosome. (A) Representative images of 3rd chromosome FISH at A I and PM/M II (B) Quantification of 3rd chromosome segregations at A I and T I.

cohesion is largely unaffected by *rod*^{MEI}.

Sister chromatid cohesion is largely unaffected by *rod*^{MEI}

In addition to cataloging the segregation patterns of the X, Y and 3rd chromosomes, the FISH experiments also allowed us to monitor sister chromatid cohesion for the X and 3rd chromosomes throughout the meiosis I division. This was not possible for the Y chromosome because the AATAC repeats are located outside the pericentromeric domain, so lack cohesion after stage S2 in prophase I. We found that, except for the equational segregations in *rod*^{MEI}, where the 359 and Dodeca sister signals segregated to opposite poles, the 359 and Dodeca signals in all A I, T I, PM II and M II cells in both *rod*^{MEI} and controls were either single spots containing two tightly fused sister alleles (fused foci) or closely adjacent or overlapping double spots (split foci). There were no examples of regular reductional (2:2) or nondisjunctional (4:0) segregations in which the sister 359 or Dodeca signals were separated sufficiently to suggest complete loss of cohesion (PSCS). Thus, an important similarity between the sex chromosome and 3rd chromosome FISH results was the absence of categories in which sister chromosome pairs lost cohesion but segregated to the same pole. Such patterns are common in mutants of genes that primarily function in the meiotic cohesion pathway, such as the SOS genes and mei-S332. But in the *rod*^{MEI} mutants, cohesion loss occurred only in the context of equational segregation; i.e., when sister chromatids lost cohesion, they always segregated to opposite poles. We also examined earlier stages to learn whether PSCS prior to anaphase I might play a role in mis-segregation. Among 24 P I, 60 PM I and 13 M I *rod*^{MEI} spermatocytes, we saw

no examples of PSCS for the 359 loci, although as described below, most 359 foci in *rod*^{MEI} were split by PM I. Similarly, although some Dodeca foci were split in PM I, none of the spermatocytes at this stage (n=206) exhibited sister signals sufficiently separated to suggest PSCS of sister 3rd chromatids (Figure 2-7). Thus, unlike in SOS mutants, in which sister chromatid cohesion loss precedes chromosome mis-segregation, becoming evident by mid-late prophase I, no loss of cohesion between sister Dodeca or 359 loci was observed in PM I or M I *rod*^{MEI} spermatocytes. This suggests that, unlike in *sos* and *mei-S332* mutants, cohesion loss is not a primary driver of mis-segregation in *rod*^{MEI} spermatocytes. Instead, it is a secondary phenomenon that occurs only in the context of equational segregation.

Lagging chromosomes are frequent in anaphase I and telophase I in *rod*^{MEI} mutants

One additional important phenotype was observed in the FISH studies of meiosis I segregation for both the sex chromosomes and chromosome 3: chromosome laggards. These are DNA masses that are separate from and located between the main segregating masses during anaphase I or telophase I. Representative examples are shown in Figure 2-8A. Based on DAPI-staining chromosome laggards were observed in 26.9 % of A I spermatocytes and in 23.4% of T I spermatocytes in *rod*^{MEI} males, frequencies were around five-fold higher than as in the controls (Figure 2-8B). Laggards in anaphase I often appeared to be stretched along the spindle axis, suggesting they are being pulled toward both poles. This indicates that the laggards do not result from failure of KT-MT attachment but rather from attachment to the

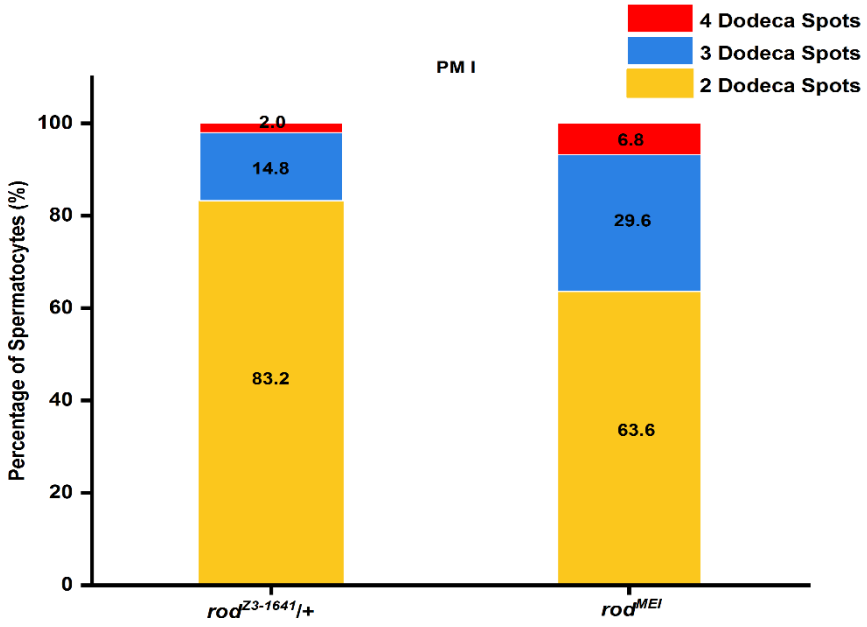

Figure 2-7. Quantification of spermatocytes at PM I with variable number of Dodeca foci.

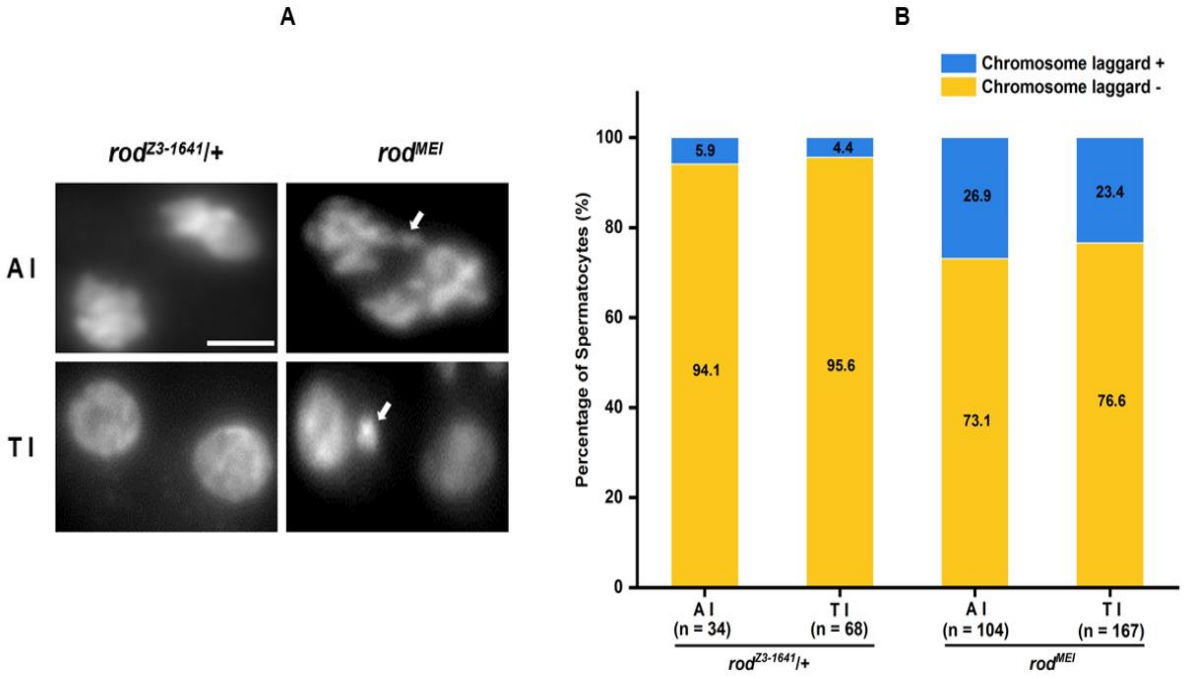

Figure 2-8. Chromosome laggards appear in *rod*^{MEI} mutants. (A) Representative images of chromosome laggards in A I and T I (B) Frequency of chromosome laggards in A I and T I.

microtubules from both poles. The identity of lagged chromosomes was ascertained by using a FISH probe for both large bivalents (the 1.686 g/cm^3 satellite that is present at one site in pericentromeric heterochromatin of both chromosomes 2 and 3) combined with the Y chromosome-specific probe (AATAC repeats). Besides the fluorescence-marked chromosome laggards, we also observed unlabeled laggards which should be either 4th chromosomes or X chromosomes (Figure 2-9A). Our results (Figure 2-9B) revealed that both the Y chromosome and the major autosomes can become trapped as laggards and non-homologous chromosomes sometimes lag simultaneously. In fact, double laggards were quite common: 2/3 of spermatocytes with Y chromosome laggards also exhibited a lagging major autosome. Since Y laggards were observed in 11.5% of spermatocytes and major autosome laggards in 14.4% of spermatocytes, the expected frequency of Y+ major autosome double laggards is only 1.7%. The observed frequency was 8.6%, suggesting that lagging Y chromosomes and lagging major autosomes are not independent events. This might suggest that the minority of anaphase I spermatocytes with laggards derive from a subset of metaphase I spermatocytes with a much higher than average likelihood of producing laggards. Analysis of the results with the Y chromosome probe revealed one further feature of the laggards: that the lagging mass can include either one or both of the sister signals. These two classes of Y chromosome laggards were observed at roughly equal frequencies (Figure 2-9C). As the AATAC block is outside the pericentromeric domain and therefore uncohesive during the meiosis I division

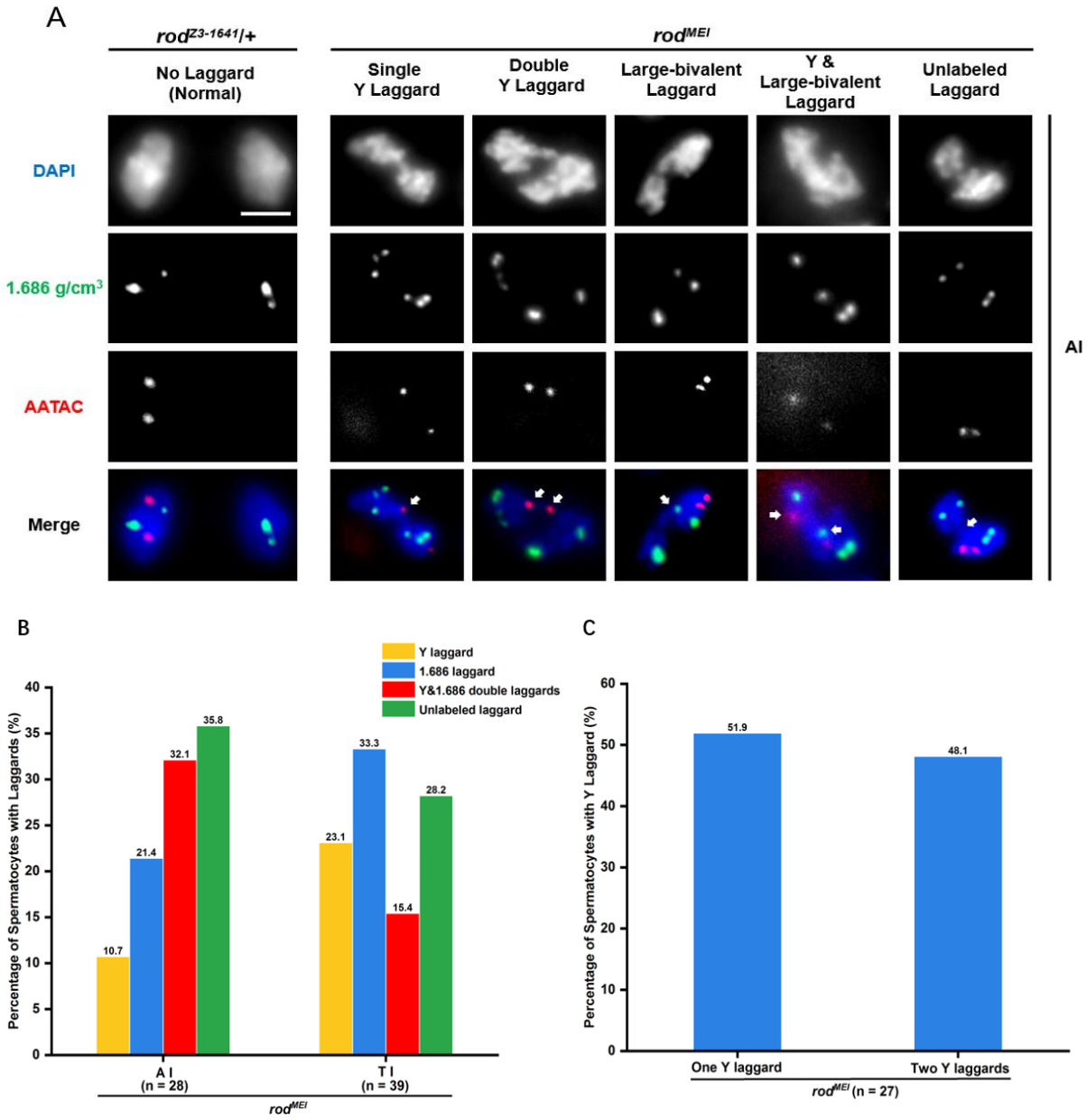

Figure 2-9. Detection of large bivalents and Y chromosome segregation by FISH. (A) Representative images for various types of chromosome laggards at A I (B) Quantification of spermatocytes with chromosome laggards labeled with distinct FISH probes (C) Quantification of single Y laggards (only one lagged AATAC focus) and double Y laggard (two lagged AATAC foci) in *rod*^{MEI} spermatocytes.

stages, so the observing two separate sister signals does not indicate that the sister chromatids have lost cohesion. However, in many of the spermatocytes with one AATAC signal at the laggards and one at a pole, the distance between the two signals is far greater than would normally pertain if pericentromeric cohesion were intact (Figure 2-9A, second column). This suggests that the sister chromatids are fully separated in these spermatocytes, one in the lagging mass and one at the pole. This implies that the single Y laggards have a single kinetochore attached to both poles, an erroneous type of attachment known as merotely. The laggards with two sister spots could represent bi-oriented dyads that have retained cohesion (or possibly two merotelic sister chromatids with or without cohesion).

What is the eventual fate of laggards in the *rod*^{MEI} primary spermatocytes?

There are three possibilities. i) For laggards involving bi-oriented dyads, spindle forces might eventually rip the two sister-pericentromeres apart, leading to equational segregation. Although equational segregations were obtained, this scenario seems unlikely. If this were a common fate, most laggards should disappear before telophase I. However, in our data laggards are almost as frequent at telophase I as at anaphase I. Moreover, in *mnm* mutants, in which homolog conjunction is absent and only univalents are present at metaphase I, there is no equational segregation despite the fact that roughly 30% of the univalents become bi-oriented by metaphase I and lag on the meiosis I spindle. To assess this possibility more thoroughly, we analyzed all of the equational segregations in the XY and Dodeca A I spermatocytes to learn how often the segregating sister spots were present in the main chromosome masses. This

turned out to be nearly always the case. Assuming that laggards are unlikely to have fused with the main masses in anaphase I, this indicates that the great majority of equational segregations occurred at the same time as reductional segregations - at the onset of anaphase I when Separase can trigger segregation by removing restraining cohesin complexes. These results indicate that meiosis I spindle forces probably cannot tear cohesive sister centromeres apart in *Drosophila*. We will return below to the question of the origin of the equational segregations. ii) Laggards might remain trapped on the spindle past the time when daughter nuclei are enclosed by nuclear envelopes. This fate could lead to loss of the lagging chromosomes, which might help account for the unequal recovery of diplo- and nullo-sperm in both the XY and 2nd chromosome cross experiments (Table 2-2 and 2-4). If this scenario occurs, it should result in a deficit of secondary spermatocytes with 4 spots (XXYY or 4 Dodeca spots) relative to secondary spermatocytes with 0 spots. However, this is not the case in *rod*^{MEI} PM II/M II spermatocytes. In the sex chromosome FISH, there is a slight, non-significant excess of nullo-XY over XXYY secondary spermatocytes (9.3% vs 8.8%) but in the Dodeca secondary spermatocytes, 4-spot nuclei exceeded 0-spot nuclei by 11.3% to 8.7% (Figure 2-10). Therefore, we conclude that in *rod*^{MEI}, meiosis I laggards do not lead to significant frequencies of chromosome loss. However, laggards were also observed in 18% of anaphase II divisions in *rod*^{MEI} (data not shown). We did not analyze the fate of these laggards so cannot rule out the possibility that meiosis II laggards do result in chromosome loss. iii) Lagging chromosomes might eventually

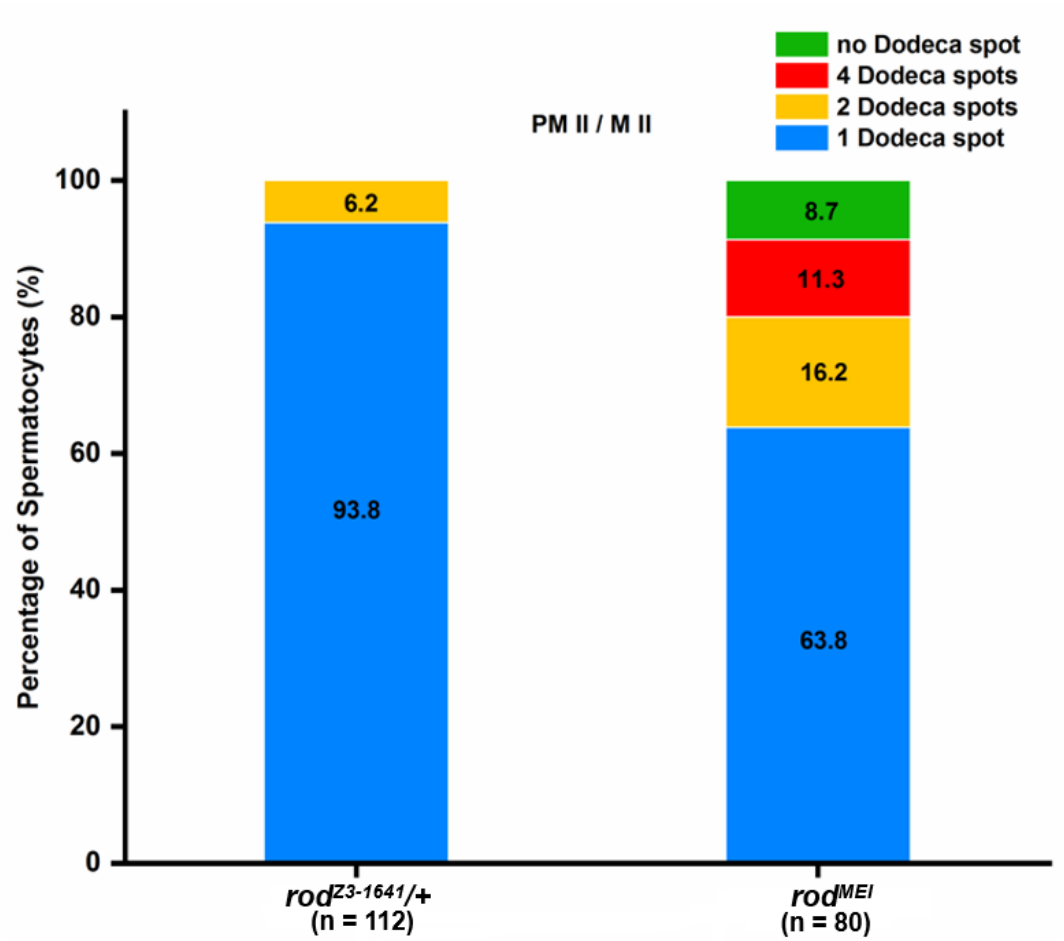

Figure 2-10. Quantification of 3rd chromosome distribution in PM/M II.

get pulled to one pole or the other on the meiosis I spindle and become incorporated into the daughter nuclei. Such fates have been described previously in *Drosophila* meiosis (Chaurasia and Lehner 2018). In light of the compelling evidence against scenarios i and ii, we conclude that this is probably the fate of most or all meiosis I lagging chromosomes in rod^{MEI}. To examine this possibility more thoroughly we assessed the positions of laggards on the spindle. In both late anaphase I and telophase I, the great majority of lagging masses were much nearer one pole than the other, and in many cases, the lagging and polar masses overlapped, suggesting a high likelihood of being incorporated into the same nucleus (e.g., Figure 2-8A). This effect was strong enough that we felt confident assigning FISH spots in the laggards to the nearby pole in our quantification of segregation patterns This fate is potentially important because it could account for some or all of the 4:0 segregations. We return to this question below.

The origin of homolog NDJ in rod^{MEI} spermatocytes

As the above results show, the most frequent mis-segregation phenotype in rod^{MEI} spermatocytes is homolog NDJ (XXYY/O). One way homolog NDJ can come about is premature dissociation of homolog conjunction resulting in mostly univalent at PM I and M I and random assortment of univalents at anaphase I, as observed in mutations for the homolog conjunction genes *snm*, *mnm*, *uno* and *tef* [Tomkiel et al 2001; Thomas et al 2005; Weber et al 2020]. However, there are two reasons to think conjunction is not impaired in rod^{MEI} mutants. First, bivalent morphology appeared entirely normal

throughout P I to M I and no univalents were evident before A I (Figure 2-11A). Second, the conjunction protein SNM showed normal localization in spermatocytes where well-established chromosome territories appeared in both *rod*$^{Z3\text{-}1641}$/+ and *rod*^{MEI}. Furthermore, conjunction appeared to be removed normally at the onset of A I in *rod*^{MEI} spermatocytes, based on the disappearance of SNM foci and regular segregation of chromosome masses (albeit often unequal masses, Figure 2-11B). These results indicate that ROD likely has no role in the establishment, maintenance and removal of the homolog conjunction complex.

Alternatively, homolog NDJ might be caused by bi-oriented dyads that remain cohesive throughout A I and eventually become incorporated into one or the other daughter nucleus through a tug-of-war between the two poles (Figure 2-12). This possibility is consistent with the high frequency of lagging chromosomes in *rod*^{MEI} meiosis I spermatocytes, and with our inference that most such laggards do get pulled to a pole and incorporated into a daughter nucleus. When both homologs of one chromosome pair form bi-oriented dyads, and both dyads become incorporated in the same daughter nucleus (as illustrated in Figure 2-12), the result would be homolog NDJ. Alternatively, the same outcome could come about through bi-orientation of one sister pair and mono-orientation of the other, followed by co-segregation of both pairs to the same pole. This model implies that either one or both two such pairs from each other or one such pair from a mono-oriented homolog is random, some bi-oriented dyads could also be present in *rod*^{MEI} spermatocytes that underwent regular 2:2

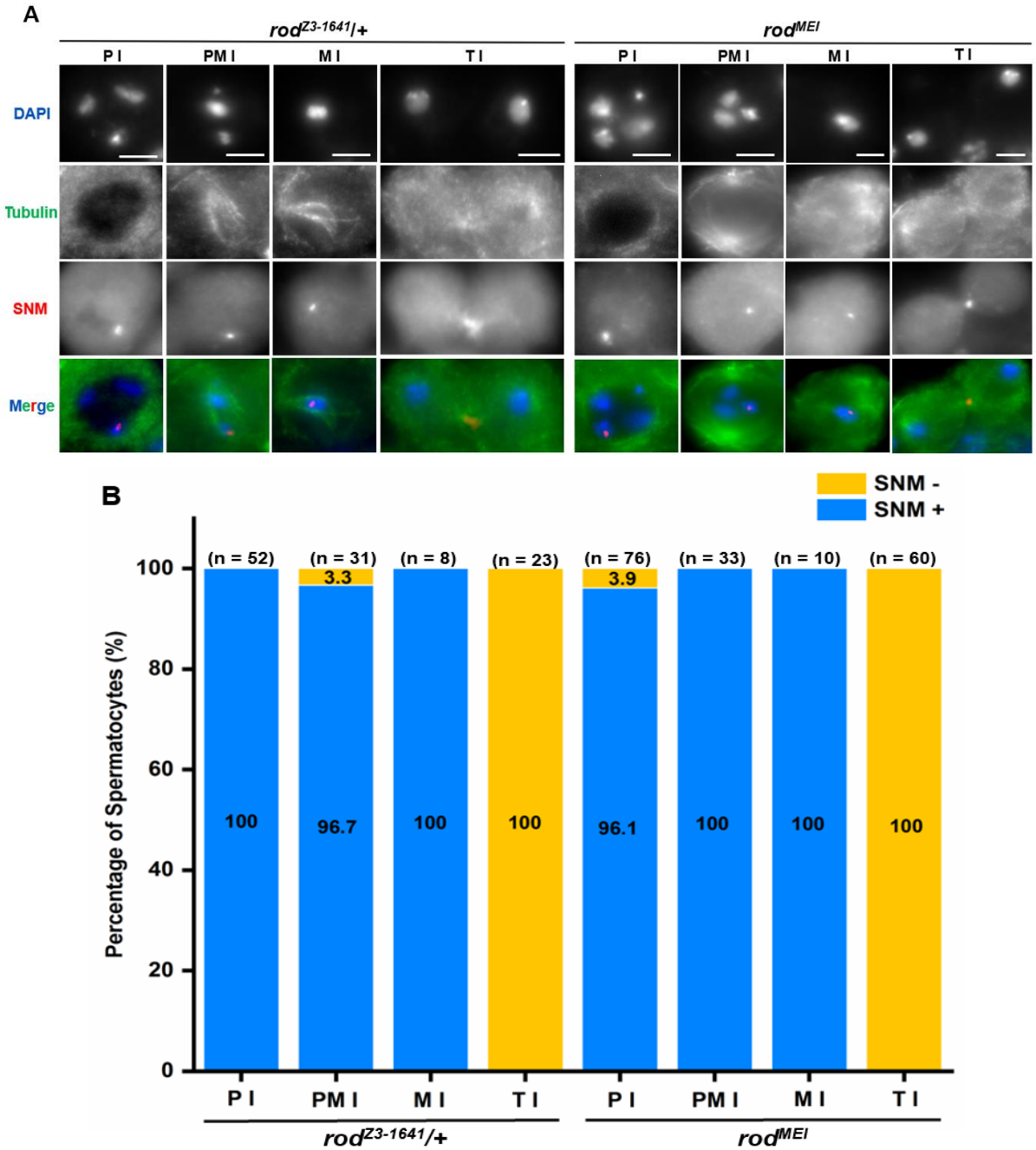

Figure 2-11. Detection of chromosome conjunction complex. (A) Representative images for the localization of SNM during meiosis I (B) Quantification of SNM-localized cells throughout meiosis I. sister chromatid pairs should be bi-oriented in all *rod*^{MEI} spermatocytes that undergo 4:0 segregation at A I. To the extent that segregation of

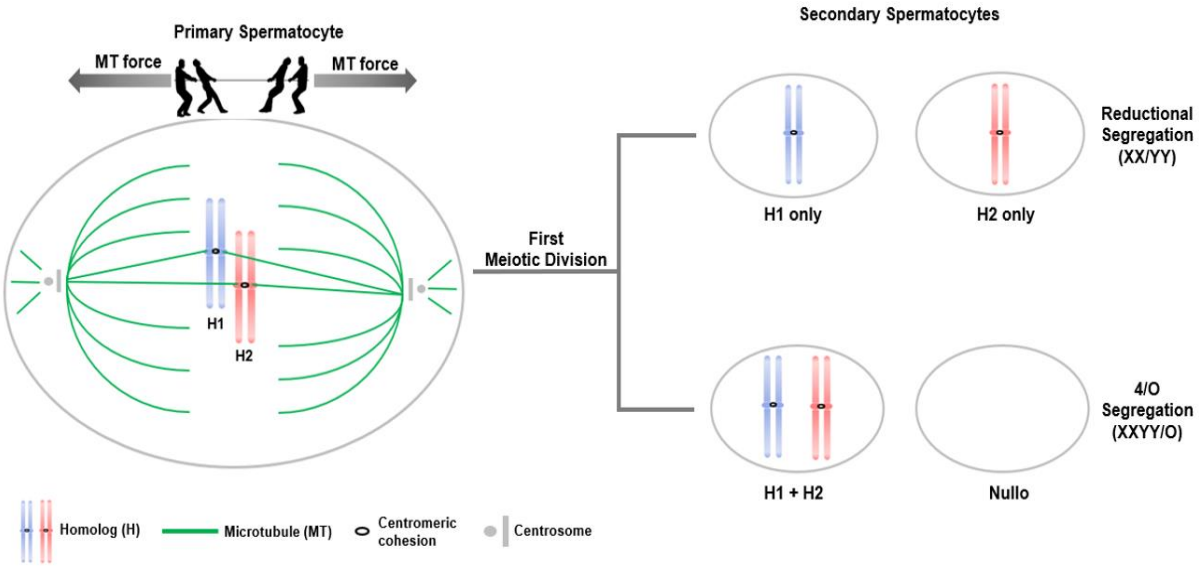

Figure 2-12. Proposed Tug-of-War model in *rod* mutants.

segregation at A I, but, since the majority of spermatocytes segregate 2:2, it seems likely that many or most 2:2 segregations would involve only mono-oriented sister chromatid pairs. If so, then there might be a difference between 4:0 and 2:2 reductional segregations with regard to the frequency of bi-oriented sister chromatid pairs. As noted above, in both the 359 and Dodeca FISH experiments, some A I/T I spermatocytes exhibited sister foci that were split slightly apart, whereas in other such spermatocytes, the sister signals were fused into a single spot. We were curious whether the presence of single or double spots related in any way to chromosome segregation patterns, so we carefully quantified the frequencies of single and double Dodeca spots in the various types of segregations in *rod*^{MEI}. Remarkably, we found a very strong correspondence between split spots and homolog NDJ and between fused spots and regular (2:2) segregation. That is, split Dodeca spots were present in all *rod*^{MEI} spermatocytes that underwent homolog NDJ for chromosome 3, whereas only fused Dodeca spots were present in *rod*^{MEI} spermatocytes that underwent regular 2:2 segregation. In equational segregations, sister foci separate completely and segregate to opposite poles, so the split vs fused categories do not apply. However, we were able to categorize the fused vs split status of the sister pair that segregated reductionally in the half-equational segregations and found that invariably those sister foci were fused (Figure 2-6). This accounts for the absence of 3-spot PM II/M II nuclei (Figure 2-10). Overall, then, the data show that sister chromatid pairs that segregate normally invariably exhibit fused Dodeca spots, whereas sister chromatid pairs that mis-segregate exhibit either split or completely separated Dodeca foci. This

relationship strongly suggests that the presence of split pericentromeric alleles at A I/T I.

Mutation of ROD disrupts sister-chromatid mono-orientation in meiosis I

Our consideration of possible mechanism responsible for mis-segregation in *rod*^{MEI} spermatocytes have led us to propose primary roles for bi-orientation of sister centromeres in the etiology of both equational segregation and homolog NDJ. Chromosome orientation is achieved during prometaphase and relies on the establishment of directional forces on kinetochores depending on the attachment of MT bundles [Hauf and Watanabe 2004; Watanabe 2012]. Since split 359 and Dodeca foci during A I/T I are correlated with mis-segregation and thus likely indicate centromere bi-orientation, we examined PM I and M I spermatocytes in *rod*^{MEI} and control spermatocytes hybridized with the 359 and Dodeca probes for evidence that splitting is present before the meiosis I divisions and is correlated with the occurrence of mis-segregation. We found that 84.8% and 76.4% of PM I and M I spermatocytes in *rod*^{MEI} mutants exhibited small gaps between sister 359 signals with mean distance and range (14.1 ± 2.3 pixels in PM I and 13.3 ± 3.2 pixel in M I, Figure 2-13C) similar to the gaps in A I spermatocytes, but such separated 359 signals appeared in only 13.6% and 19.5% of PM I and M I spermatocytes, respectively in *rod*$^{Z3\text{-}1641}$/+ controls (Figure 2-13A and B). Additionally, split Dodeca foci were present at PM I in 36.4% of *rod*^{MEI} spermatocytes but only 16.8% of control spermatocytes (Figure 2-7), indicating that the *rod*^{MEI} mutation disrupts the proper orientation of pericentromeric regions of

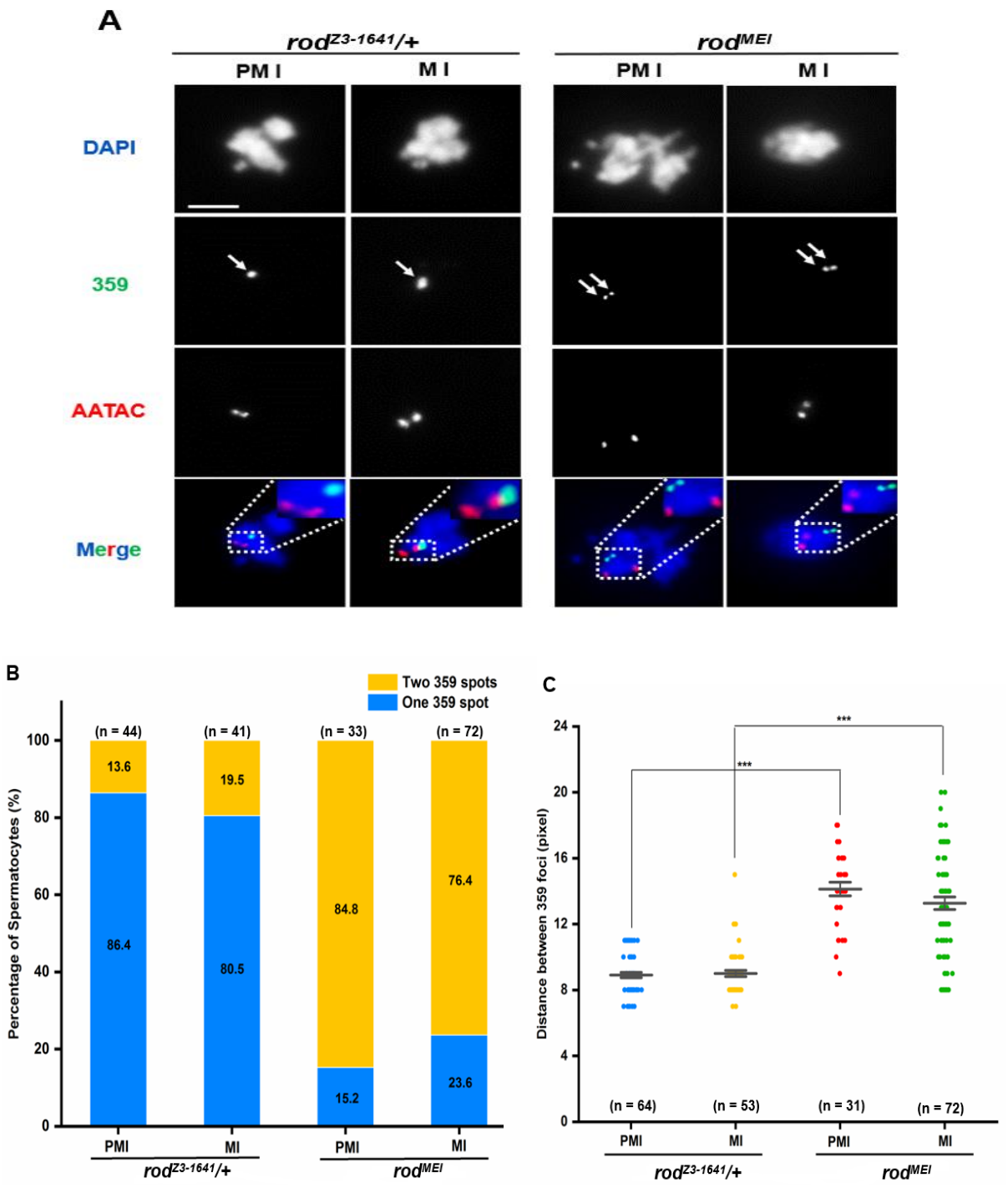

Figure 2-13. Formation of X-chromosome gaps at pericentromeres in *rod* mutants. (A) Representative images for pericentromeric gaps (B) Percentage of spermatocytes with or without sister gap of X chromosome (C) Distance between pericentromeres of X chromosome.

both autosomes and sex chromosomes. The increased distance at pericentromeric regions (as illustrated in Figure 2-14) in *rod*^{MEI} spermatocytes might result from opposing spindle forces on bi-orientated sister centromeres still held together by peri-centromeric cohesion.

Separation of pericentromeres in *rod*^{MEI} depends on microtubule forces

To test this hypothesis, we exposed primary spermatocytes to the MT depolymerizing agent colchicine, reasoning that if spindle-generated tension is required for splitting, disassembly of the spindle should lead to reduction of split foci. Testes dissected from *rod*^{MEI} and *rod*$^{Z3\text{-}1641}$/+ males were incubated in insect culture medium supplemented with colchicine for 15 minutes followed by FISH with 359 probe. We found that the percentage of PM I spermatocytes in *rod*^{MEI} mutants with sister gaps (two 359 spots) decreased from 84.8% in untreated controls (dissected testes exposed to colchicine-free buffer) to 32.4% in the colchicine-treated testes. The frequency of 2-spot spermatocytes recovered to 73.4% when colchicine-treated testes were subsequently incubated in colchicine-free buffer for 15 minutes prior to performing FISH (Recovery condition) (Figure 2-15A and B). Similarly, the average distance between 359 foci diminished to 11 ± 1.88 pixel when treated by colchicine and restored to 12.89 ± 2.34 pixels after recovery (Figure 2-15C).

However, drastic fluctuation was not appeared in PM I of *rod*$^{Z3\text{-}1641}$ spermatocytes at which the two-spotted spermatocytes did not change that much when treated with colchicine and in the following recovery (Figure 2-16). The reaction of 359 foci in response to MT polymerizing states underscores the role of MT force in the gap formed

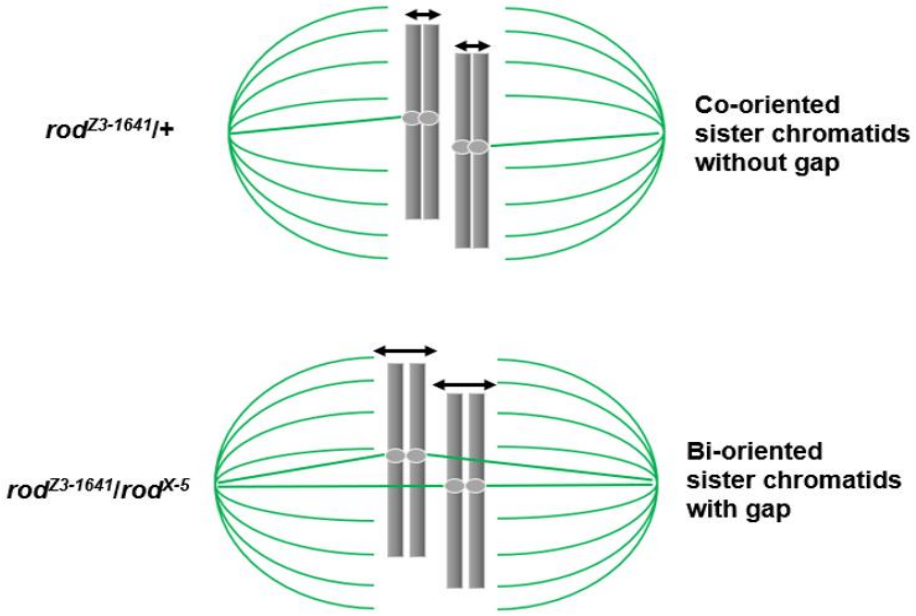

Figure 2-14. Proposed model for sister chromatid orientation in control and *rod* mutant spermatocytes.

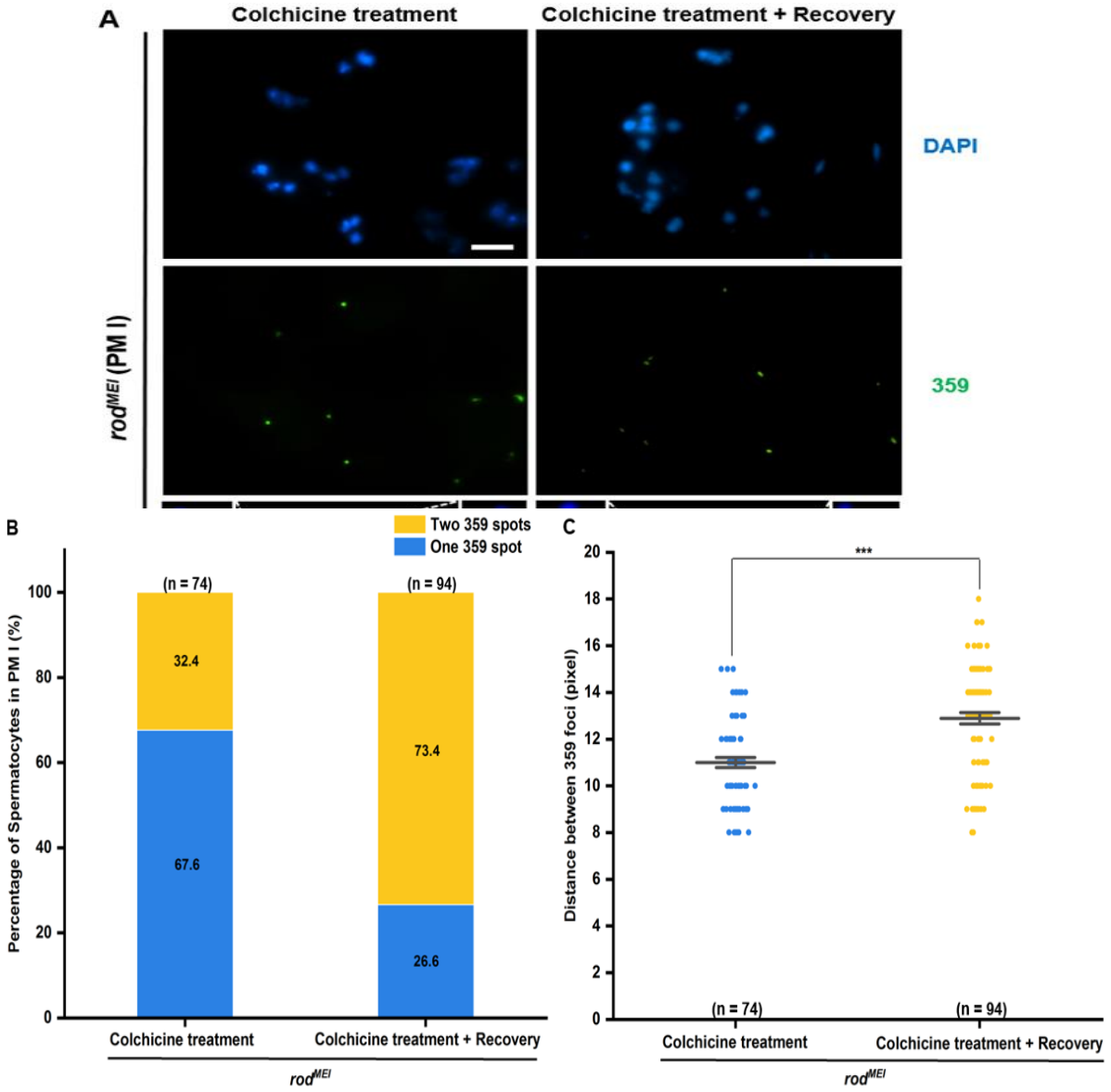

Figure 2-15. Pericentromeric separation in *rod* mutants is under the regulation of microtubule force. (A) Representative images for X chromosome FISH (B) Quantification of PM I spermatocytes with (two 359 spots) or without (one 359 spot) sister gap (C) Distance between pericentromeres of X chromosome in PM I.

between sister pericentromeres and further verifies our presumption that mutations in *rod* disrupt the mono-orientation of sister chromatids in meiosis I.

Sister chromatid cohesion is lost at A I in a significant minority of chromosome in *rod*^{MEI}

Although loss of cohesion is not a primary driver of mis-segregation in *rod*^{MEI} spermatocytes, it is nevertheless an essential part of the process that generates equational segregations; if pericentromeric cohesion is not released before the end of meiosis I division, sister chromatids cannot segregate. SUNN, serving as a potential structural homolog of SA, colocalizes with SMC1 and SOLO at centromere until A II, and mutations in *sunn* cause premature release of sister chromatid cohesion starting from Prophase I (P I) [Krishnan et al 2014]. To better understand the role of cohesion in equational segregation in *rod*^{MEI} spermatocytes, we used a Venus tagged allele of SUNN (UASp-sunn::Venus) to track centromeric cohesion during meiosis I. We found that from P I to M I SUNN localization and foci numbers were similar in *rod*^{MEI} and *rod*$^{Z3\text{-}1641}$/+ (between 6 and 8 per nucleus) similar to previous results from wild-type genotypes (Figure 2-17). However, significant differences between rodMEI and control spermatocytes emerged after the onset of the meiosis I division. Whereas nearly all *rod*$^{Z3\text{-}1641}$/+ spermatocytes continued to show 7-8 SUNN foci at A I (counting both daughter nuclei), as expected, among *rod*^{MEI} A I spermatocytes 27.8% exhibited fewer than 7 SUNN foci (range from 2-6 foci) and 11.7% exhibited more than 8 SUNN foci

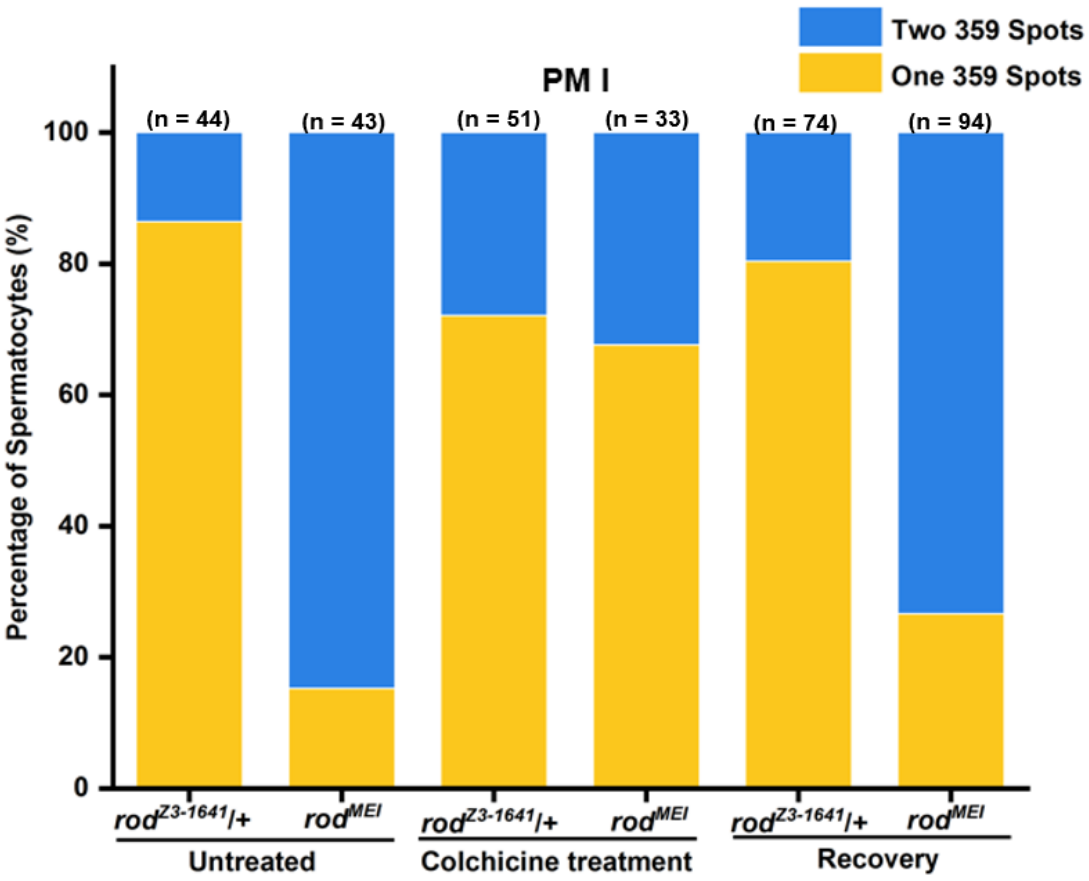

Figure 2-16. Comparison of PM I spermatocytes with one or two 359 spots.

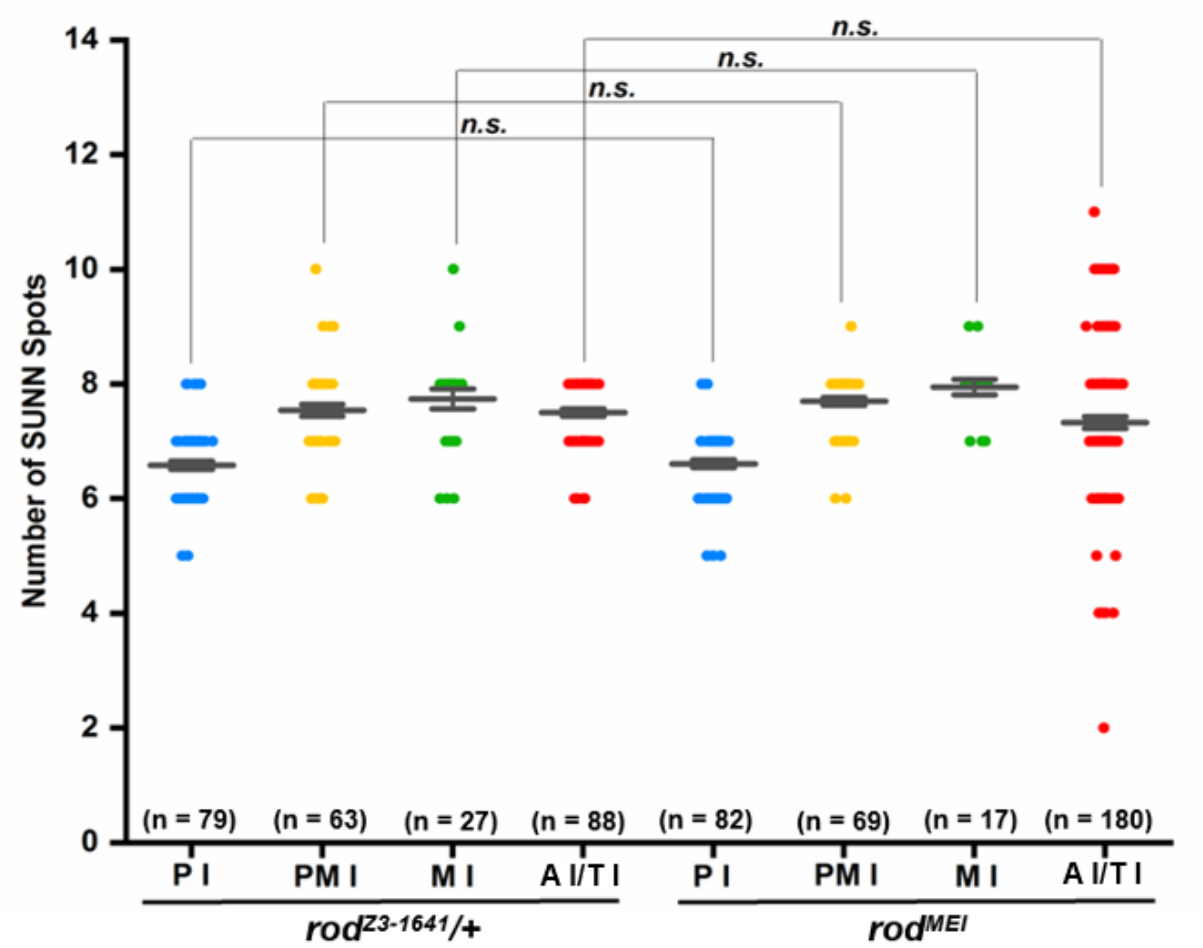

Figure 2-17. Quantification of SUNN spots during meiosis I.

(range 9-11) (Figure 2-18A and B). We hypothesize that the spermatocytes with more than 8 foci have undergone loss of cohesion, allowing sister centromere regions (along with associated SUNN proteins) to separate, but have not yet undergone removal of the inactivated cohesion complexes, whereas the spermatocytes with fewer than 7 foci have lost cohesion from one or more sister pairs and have undergone removal of the inactivated cohesion complexes.

A brief transition period between initiation of chromosome segregation and removal of cohesion proteins has been reported in Separase-dependent removal of both conjunction and cohesion proteins. Time-lapse imaging clearly reveals that *Drosophila* MNM persists on one of the segregating nuclei migrating to one spindle pole and disappears within 3 minutes after the onset of A I [Blattner et al 2016]. Similarly, in human cell culture, Separase-cleaved SCC1 retains on chromosomes up to 12.5 minutes after they begin to segregate [Rosen et al 2019]. Such evidence confirms that both conjunction and cohesin proteins can linger on their chromosome-deposition sites after Separase cleavage but the duration may vary among various Separase targets or among different species.

The above results demonstrate that the sister chromatid cohesin SUNN is removed prematurely from a small but significant fraction of pericentromeric domains during A I. This likely implies a loss of cohesion and is consistent with our proposal that equational segregation in rod^{MEI} spermatocytes results from a mechanism involving abnormal bi-orientation of dyads on the meiosis I spindle followed by loss of

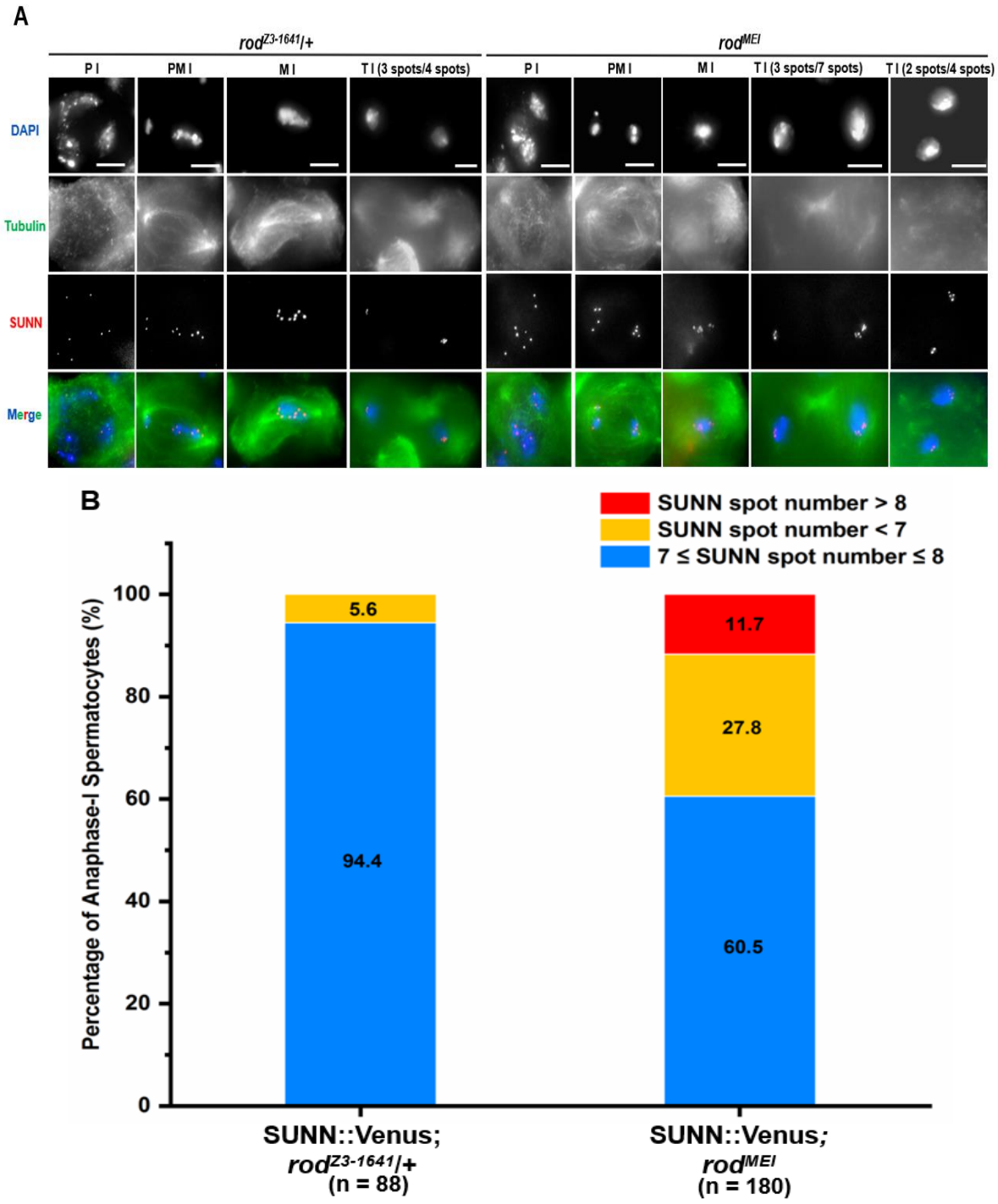

Figure 2-18. Detection of centromere cohesion in meiosis I spermatocytes. (A) Representative images for SUNN localization (B) Quantification of SUNN distribution at A I.

the restraining pericentromeric cohesion.

ROD is required for the suppression of MEI-S332 redistribution in meiosis I

A crucial question raised by these observations is why cohesion is lost during A I. In *Drosophila*, as in other eukaryotes, cohesion removal during anaphase of both meiotic divisions requires Separase. Separase is activated at male A I to mediate removal of the conjunction complexes that constrain homologs [Blattner et al 2016]. Pericentromeric cohesion in *Drosophila* is normally protected from Separase at A I by the *Drosophila* SGO ortholog MEI-S332 [Kerrebrock et al 1992]. In *mei-S332* mutants, centromeric foci of SUNN, SOLO and SMC1 are removed at A I instead of at A II [Yan et al 2010; Krishnan et al 2013]. We, therefore, wondered whether reduced *rod* function might somehow impair the level or function of MEI-S332 during meiosis I. To address these questions, we introduced a GFP-tagged MEI-S332 allele (GrM1 driven by native MEI-S332 sequences) in both control and *rod* mutant backgrounds to detect the localization of MEI-S332 in meiosis I [Kerrebrock et al 1995]. We found no evidence for reduced levels of MEI-S332 or for any gross abnormality in MEI-S332 localization in rod^{MEI} spermatocytes. From PM I through M I, MEI-S332 localized to one prominent site, presumably the centromere/ pericentromere region, per chromosome in both rod^{MEI} and $rod^{Z3\text{-}1641}$/+ spermatocytes. However, whereas the MEI-S332 foci in $rod^{Z3\text{-}1641}$/+ spermatocytes were invariably single, detailed analysis of rod^{MEI} spermatocytes revealed that some chromosomes had two closely adjacent foci on opposite sides of the DNA instead of the single centromere-spanning foci normally present at these stages. These double foci give the impression of resulting

from splitting of the single foci (Figure 2-19A). Quantitative data obtained by counting the double foci as two foci showed a significant increase in the average number of MEI-S332 foci in rod^{MEI} versus $rod^{Z3-1641}$/+ spermatocytes: 9.67 ± 0.16 versus 7.75 ± 0.12 at PM I and 10.05 ± 0.32 versus 7.88 ± 0.13 at M I (Figure 2-19B). These results imply that in rod^{MEI} spermatocytes, slightly more than one-fourth of PM I and M I chromosomes, on average, have split foci. However, this is surely an underestimate: the double foci are close enough that their discrimination would be highly dependent on the angle between the imaging plane and the axis of the chromosome (reflected by the appearance of elliptical MEI-332 foci in *rod* mutants). Very roughly, then, chromosomes with split MEI-S332 foci likely comprise more than one-fourth up to one-third of the total population of PM I/M I chromosomes in rod^{MEI} spermatocytes.

Splitting of sister MEI-S332 foci also occurs in mitosis or meiosis II in several organisms. In dividing *Drosophila* cells, MEI-S332 foci are initially single but split into two closely associated foci on opposite faces of the kinetochore when the sisters come under tension in metaphase [Yamada et al 2017]. Although MEI-S332 does not play an essential role in mitosis, it localizes to centromeric domains throughout mitosis and contributes to the protection of pericentromeric cohesion during prophase when arm cohesins are removed by the non-proteolytic WAPL pathway. In human cells, a similar splitting of SGO1 signals results from redistribution of the foci from inner centromeres to kinetochores in response to inter-kinetochore tension [Liu et al 2013]. In mouse spermatocytes, SGO2 redistributes from centromeres to kinetochores as sisters are

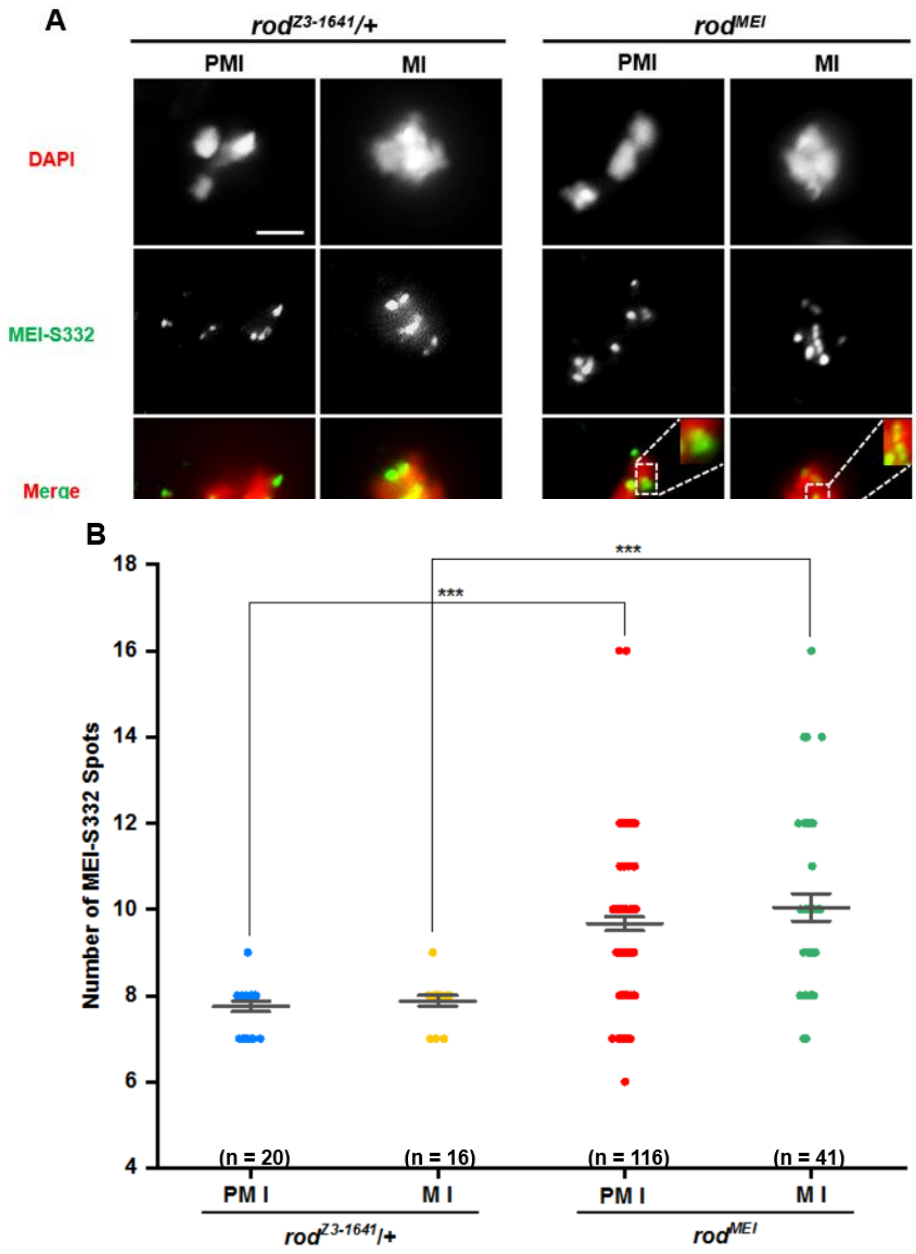

Figure 2-19. The analysis of MEI-S332 behavior in PM I and M I. (A) Representative images for the localization of MEI-S332 (B) Quantification of MEI-S332 foci.

bi-oriented during PM II [Gómez et al 2007]. In all of these cases, the removal of Shugoshins from pericentromeric sites apparently serves to expose pericentromeric cohesion to phosphorylation and subsequent cleavage by Separase, a maneuver that can only be carried out safely once the sister centromeres are bi-oriented.

No such relocation is a normal part of meiosis I since Shugoshin is essential for protecting pericentromeric cohesion during anaphase I. Moreover, in the normal course of meiosis I, inter-kinetochore tension is not stably generated. However, we have provided several lines of evidence consistent with bi-orientation of at least some dyads at PM I and M I and for loss of pericentromeric cohesion in early anaphase I in some *rod*^{MEI} spermatocytes. This raises the question of whether the relocation of MEI-S332 is a result of inter-kinetochore tension on bi-oriented dyads. To address this question, we incubated testes dissected from the GrMEI-S332-GFP; *rod*^{MEI} stock (and the corresponding control stock) to colchicine as described above. Surprisingly, we did not observe any reduction in the numbers of split MEI-S332 foci as a result of colchicine treatment, nor any effect of the recovery condition (Figure 2-20A and B). The average number of MEI-S332 spots was nearly the same in all conditions, much higher than 8 as in untreated *rod*^{MEI} spermatocytes, after colchicine treatment (10.43 ± 1.79) and after a brief recovery (10.71 ± 1.97). This result is very different than that for 359 foci which showed strong and rapid reactions to both MT depolymerization and repolymerization. This result could indicate that MEI-S332 redistribution occurs independently of spindle forces. However, an alternative possibility is that the redistribution of MEI-S332 occurs in response to bipolarity and inter-kinetochore

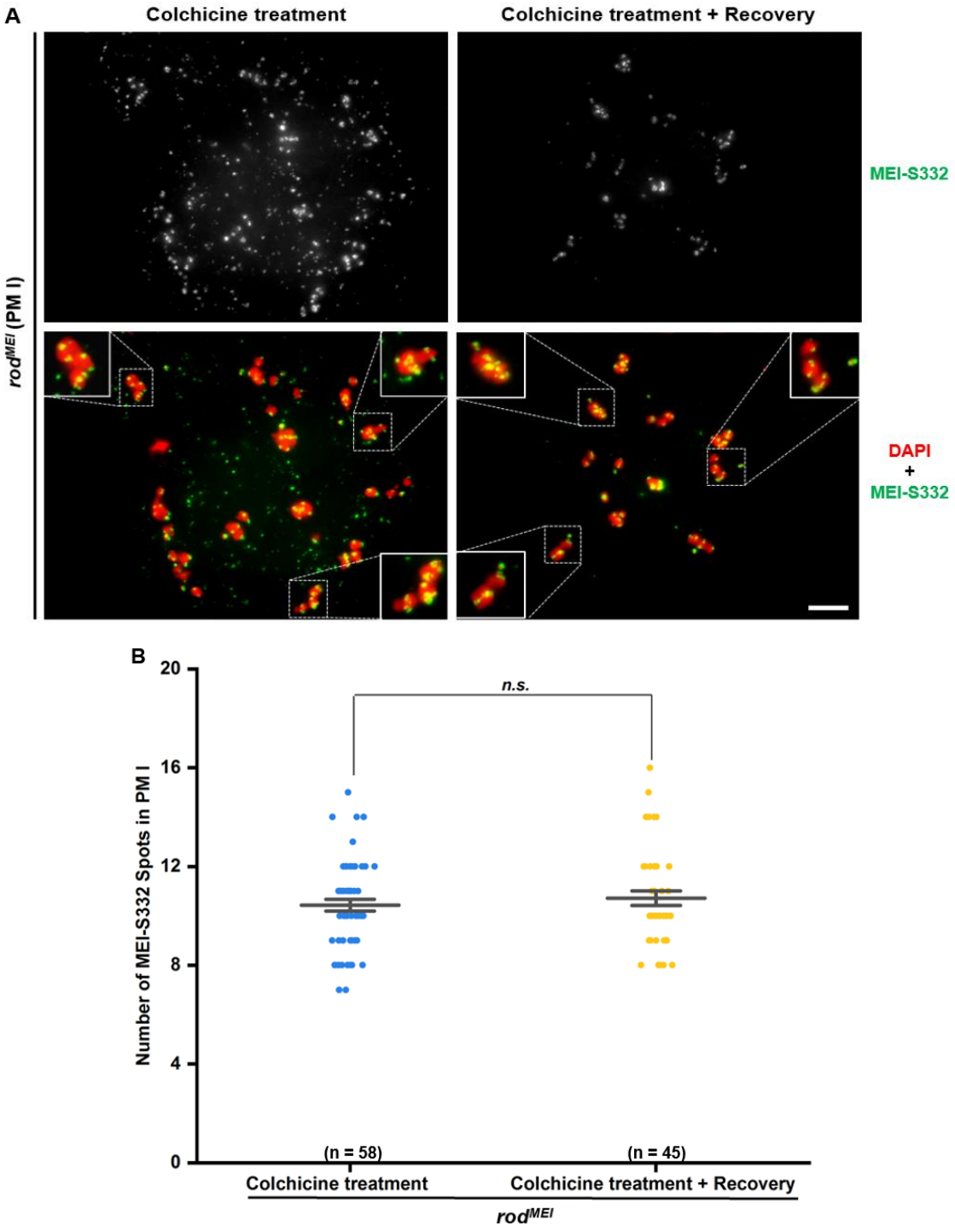

Figure 2-20. Redistribution of MEI-S332 is not reversed by compromised microtubule force. (A) Representative images for the localization of MEI-S332 at PM I under colchicine-treated and recovery conditions (B) Quantification of MEI-S332 foci at PM I under colchicine-treated and recovery conditions.

tension, but that once it occurs, it is irreversible, which could be for a variety of different reasons. These results also suggest that stable bi-orientation and MEI-S332 redistribution must usually occur quite early in prometaphase I in *rod*^{MEI} spermatocytes. If a substantial population of early prometaphase dyads was uncommitted with respect to centromere orientation, colchicine exposure would be expected to prevent stable bi-orientation and block MEI-S332 redistribution, resulting in increased frequencies of single foci. This conclusion is supported by the fact that the frequencies of split foci (both 359 foci and MEI-S332 foci) are nearly the same in PM I and M I. It is also consistent with the established role of ROD to inhibit end-on KT-MT attachments during early prometaphase. Whether the redistribution of MEI-S332 foci is a response to the establishment of dyad bipolarity or is an independent effect of the *rod*^{MEI} genotype is an important question for future research.

Summary of ROD's role in chromosome segregation in *Drosophila* male meiosis

In the present study, we uncovered checkpoint-independent functions of ROD protein during meiosis I of male *Drosophila* by using trans-heterozygous *rod*^{MEI} mutants. Our results indicated the novel roles of ROD in sister-chromatid mono-orientation and the maintenance of centromere cohesion in the first meiotic division.

In prometaphase I, *rod*^{MEI} mutations disrupt sister-chromatid orientation and convert mono-oriented sister chromatid to bi-orientation sisters, thereby triggering the redistribution of Shugoshin MEI-S332 and abrogating the preservation of cohesion complexes at centromeres prior to A I begins.

After A I onset, the activated protease Separase cleaves on the exposed cohesion

complexes and releases two sister chromatids prematurely. Therefore, these prematurely separated sisters move to opposite spindle poles under the direction of ectopically formed bi-orientation, forming equational segregation in meiosis I. Meanwhile, some bi-oriented homologs are still cohesive with a functional centromere cohesion but are also affected by aberrant bi-orientation. Some bi-oriented homologs normally adopt mono-orientation before A I onset and move back-to-back to opposite poles, but others mis-segregate side-by-side with another homolog (homologous chromosome pair) to the same pole to form 4:0 nondisjunction.

In previous studies, it has been reported that kinetochores tend to form a ring and crescent structure observed by electron microscopy prior to the attachment of MT [Ris and Witt 1981; Rattner and Bazett-Jones 1989]. Kinetochore expansion, particularly as in MT-unattached status, is assisted by the addition of outer-domain proteins to establish the outmost fibrous corona and the expanded surface of kinetochores are prone to recruit proteins involved in SAC and MT-related pathway to reinforce the checkpoint and lateral MT-kinetochore interaction. After the formation of end-on attachment, the expanded kinetochores undergo compaction to adopt bipolar orientation [Magidson et al 2015]. As an essential SAC component, it recently has been demonstrated that RZZ complex and its downstream partner SPINDLY are essential for both kinetochore expansion and compaction. ROD has a strong propensity to self-assemble into micrometer-scale filaments in *C .elegans* [Pereira et al 2018], and it might contribute to the construction of fibrous corona where further recruit the downstream effectors. ROD, on the other hand, helps the compaction of

kinetochore upon MT-attachment together with SPINDLY in a DYNEIN-dependent manner [Gama et al 2017]. Even though lateral MT attachment promoters the active kinetochore rotation and position adjustment, exaggerated kinetochores and prolonged time could give rise to errors in the conversion from lateral to end-on attachment, leading to chromosome mis-segregation [Magidson et al 2015]. Therefore, we speculate that kinetochore mis-orientation in *rod* mutants might be caused by the disrupted dynamic of the fibrous corona.

REFERENCES

Abad, J. P., Carmena, M., Baars, S., Saunders, R. D., Glover, D. M., Ludena, P., and Villasante, A. et al. (1992). Dodeca satellite: a conserved G+ C-rich satellite from the centromeric heterochromatin of Drosophila melanogaster. *Proceedings of the National Academy of Sciences*, *89*, 4663-4667.

Balicky, E. M., Endres, M. W., Lai, C., and Bickel, S. E. (2002). Meiotic cohesion requires accumulation of ORD on chromosomes before condensation. *Molecular Biology of the Cell*, *13*, 3890-3900.

Basto, R., Scaerou, F., Mische, S., Wojcik, E., Lefebvre, C., Gomes, R., and Karess, R. et al. (2004). In vivo dynamics of the rough deal checkpoint protein during Drosophila mitosis. *Current Biology*, *14*, 56-61.

Barbosa, J., Martins, T., Bange, T., Tao, L., Conde, C., and Sunkel, C. (2020). Polo regulates Spindly to prevent premature stabilization of kinetochore–microtubule attachments. *The EMBO journal*, *39*, e100789.

Bickel, S. E., Wyman, D. W., Miyazaki, W. Y., Moore, D. P., and Orr-Weaver, T. L. (1996). Identification of ORD, a Drosophila protein essential for sister chromatid cohesion. The EMBO Journal, 15, 1451-1459.

Blattner, A. C., Chaurasia, S., McKee, B. D., and Lehner, C. F. (2016). Separase is required for homolog and sister disjunction during Drosophila melanogaster male meiosis, but not for biorientation of sister centromeres. *PLoS genetics*, *12*, e1005996.

Bonaccorsi, S., Giansanti, M. G., Cenci, G., and Gatti, M. (2000). Cytological analysis of spermatocyte growth and male meiosis in Drosophila melanogaster. *Drosophila Protocols*, *87*, 109.

Carmena, M., Abad, J. P., Villasante, A., and Gonzalez, C. (1993). The Drosophila melanogaster dodecasatellite sequence is closely linked to the centromere and can form connections between sister chromatids during mitosis. *Journal of cell science*, *105*, 41-50.

Carrell, D. T., Wilcox, A. L., Lowy, L., Peterson, C. M., Jones, K. P., Erickson, L., and Hatasaka, H. H. et al. (2003). Elevated sperm chromosome aneuploidy and apoptosis in patients with unexplained recurrent pregnancy loss. *Obstetrics and Gynecology*, *101*, 1229-1235.

Chan, G. K., and Yen, T. J. (2003). The mitotic checkpoint: a signaling pathway that allows a single unattached kinetochore to inhibit mitotic exit. *PROGRESS IN CELL CYCLE RESEARCH.*, *5*, 431-440.

Chaurasia, S., and Lehner, C. F. (2018). Dynamics and control of sister kinetochore behavior during the meiotic divisions in Drosophila spermatocytes. *PLoS genetics*, *14*, e1007372.

Cheerambathur, D. K., Gassmann, R., Cook, B., Oegema, K., and Desai, A. (2013). Crosstalk between microtubule attachment complexes ensures accurate chromosome segregation. Science, 342, 1239-1242.

Corbett, K. D., and Harrison, S. C. (2012). Molecular architecture of the yeast monopolin complex. *Cell reports*, *1*, 583-589.

Galander, S., and Marston, A. L. (2020). Meiosis I kinase regulators: conserved orchestrators of reductional chromosome segregation. *BioEssays*, *42*, 2000018.

Goldstein, L. S. (1981). Kinetochore structure and its role in chromosome orientation during the first meiotic division in male D. melanogaster. *Cell*, *25*, 591-602.

Gómez, R., Valdeolmillos, A., Parra, M. T., Viera, A., Carreiro, C., Roncal, F., and Suja, J. A. et al. (2007). Mammalian SGO2 appears at the inner centromere domain and redistributes depending on tension across centromeres during meiosis II and mitosis. *EMBO reports*, *8*, 173-180.

Hamer, G., Novak, I., Kouznetsova, A., and Höög, C. (2008). Disruption of pairing and synapsis of chromosomes causes stage-specific apoptosis of male meiotic cells. *Theriogenology*, *69*, 333-339.

Harton, G. L., and Tempest, H. G. (2012). Chromosomal disorders and male infertility. *Asian Journal of Andrology*, *14*, 32.

Hauf, S., and Watanabe, Y. (2004). Kinetochore orientation in mitosis and meiosis. *Cell*, *119*, 317-327.

Hochwagen, A. (2008). Meiosis. *Current Biology*, *18*, R641-R645.

Izawa, D., and Pines, J. (2015). The mitotic checkpoint complex binds a second CDC20 to inhibit active APC/C. *Nature*, *517*, 631-634.

Karess, R. E., and Glover, D. M. (1989). rough deal: a gene required for proper mitotic segregation in Drosophila. *The Journal of Cell Biology*, *109*, 2951-2961.

Kerrebrock, A. W., Miyazaki, W. Y., Birnby, D., and Orr-Weaver, T. L. (1992). The Drosophila mei-S332 gene promotes sister-chromatid cohesion in meiosis following kinetochore differentiation. *Genetics*, *130*, 827-841.

Kerrebrock, A. W., Moore, D. P., Wu, J. S., and Orr-Weaver, T. L. (1995). Mei-S332, a Drosophila protein required for sister-chromatid cohesion, can localize to meiotic centromere regions. *Cell*, *83*, 247-256.

Kim, J., Ishiguro, K. I., Nambu, A., Akiyoshi, B., Yokobayashi, S., Kagami, A., and Watanabe, Y. et al. (2015). Meikin is a conserved regulator of meiosis-I-specific kinetochore function. *Nature*, *517*, 466-471.

Kops, G. J., and Gassmann, R. (2020). Crowning the kinetochore: the fibrous corona in chromosome segregation. *Trends in Cell Biology*, *30*, 653-667.

Krishnan, B., Thomas, S. E., Yan, R., Yamada, H., Zhulin, I. B., and McKee, B. D. (2014). Sisters unbound is required for meiotic centromeric cohesion in Drosophila melanogaster. *Genetics*, *198*, 947-965.

Lara-Gonzalez, P., Westhorpe, F. G., and Taylor, S. S. (2012). The spindle assembly checkpoint. *Current Biology*, *22*, R966-R980.

Liu, H., Jia, L., and Yu, H. (2013). Phospho-H2A and cohesin specify distinct tension-regulated Sgo1 pools at kinetochores and inner centromeres. *Current Biology*, *23*, 1927-1933.

Marston, A. L., and Amon, A. (2005). Erratum: Meiosis: Cell-cycle controls shuffle and deal. *Nature Reviews Molecular Cell Biology*, *6*, 818-818.

MacLennan, M., Crichton, J. H., Playfoot, C. J., and Adams, I. R. (2015). Oocyte development, meiosis and aneuploidy. In *Seminars in cell & developmental biology* , *Vol. 45*, pp. 68-76. Academic Press.

McKee, B. D., Yan, R., and Tsai, J. H. (2012). Meiosis in male Drosophila. *Spermatogenesis*, *2*, 167-184.

Musacchio, A., and Salmon, E. D. (2007). The spindle-assembly checkpoint in space and time. *Nature Reviews Molecular Cell Biology*, *8*, 379-393.

Ni, J. Q., Zhou, R., Czech, B., Liu, L. P., Holderbaum, L., Yang-Zhou, D., and Perrimon, N. et al. (2011). A genome-scale shRNA resource for transgenic RNAi in Drosophila. *Nature Methods*, *8*, 405-407.

Onn, I., Heidinger-Pauli, J. M., Guacci, V., Ünal, E., and Koshland, D. E. (2008). Sister chromatid cohesion: a simple concept with a complex reality. *Annual Review of Cell and Developmental Biology*, *24*, 105-129.

Orr-Weaver, T. L. (1995). Meiosis in Drosophila: seeing is believing. *Proceedings of the National Academy of Sciences*, *92*, 10443-10449.

Pereira, C., Reis, R. M., Gama, J. B., Celestino, R., Cheerambathur, D. K., Carvalho, A. X., and Gassmann, R. (2018). Self-assembly of the RZZ complex into filaments drives kinetochore expansion in the absence of microtubule attachment. *Current Biology*, *28*, 3408-3421.

Peters, J. M., Tedeschi, A., and Schmitz, J. (2008). The cohesin complex and its roles in chromosome biology. *Genes & Development*, *22*, 3089-3114.

Potapova, T., and Gorbsky, G. J. (2017). The consequences of chromosome segregation errors in mitosis and meiosis. *Biology*, *6*, 12.

Rahmani, Z., Gagou, M. E., Lefebvre, C., Emre, D., and Karess, R. E. (2009). Separating the spindle, checkpoint, and timer functions of BubR1. *The Journal of Cell Biology*, *187*, 597-605.

Rosen, L. E., Klebba, J. E., Asfaha, J. B., Ghent, C. M., Campbell, M. G., Cheng, Y., and Morgan, D. O. (2019). Cohesin cleavage by separase is enhanced by a substrate motif distinct from the cleavage site. *Nature communications*, *10*, 1-10.

Scaërou, F., Aguilera, I., Saunders, R., Kane, N., Blottière, L., and Karess, R. (1999). The rough deal protein is a new kinetochore component required for accurate chromosome segregation in Drosophila. *Journal of Cell Science*, *112*, 3757-3768.

Thomas, S. E., Soltani-Bejnood, M., Roth, P., Dorn, R., Logsdon Jr, J. M., and McKee, B. D. (2005). Identification of two proteins required for conjunction and regular segregation of achiasmate homologs in Drosophila male meiosis. *Cell*, *123*, 555-568.

Tomkiel, J. E., Wakimoto, B. T., and Briscoe Jr, A. (2001). The teflon gene is required for maintenance of autosomal homolog pairing at meiosis I in male Drosophila melanogaster. *Genetics*, *157*, 273-281.

Tóth, A., Rabitsch, K. P., Gálová, M., Schleiffer, A., Buonomo, S. B., and Nasmyth, K. (2000). Functional genomics identifies monopolin: a kinetochore protein required for segregation of homologs during meiosis I. *Cell*, *103*, 1155-1168.

Vendrell, X., Ferrer, M., García-Mengual, E., Munoz, P., Trivino, J. C., Calatayud, C., and Ruiz-Jorro, M. et al. (2014). Correlation between aneuploidy, apoptotic markers and DNA fragmentation in spermatozoa from normozoospermic patients. *Reproductive Biomedicine Online*, *28*(4), 492-502.

Watanabe, Y. (2005). Shugoshin: guardian spirit at the centromere. *Current Opinion in*

Cell Biology, *17*, 590-595.
Watanabe, Y. (2006). A one-sided view of kinetochore attachment in meiosis. *Cell*, *126*, 1030-1032.
Watanabe, Y. (2012). Geometry and force behind kinetochore orientation: lessons from meiosis. *Nature Reviews Molecular Cell Biology*, *13*, 370-382.
White-Cooper, H. (2004). Analysis of Meiosis and Morphogenesis. *Drosophila Cytogenetics Protocols*, 45.
Yamada, T., Tahara, E., Kanke, M., Kuwata, K., and Nishiyama, T. (2017). Drosophila Dalmatian combines sororin and shugoshin roles in establishment and protection of cohesion. *The EMBO journal*, *36*, 1513-1527.
Yan, R., Thomas, S. E., Tsai, J. H., Yamada, Y., and McKee, B. D. (2010). SOLO: a meiotic protein required for centromere cohesion, coorientation, and SMC1 localization in Drosophila melanogaster. *The Journal of Cell Biology*, *188*, 335-349.
Yokobayashi, S., and Watanabe, Y. (2005). The kinetochore protein Moa1 enables cohesion-mediated monopolar attachment at meiosis I. *Cell*, *123*, 803-817.
Zhou, J., Yao, J., and Joshi, H. C. (2002). Attachment and tension in the spindle assembly checkpoint. *Journal of Cell Science, 115*, 3547-3555.

CHAPTER III: EVALUATION OF DROSOPHILA SITE-SPECIFIC DNA INTEGRATION ACHIEVED BY CRISPR-MEDIATED KNOCK-IN AND PHIC31 INTEGRASE-MEDIATED RECOMBINATION

ABSTRACT

Gene editing is a powerful tool to change the genetic information stored in the organism's genome which can be inherited by the offspring. Recently, a novel gene-editing technique CRISPR, derived from bacterial adaptive immune system, brought a revolution into the biological field. Due to the extraordinary simplicity and specificity, CRISPR-mediated gene editing has been extensively used in eukaryotic organisms, from yeast to humans. Through the DNA repair pathway of double-strand break, CRISPR is capable of creating deletions, insertions and point mutations as well as DNA integration at specific sites in the genome, depending on Cas nuclease and the presence of PAM sites. Previously, we have identified novel functions of the checkpoint protein ROD in *Drosophila* spermatocytes. The mutations in *rod* resulted in premature loss of sister chromatid cohesion and a disrupted sister-chromatid orientation, eventually leading to chromosome mis-segregation in anaphase I. However, the frequency of chromosome nondisjunction and incomplete loss of sister centromere cohesion indicated a hypomorphic effect of the trans-heterozygous rod^{MEI} alleles. Since the rod gene is essential for both mitosis and meiosis, homozygosity of previously identified *rod* mutant alleles causes lethality in early development and sterility in the rare adult survivors. Therefore, we endeavored to combine CRISPR-mediated genome editing and plant-derived auxin-inducible degradation system to create conditional null-like *rod* mutants, which would allow us to further investigate the potential mechanisms associated with the phenotype we observed in rod^{MEI} mutants. We introduced an auxin-inducible degron into rod locus

through HDR- and MMEJ-mediated CRISPR, while achieved the genome integration of ubiquitin ligase-related F box protein TIR1 by phage phiC31 site-specific recombinase. Our result showed that no transformant was observed in genome integration through the MMEJ pathway and short homology arm-mediated HDR pathway. However, successfully transformed flies were obtained in the integration by CRISPR using long homology arms and phiC31 integrase system. PCR-based verification and Sanger DNA sequencing provided evidence that the size and position of the integrated DNAs were correct in transformed flies.

INTRODUCTION

In Chapter 2, we deployed a comprehensive study of ROD's role, as narrated in Chapter 2, by using the combination of genetic and cytological approaches in *Drosophila* spermatocytes. Our results have demonstrated that ROD is required for the establishment of meiosis-specific mono-orientation and the maintenance of centromere cohesion after metaphase I. Mutations in *rod* gene gave rise to the perturbed orientation on homologs or chromatids reflected by the high frequency of various chromosome laggards in anaphase I and led to the premature destruction of centromere cohesion by ectopic redistribution of *Drosophila* Shugoshin protein MEI-S332, by which chromosome mis-segregation was prevalent in the first meiotic division. Based on the obtained phenotypic defects in *rod*-mutant spermatocytes, the top priority is to understand how kinetochore-bound ROD protein interacts with microtubules and cohesion-associated proteins. However, the overall NDJ frequencies in rod^{MEI} mutants on both sex chromosomes and autosomes are much lower than those in the null mutation of either conjunction or cohesion proteins. Besides, the *rod* null mutants are lethal at the early developmental stage, but rod^{MEI} mutants were viable and only showed the meiosis-specific phenotype of chromosome segregation in our study. Although homolog conjunction was not affected by the mutations in *rod*, a clear phenotype of premature loss of centromere cohesion was evident in rod^{MEI} mutants. However, the frequency of equational segregation, a hallmark of precocious cohesion loss, was less than 40%, which is much lower than that observed in *solo* and *sunn* mutants (approximately 70% in both) [Yan et al 2010; Krishnan et al 2014]. Taken

together, we hypothesized that the genotype of *rod*^{MEI} may bear a reduced function, not null, on kinetochores that might obscure the characterization of ROD's comprehensive roles in meiotic chromosome segregation.

To fully understand ROD's function in *Drosophila* meiosis, the subsequent mechanism investigations would favor a genetically null-like background of *rod* to display the phenotype more clearly and increase the signal/noise ratio in the ensuing cytological and biochemical analysis. Unfortunately, the previously identified *rod* mutant alleles, like *rod*$^{X-1}$ to *rod*$^{X-5}$, contained severe DNA lesions and the homozygotes with these *rod* alleles were inviable and sterile [Karess and Glover 1989]. In higher eukaryotic organisms, the spermatogenesis undergoes four rounds of mitotic divisions from differentiated blast cells to pre-meiotic spermatogonia. Along with this process, the detrimental effects are accumulated in the germline, which can result in sterility eventually. So, the ideal manipulation is to deplete the function of ROD in meiotic cells only, by which a clear role of ROD in meiosis can be captured without any interference coming from mitotic defects.

In *Drosophila melanogaster*, conventional genomic engineering for precise mutations, like point mutations, involves the construction of genes with desirable mutations and the transformation of germline with constructed genes carried by insect-specific transformation vectors. The transposable elements, such as P-element, on the transformation vector, mediates the integration of the transgenes into the genome and the functional detection is performed by the introduction of the allele with a transgene into a null background of the gene of interest. This technique is time-

consuming since it demands a long time for the screening of transformed progeny and additional steps to wipe out the endogenous gene. Moreover, the location of transgene insertion sites is nearly random, so it brings, at least, two disadvantages: 1) it is possible to create an unpredictable secondary mutation anywhere in the genome; 2) the expression of integrated transgene might be unstable and affected by the transcriptional regulators or genomic landscape near the insertion site.

Alternatively, precise gain/loss-function of a gene can be achieved by gene editing, which depends on the generation of DNA double-strand break on a particular site of chromosome and the endogenous DNA repair pathways. In eukaryotic organisms, DNA double-strand break is usually repaired by two classic pathways: non-homologous end joining (NHEJ) and homology-directed repair (HDR). NHEJ events are prevalent throughout the cell cycle and are responsible for the DNA repair without a homologous template, even though it is an error-prone event. NHEJ repair pathway recruits protein factors to re-ligate the break ends, on which it often induces deletions or insertions (referred to as indels) during this process. In contrast, HDR requires the presence of a homologous donor DNA, such as duplicated sister chromatid, to precisely repair double-strand breaks. So, HDR is mainly involved and active in the late S and G2 phase in which sister chromatids appear after DNA replication. In terms of the applications, NHEJ is commonly used for the disruption of genes' function by introducing indels, whereas HDR is a sophisticated DNA repair pathway that can be employed to faithfully introduce a desired mutation or mediate gene knock-in [Rothkamm et al 2003; Wyman and Kanaar 2006; Salsman and Dellaire 2017].

How to induce a DNA double-strand break artificially in a desired site on a chromosome has long been a question for gene editing. The first breakthrough in this field was the identification and engineering of zinc finger nucleases (ZFNs), consisting of a sequence-specific Cys2-His2 zinc finger protein and a non-specific restriction enzyme FOKI. Zinc finger proteins are commonly associated with the transcription regulation and protein-protein interactions, while FOKI is responsible for the creation of DNA double-strand break [Urnov et al 2010; Carroll 2011]. Several years later, another DNA binding protein called transcription activator-like effector (TALE) was identified in plant pathogenic bacterial, composed of two flanking amino acid repeats with a central DNA binding region, named repeat variable di-residues. Then, TALEs have been fused with FOKI to form a new DNA-cutting weapon, termed TALE nucleases (TALENs). Compared to the previous ZFNs, TALENs take less time to produce and are able to bind more types of genomic sites, not so limited as zinc finger proteins. However, the large size of TALENs is a flaw and the other one is the off-target effect [Zhang et al 2013; Joung and Sander 2013].

In the past decade, a novel genome-editing tool was invented based on clustered regularly-interspaced short palindromic repeats, also known as CRISPR, which was derived from the adaptive prokaryotic immune system (CRISPR-associated system or Cas) [Mojica, et al 2005; Van der Oost et al 2009]. The extensive applications of CRISPR, due to its simplicity and specificity, brought a revolution in the field of gene editing and accelerated the pace of biomedical research. Transplantation and development of this technique in different eukaryotic organisms intensify and enhance

the studies of, but not restricted to, the mechanism of genetic diseases, the development of novel gene therapies, and the engineering of transgenic animals [Gaspar et al 2011; Wang et al 2013; Findlay et al 2014]. Recently, six types of CRISPR systems have been identified but the type II CRISPR system that requires only one Cas9 protein has emerged as a powerful tool for the introduction of a site-specific DNA double-strand break in a variety of organisms. In principle, type II system-mediated double-strand break depends on three core components: trans-activating RNA (tacrine), Cas9 protein and CRISPR RNA (crRNA) with site-specific spacer sequence (Figure 3-1). Once transcribed, tracer and pre-crRNA are bound and stabilized by the Cas9 protein. Then, pre-crRNA is processed by endogenous RNase III to form a mature crRNA:tracrRNA:Cas9 complex. In order to simplify the two components into one, tharra and crRNA can be combined to form a functional single-guide RNA (sgRNA). Target specificity is derived from the designed spacer sequence which recognizes the short protospacer-adjacent motif (PAM, 5'-NGG-3' in *Streptococcus pyogenes*) and unwinds double-strand DNA in the adjacent area. In *Drosophila*, numerous studies have demonstrated the feasibility of site-specific mutagenesis in different target genes by the CRISPR-Cas9 system. The first attempt was reported by Gratz et al who co-injected two plasmids containing Cas9 and sgRNA into *Drosophila* embryo to disrupt the expression of *yellow* (*y*) gene, but the transmission rate of mutagenesis was only 5.9%. Later, the authors found that the mutagenesis rate was significantly increased when they supplied the injection with one more sgRNA to the other end of *y* gene [Gratz et al 2013]. In the subsequent studies, *Drosophila*

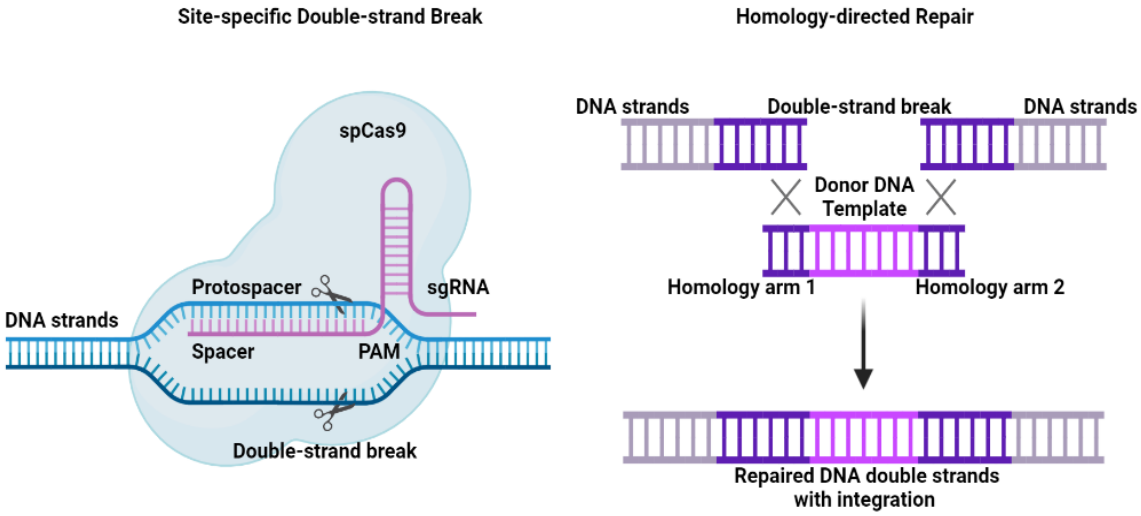

Figure 3-1. CRISPR-induced DNA double-strand break and homology-directed repair.

researchers modified a variety of approaches on the delivery methods for Cas9 and gRNA, the optimization of the driver for sgRNA expression and the prevention of off-target effect to achieve high efficiency of CRISPR in gene- or tissue-specific mutagenesis [Bassett et al 2014; Meltzer et al 2019]. One of the advanced CRISPR-boosting techniques is the employment of tRNAs in sgRNA expression cassette, which not only benefits the multiple gene targeting but also significantly increases the efficiency of gene editing. This approach highlights the efficient transcription of multiple sgRNAs flanking by tRNAs in one unit and the separation of tRNA-linked sgRNA is mediated by the conserved tRNA-processing pathway that cut the tRNA on 5' leader and 3' trailer by RNase P and RNase Z, respectively. In recent studies, tRNA-associated sgRNAs not only realized the targeting of multiple gene sites (up to 4) in rice but further enhanced the efficiency of single-gene disruption in *Drosophila* by 17% [Xie et al 2015; Port, & Bullock 2016].

The repair of DNA double-strand break is the central event in gene editing, and it mainly depends on NHEJ and HDR pathways. However, the latest studies uncovered an alternative mechanism for double-strand break repair, termed microhomology-mediated end joining (MMEJ). When a short homologous DNA strand exists, the two ends of double-strand break tend to take advantage of the microhomology of the short homologous DNA to implement the repair process. MMEJ takes place in M and early S phase when HDR is inactive, so it can serve as a complementary homology-dependent process in DNA repair. In human cells, MMEJ has been shown to mediate the high frequency of site-directed deletions by using TALENs and CRISPR, which

exhibited its extraordinary capacity and compatibility in gene editing [Bae et al 2014]. Recently, multiple studies pointed out that the mechanism of MMEJ is conserved in *Drosophila*, *C.elegans*, Zebrafish and Mouse, and, in these species, MMEJ relies on the endogenous polymerase θ (Pol θ), a polymerase-helicase fusion protein encoded by mus308 gene [Koole et al 2014; Yousefzadeh et al 2014; Thyme & Schier 2016; Beagan et al 2017]. Pol θ acts on the 3' single-strand DNA overhangs generated by 5'-3' exonuclease resection to execute DNA repair for double-strand breaks and interstrand crosslinks by the activation of the MMEJ pathway [Black et al 2019]. Therefore, MMEJ is an efficient mean for the loss-of-function study, but it has also been reported to efficiently mediate genome integration in vertebrates. Nakade et al developed a novel system of MMEJ-based gene knock-in, termed precise integration into target chromosome (PITCh), and the exogenous DNA can be delivered accurately into specific genomic sites by short homology arms (8-40 bp) on double-strand donor DNA. However, shorter homology arms might undermine the accuracy of the junction and result in compromised knock-in efficiency. Besides the feature of microhomology, this system highlights the addition of short PITCh sequences flanking homology arms, on which an integrated PITCh sgRNA triggers the Cas9-mediated cleavage and liberates donor DNA from the vector. Then, the free donor DNA largely prevents the incidence of the whole-vector integration and the unexpected variations on the integration site. However, the efficiency of PITCh in *Drosophila* has not been tested as yet.

Regardless of the types of gene editing, the alteration of endogenous DNA

depends on the directions of the artificially produced transformation vectors (exogenous DNA). Current molecular cloning involved a high-frequent DNA shuffling from one vector to another, e.g. from the entry vector to expression vector. Although some recombination-based strategies create user-friendly and flexible approaches to assist DNA relocations, the biggest issue is the remaining residual nucleotides on the recombination site, which might cause the addition of unwanted amino acids or influence gene transcription, like frameshift mutation. A desirable DNA transfer plan requires a convenient DNA breakage & ligation and a scarless shuffling between each step of construct assembly. Recently, a powerful cloning strategy, named Golden Gate cloning, has been developed to support this idea by Engler et al who designed a comprehensive vector system allowing the modular assembly of vectors for complicated DNA cloning [Engler et al 2008; 2009]. The operation of Golden Gate cloning depends on the application of type IIs restriction endonucleases, such as BbsI and BsaI, which cleaves DNA double strands outside of their recognition sites, leaving 5’ or 3’ DNA overhangs that consist of any nucleotides. Therefore, it can realize the scar-free shuffling from the entry clone to the destination vector by incorporating the first or last several nucleotides on DNA constructs into enzyme recognition sites. To achieve great convenience during DNA transfer, the authors produced several sets of vectors and each of them contained linear linked recognition sites for two different Type IIs enzymes in a simplified plasmid backbone. In the first digestion, a DNA construct can be inserted into the vector accompanying with the destruction of one recognition site inside while another restriction enzyme can recognize the other one

outside in the next round of assembly, by which the DNA construct can be shuffled to another vector by itself or together with other constructs with complementary overhangs. Golden gate cloning encompasses two advantages - one-step DNA digestion & ligation in the same tube and the maximum flexibility of vector assembly without the concern of unnecessary DNA sequences.

MATERIALS AND METHODS

The vector constructions for CRISPR-mediated genome integration

In this project, the utmost goal is to incorporate comprehensive protein tags in the endogenous *rod* gene locus on chromosome 3, including a fluorescent Venus tag, an auxin-inducible degron and a short Twin-Strep tag. Based on previous studies, various fluorescence tags turned out to be functional in either C- or N-terminus of ROD, so we located a PAM site 17 bp upstream of the stop codon as the sgRNA-recognition site, not only because this site was extremely close to the desired insertion site but the evaluation of off-target was considerably lower than other PAM sits in the two ends of ROD protein (performed by using CRISPR Optimal Target Finder [Gratz et al 2014]). Based on this design, all the integrated tags were transcribed along with the endogenous *rod* gene under the same regulation. To drive the expression of sgRNA efficiently in vivo, we used U6:3 RNA promoter and integrated the sgRNA in a tandemly arrayed tRNA cassette. U6:3 promoter exhibited an extraordinary potency in *Drosophila* CRISPR/Cas9-mediated genome editing among the three U6 promoters [Port et al 2014]. The tRNA constructs flanking the sgRNA, by utilizing an in-vivo tRNA process system, can significantly enhance the efficiency and accuracy of a double-strand break on the PAM site (explained in the introduction).

Unlike the single type of sgRNA targeted to the C-terminal PAM site of ROD, donor DNA, containing all the tags, was designed in three different forms corresponding to three distinct mechanisms. First, we would like to test whether the

overall length of homology arms is associated with the success of long sequence integration through homology-directed repair (HDR), as reported in *Drosophila* culture cell (S2 cell) where the sgRNA was transfected into cells. Therefore, we designed two homology arms in the length of 600 bp (short HA arms) and 1 kb (long HA arms). In addition, the alternative microhomology-mediated end joining can mediate DNA repair efficiently during M to early S phase and was also included in our trial by designing a pair of short homology arms with 23 nucleotides, which was anticipated to facilitate the genomic integration in the Cas9-induced DSB sites better than the traditional HDR pathway. Between the two homology arms on the vector, the first element was auxin-induced degron which can be recognized by plant F-box protein TIR1 resulting in the ubiquitination-mediated degradation at the presence of auxin. The following two components were yellow fluorescence tag mVenus and pulldown tag Twin-strep. mVenus is a monomeric yellow fluorescent protein derived from green fluorescent protein (GFP) in *Aequorea victoria*, and multiple point mutations created in EYFP scaffold that not only slightly shift the light wavelength of excitation and emission but enhance the quantum yield and maturation in vivo [Kremers et al 2006]. In our previous studies in *Drosophila* spermatocytes, mVenus tag has been used for tracking the localization of centromeric cohesion proteins (SOLO and SUNN) until Anaphase II [Yan et al 2010; Krishnan et al 2014], so we believed that it might show a good capacity to label ROD in the same physiological condition. Twin-strep was selected as a pull-down tag due to its short length and high binding affinity for the sake of purification specificity. Strep-tag is developed based on

the well-known binding between biotin and streptavidin, and it is only composed of 8 amino acids (Trp-Ser-His-Pro-Gln-Phe-Glu-Lys). Twin-strep contains two copies of Strep-tag including a flexible linker in between. The purification of the fusion protein can be performed in a commercially available Strep-Tactin column with a high capacity of up to 500nmol and the pull-down efficiency of Twin-strep tag has been well-documented in *Drosophila* S2 cells [Barišić-Jäger et al 2013]. Outside the main functional units, we supplied the donor construct with a dsRed gene flanking by transposable PiggyBac sequences, by which the successfully transformed flies bear red fluorescence eyes and, after the screening of transformants, a scarless removal of dsRed can be realized by the artificial activation of PiggyBac transposable ability.

Conditional depletion of ROD requires the coincidence of three essential components - degron signal, auxin and plant F-box protein TIR1. Since the transformation of F box protein not necessarily coincided with the CRISPR-integration system, we constructed another vector to allow the expression of TIR protein, exclusively in spermatocytes. Spermatocytes-specific expression was regulated by the promoter of bam (bags of marbles) that has been verified to efficiently drive the expression of conjunction protein (MNM) in early *Drosophila* spermatocytes. Even though it is unknown where the exogenously expressed TIR1 protein localizes in the cell and whether it exists in a structure-bound form or in a diffusible form, we tagged TIR1 protein with a monomeric red fluorescent protein, called mScarlet and bam promoter-TIR1-mScarlet construct was enclosed in one-single transcriptional unit separated from other functional elements by Gypsy

insulators. Genomic integration was achieved by phage phiC31 integrase, so an attB sequence was inserted in the TIR1 expression vector. With the presence of the phiC31 integrase, site-specific recombination mediates the integration of attB-containing construct in a chosen attP sites [Growth et al 2004; Huang et al 2009]. The last piece in this vector was *mini-white* gene which served as a transformation marker in offspring screening, thereby the transformed progeny were those with orange eyes in a *w* background.

Some technical details involving the design of the constructs are also of significance to assure the success and accuracy of gene editing. First, to prevent recurrent Cas9-dependent DNA breaks, the nucleotides on the PAM site deployed for the integration were replaced by the substitutions that encode the same amino acids. Moreover, all of the functional DNA sequences used in this study, such as AID, mVenus and TIR1, underwent codon optimization to replace the rare codons for the sake of better expression in *Drosophila* cells. In addition, Golden Gate DNA shuffling provides great convenience for the stepwise assembly of a large destination vector from many small entry vectors, but each DNA shuffling from one vector to another brings the addition of short adaptor sequences (three nucleotides in both ends) to the new vector. Therefore, the newly inherited nucleotides from old vectors should be taken into consideration in the design of DNA constructs in each reaction and this issue usually can be addressed by incorporating them in a short flexible linker to separate linearized-arrayed functional units on the vector.

Molecular Constructions of Transformation Vectors

In CRISPR-mediated knock-in, the Golden Gate assembly allows us to use a concise destination vector only bearing desired DNA constructs, so we were able to combine both sgRNA-coding sequence and donor DNA with homology arms and they can be transformed concomitantly and efficiently into *Drosophila* embryos. Since we included the trial for the three types of homology arms, we anticipated to make three destination vectors in total: 1) sgRNA-HA(23 bp, MMEJ)-donor DNA; 2) sgRNA-HA(600 bp, HDR)-donor DNA; 3) sgRNA-HA(1 kb, HDR)-donor DNA. All the plasmids used in Golden Gate assembly were contained in a MoClo toolkit purchased from addgene and preserved in bacterial cells on a 96-well plate with a specific code (for example: pAGM or pICH).

The first step in the assembly of gRNA cassette was to load the DNA sequences of FRT sites, U6::3 promoter, sgRNA (including scaffold and spacer) and polymerase III terminator (Pol-III T) into the entry vector (pAGM1311) by using BbsI to create the following entry clones: CAGA-FRT1-CCAT, CCAT-U6::3-TGCA, TGCA-sgRNA-tRNA-GTTT, GTTT-Pol-III T-TGTG, GAGC-FRT2-TGCC (Figure 3-2). Then, these entry clones were further transferred into a level-M vector (pAGM8079) together with TGTG-attB-GAGC (pICH47781) and TGCC end-linker (pICH50932) by using BsaI. In the next step, the integrated construct CAGA-FRT1-U6::3-sgRNA-Pol-III T-attB-FRT2-TGCC was transferred from a level-M vector to a level-P vector (pICH75366) by using a TGCC-end linker (pICH79311).

For the donor DNA construction, the assembly was initiated from insertions of

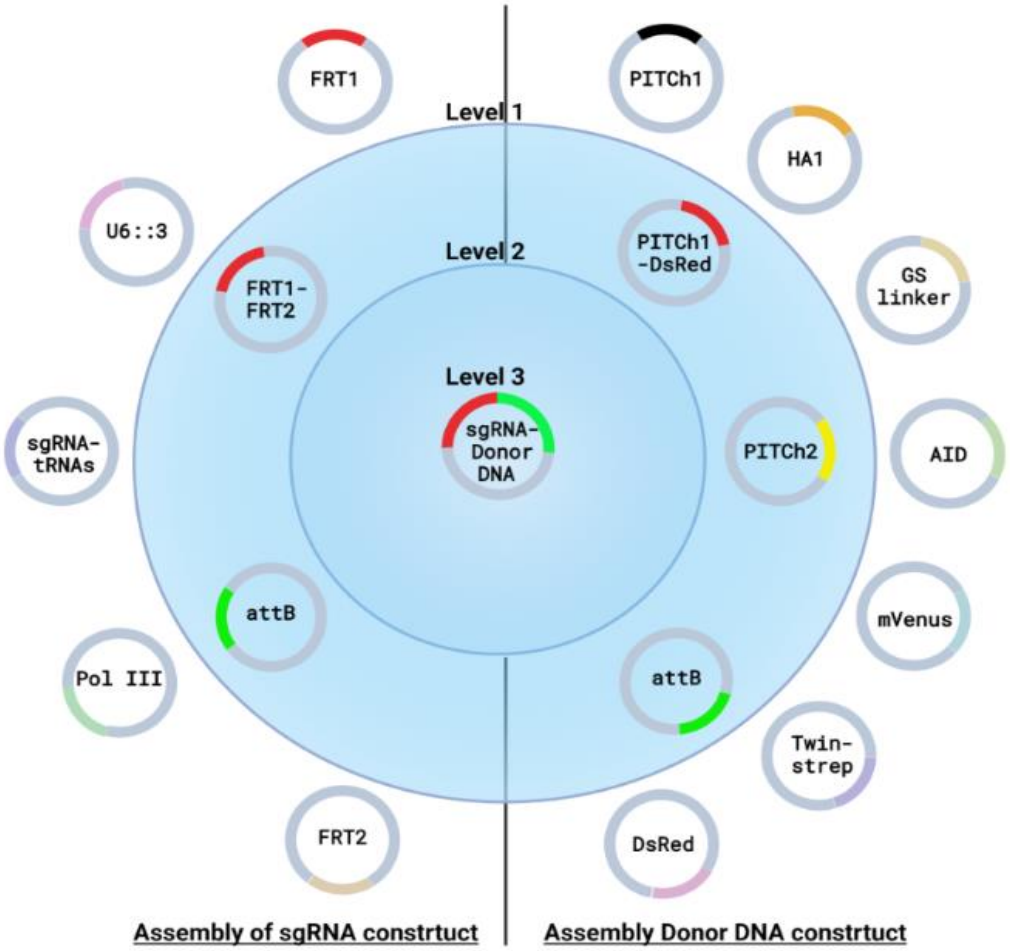

Figure 3-2. Hierarchical assembly of sgRNA and donor DNA constructs.

eight components into corresponding entry vectors with the same vector-adaptors to form head-to-tail links by using BbsI: GGAG-PITCh1-TACT (pICH41233), TACT-HA1-CCAT (pAGM1263), CCAT-GS linker-AATG (pAGM1276), AATG-AID-AGGT (pICH41258), AGGT-mVenus-TTCG (pAGM1299), TTCG-Twin-strep-GCTT (pAGM1301), GCTT-piggyBacDsRed-GGTA (pICH53388) and GGTA-HA2-CGCT (pICH53399).The overlapped adaptors between each two constructs allowed them to assembly into a linearized unit on an intermediate vector (pICH47732) by using BsaI and to form an integrated construct TGCC-PITCh-HA1-GS linker-AID-mVenus-Twin-strep-PiggyBacDsRed-HA2-GCAA.

The final assembly was to form a combined vector with both gRNA and donor DNA, and it was accomplished in an additional Golden Gate reaction in which the previous obtained CAGA-FRT1-U6::3-sgRNA-Pol-III T-attB-FRT2-TGCC and TGCC-PITCh-HA1-GS linker-AID-mVenus-Twin-strep-PiggyBacDsRed-HA2-GCAA were transferred by using BbsI, together with GCAA-PITCh2-ACTA (pAGM1311) and end-linker TTAC into a modified destination vector - M8079delta (derived from pAGM8079), favoring of the expression in animal cells.

Separating from CRISPR vector construction, the assembly of the TIR1 vector started from the insertion of the TIR1 transcription unit in the entry vectors (pAGM1311) and then shuffling them to five intermediate clones: GGAG-bam promoter-AATG (pICH41295), AATG-TIR1-AGGT (pICH41258), AGGT-mScarlet-GCTT (pICH41264), GCTT-P10 terminator-GGTA (pICH53388) and GGTA-Gypsy2-CGCT (pICH53399) (Figure 3-3). The final step was conducted by combining the

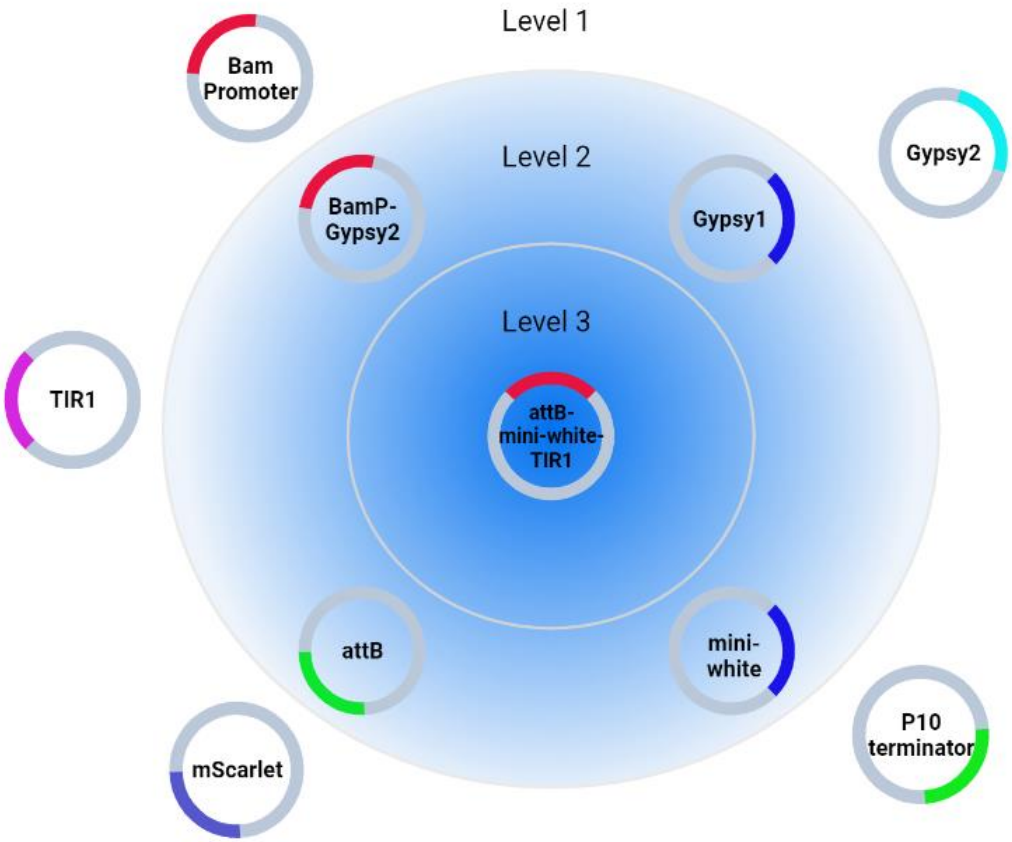

Figure 3-3. Hierarchical assembly of TIR1-expressing construct.

entire TIR1 transcriptional unit with attB site, *mini-white* gene, Gypsy1 and end-liner GGGA into the destination M8079delta vector.

Fly transformation, screening and verification

Drosophila transformation was conducted by embryo microinjection (Bestgene) and three sgRNA-donor DNA vectors were purified by midi-prep kit (Qiagen) with distinct homology arms (23 bp, 600 bp and 1 kb, respectively) were injected independently into different batches of embryos collected from Cas9-expressing stock (*yw*; *nos*-Cas9 attP40/*CyO*) (Figure 3-4). More than 300 embryos were injected for each line, from which the surviving larvae were collected, named MMEJ, HA600 and HA1000. Since *rod* gene locates on chromosome 3, we decided to use the att40 site on chromosome 2 as the landing position of attB on the TIR1 expression vector, so the plasmid after purification was injected in the embryos of P{nos-phiC31.NLS}X; P{attP40} and the use of nanos driver allowed the expression of phiC31 integrase exclusively in the germline, and thereby located TIR1 construct on the 2nd chromosome.

The hatched individuals from the three injected lines were crossed to males and virgins from the double-balancer stock *w*; *CyO*/*Sco*; *MKRS*/*TM6B*. Among the progeny, we screened the individuals with the genotype of CyO/*Sco*; *rod** (potentially modified *rod*) or +/*TM6B* or *MKRS,* by which the cas9-containing allele was removed from the genome and the potential *rod** allele was balanced. After that, they underwent the detection of the DsRed signal (bright red color) in their eyes to getting rid of +/*TM6B* or *MKRS* without the DsRed signal, and the DsRed-positive

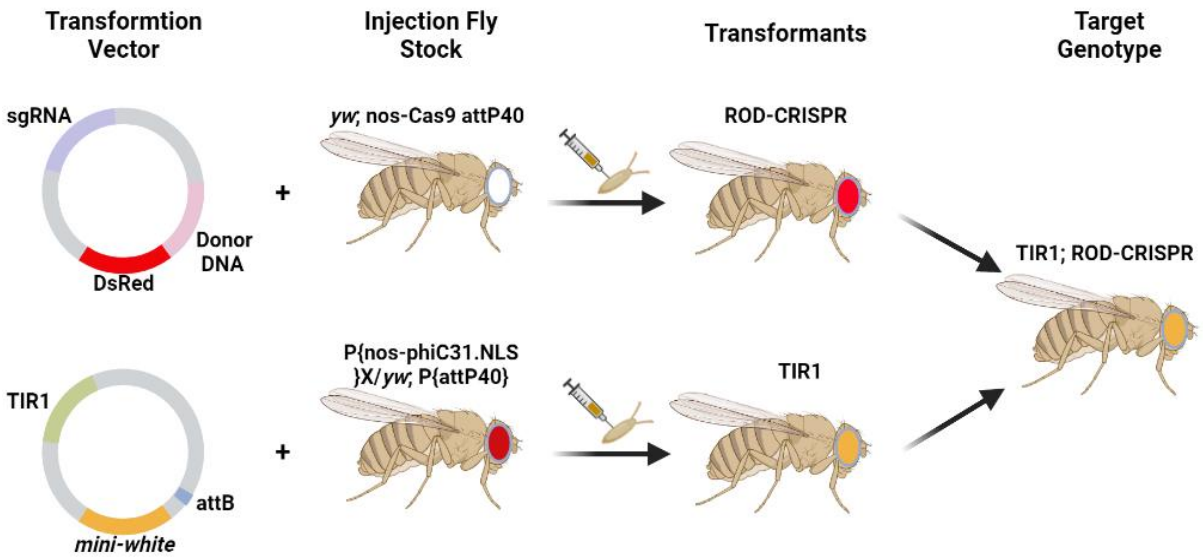

Figure 3-4. Fly transformation and transformants' screening.

transformants were maintained. To removal the DsRed maker from the genome, we crossed DsRed-positive males (*w*; *CyO*/*Sco*; rod-AID-mVenus-Twin-strep-piggyBacDsRed*/MKRS*) with the virgins from the stock of *w*; Tub-PBac transposase/*CyO*; *MKRS*/*TM6B* (where PBac transposase was expressed) and, in the population of progeny, those showed white eyes without fluorescence, indicating the successful removal of piggBacDsRed sequence, were undergone another round of cross to the flies from double-balancer stock, by which Tub-PBac transposase allele was removed from the isolated stock. The screening of transformants for TIR1 integration was relatively easier. Since TIR1 construct bearing *mini-white* was injected into a *w* mutant background, the successfully transformed flies showed orange eyes in the F1 generation and were balanced by the following two crosses to the flies from double-balancer stock. Finally, the stock of *w*; TIR1 *mini-white*/*CyO*; *MKRS/TM6B* was maintained in the lab.

Although the DsRed marker in the eyes of transformants is a good indicator for the success of CRISPR-mediated integration, the most convincing evidence would be the exhibition of a modified *rod* locus in the transformants' genome. Polymerase chain reaction (PCR)-based verifications were used along the process of genome editing. First, the sequence of each functional unit in the entry vector was confirmed by gene-specific PCR and Sanger DNA sequencing, after which only the constructs showed correct results in both tests were used in the next-step DNA assembly. The other two rounds of PCR confirmations were carried out for the inspections of *rod* gene in transformants' genome before and after the removal of the DsRed sequence

by using two primers targeted to 3' *rod* sequence (V3F+V5R). In addition, the obtained PCR products were confirmed by the restriction digestions using NotI-HF. The verification of TIR1 constructs was performed by both PCR and sanger DNA sequencing by using both TIR1-specific forward and reverse primers plus a vector backbone-specific forward primer.

Polymerase chain reaction (PCR)

For different purposes in molecular cloning and construction verification, PCR was performed throughout the entire project. For the operations of reactions, we used a commercially available PrimeSTAR GXL DNA polymerase kit (Takara) which included the 5X PCR buffer, dNTPs and high-fidelity DNA polymerase. In different PCRs, DNA templates varied from extracted genomic DNA to various plasmids (addgene) and gene- or sequence-specific primers were synthesized on a case-by-case basis (Integrated DNA technologies). All thermal cycles were accomplished in a thermocycler (Bio-Rad) as the following detail: denature at 95 °C for 30 seconds; annealing at 50 -60 °C for 1 minute; extension at 68 °C for 1-4 minutes; repeat the cycle for 30 times; final extension at 68 °C for 5 minutes; cycles stop and store DNA sample at 4 °C. Electrophoresis of PCR products was conducted on 1% agarose gel (Fisher Scientific) prepared by 1X TBE buffer for 1 hour at 100 Volts. The length for each DNA band on agarose gel was determined assisting by using 1 kb plus DNA ruler (Thermo Scientific).

RESULTS

Long homology arms favor large DNA insertion in CRISPR-mediated genome integration

Embryo injections were performed independently by using the destination vectors with three types of homology arms - 25 bp (MMEJ), 600 bp (HA600) and 1 kb (HA1000). In each of the three lines, more than 300 embryos were injected and around 100 survival larvae were collected for the screening of transformants (Table 3-1). The great majority of embryos and obtained larvae developed to adult flies in both sexes and the survival rate was 98% for MMEJ, 83% for HA600 and 100% for HA1000. However, after the first crossing, the progeny with red fluorescence in eyes only accounted for 3% in the line of HA1000 and no such offspring were observed in both MMEJ and HA600 lines. Therefore, the genomic DNAs (gDNAs) extracted from the potential transformants isolated from the HA1000 line were used for the subsequent verification of the DNA sequence.

PCR-based verification of CRISP-mediated genome integration

During the initial stage of Golden Gate assembly, a complete sequence inspection was performed for all the components involved in the construction of sgRNA and donor DNA, including homology arms. The biggest concerns, on the DNA level, would be whether the donor DNA was accurately inserted into the expected integration site and whether only one single copy of each DNA construct was precisely integrated without any addition of an unwanted sequence. To answer these questions, six primers were designed for the 3' of wild type rod gene (rod-WT) and targeted to distinct DNA sequences before homology arm 1 (forward primers:

Table 3-1. Screening of transformants after the microinjection of *Drosophila.*

Type of homology arms	Number of injected embryo	Number of survival larvae	Survival adult males	Survival adult females	Adult survival rate	DsRed-positive Rate
MMEJ	> 300	100	50	48	98%	0
HA600	> 300	120	49	51	83%	0
HA1000	> 300	100	49	51	100%	3%

VP1, VP2 and VP3) and after homology arm 2 (reverse primers: VP4, VP5 and VP6). To test their efficiencies, the first PCR was conducted by using different combinations of forward and reverse primers together with gDNAs extracted from *yw* flies with wild type *rod* gene. Based on the result, three primer pairs did not produce wild type 3' rod-specific band at the position of 2000 bp while the rest of the six primer combinations showed rod-WT bands on the gel, particularly the pair of VP3 and VP5 with the lightest background and non-specific bindings (Figure 3-5).

Next, another round of PCR by using the VP3 and VP5 as primers but DNA templates were replaced by gDNAs extracted from the adults of *yw*, transformed rod-CRISPR heterozygotes and homozygotes. Clearly, based on the result (Figure 3-6), a prominent band, representing wild type rod, appeared and was the only band showed in *yw* genome, whereas another band with higher molecular weight was observed in the two rod-CRISPR lines matching the overall length of endogenous 3' the sequence of rod gene and integrated tags. In rod-CRISPR homozygotes, the only band above 5 kb exhibited that both copies of rod on the diploid chromosomes were tagged by CRISPR-mediated integration, while two bands in rod-CRISPR heterozygotes indicated that one of the two rod alleles carried integrated tags and the other remained in wild type form. Thus, this result was manifested that the donor DNA has been incorporated into the correct landing site in 3' of rod gene and, according to the total length of 3' rod in transformants, it was very likely that this region only contained one copy of inserted tags.

To confirm our reasoning, restriction digestion was conducted by using NotI-HF

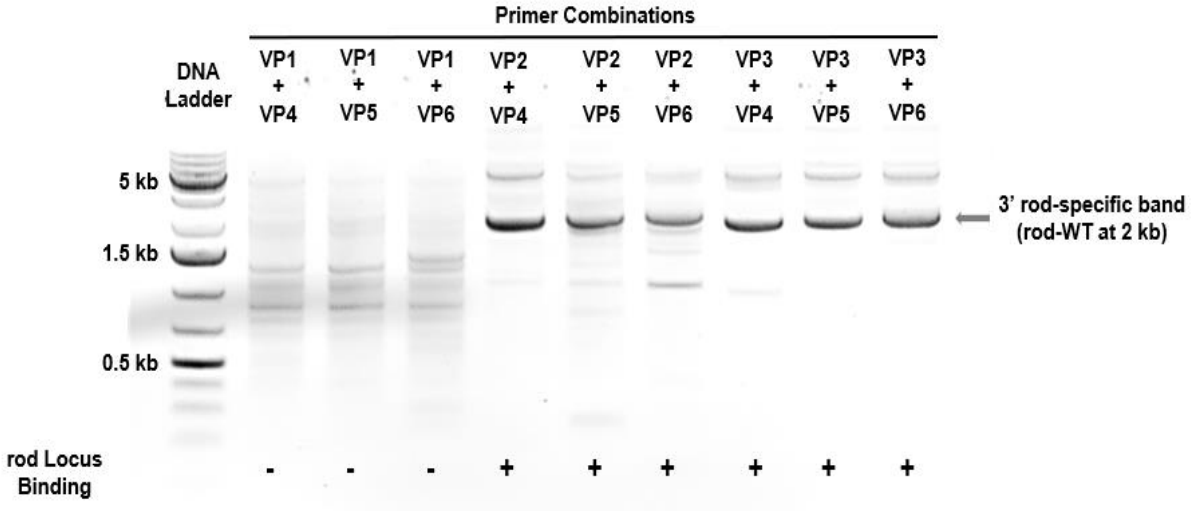

Figure 3-5. Comparison of PCR primer pairs for the detection of *rod* gene locus.

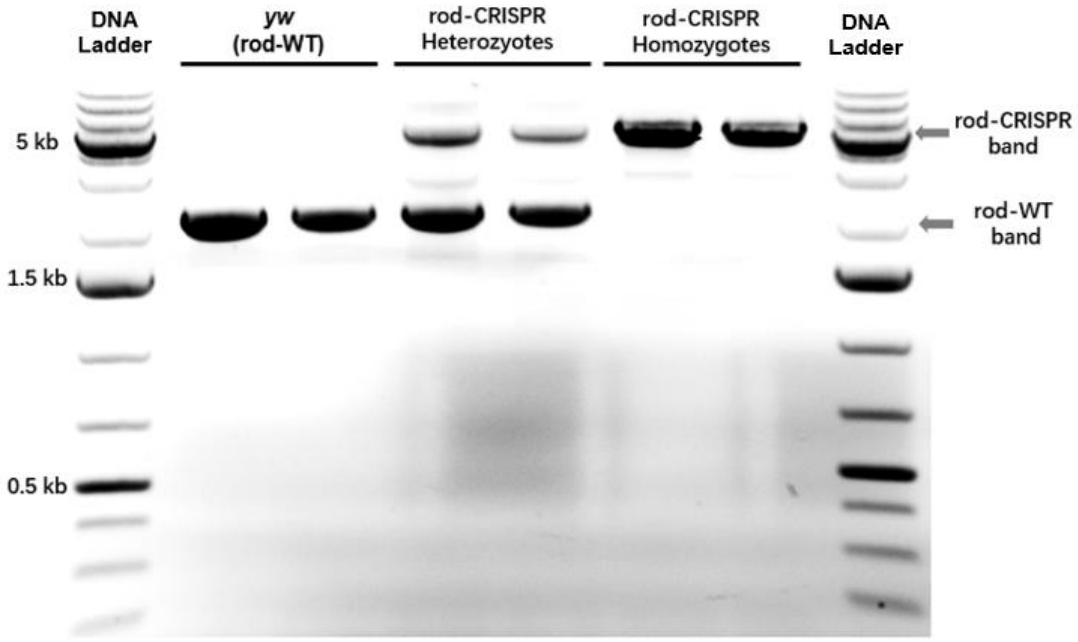

Figure 3-6. Detection of 3' sequence in rod locus in *yw* and transformed stocks.

which has only one cut site within the inserted tag. This digestion would split the rod-CRISPR band into two, positioning at around 4 kb and 1.5 kb respectively, but the rod-WT band would not be affected. Therefore, we anticipated to see a diagnostic band pattern of the PCR products in the three groups. Indeed, after digestion, the PCR products derived from *yw* flies remained the same which only showed one band at 2 kb, but the digestion-resultant two bands, one at 4 kb and the other one at 1.5 kb, were evident in the enzyme-treated PCR products derived from rod-CRISPR heterozygotes and homozygotes (Figure 3-7). Meanwhile, the digested products at 4 kb and 1.5 kb were lighter in rod-CRISPR heterozygotes than those in rod-CRISPR homozygotes, but the PCR product at 2 kb in rod-CRISPR heterozygotes did not change, similar to that in *yw* flies, which confirmed that NotI-HF cut site only exist in the integrated rod, instead of WT rod gene. In addition, the presence of rod-CRISPR homozygotes implicated that the rod-CRISPR allele did not cause severe developmental defects and the adult flies bearing two copies of the modified rod allele were viable.

After the removal of DsRed marker, ten progeny without red-fluorescent eyes were obtained but only two of which showed the representative rod-CRISPR band on the gel, named M9 and F2. PCR-based verification was performed by using VP3 and VP5 primers and templates were the gDNAs extracted from M9 and F2 homozygous adults. The result indicated that only one rod-CRISPR band showed in homozygotes, while two bands (one for rod-CRISPR and the other for rod-WT) were observed in heterozygotes (Figure3-8). More importantly, a reduced molecular weight was

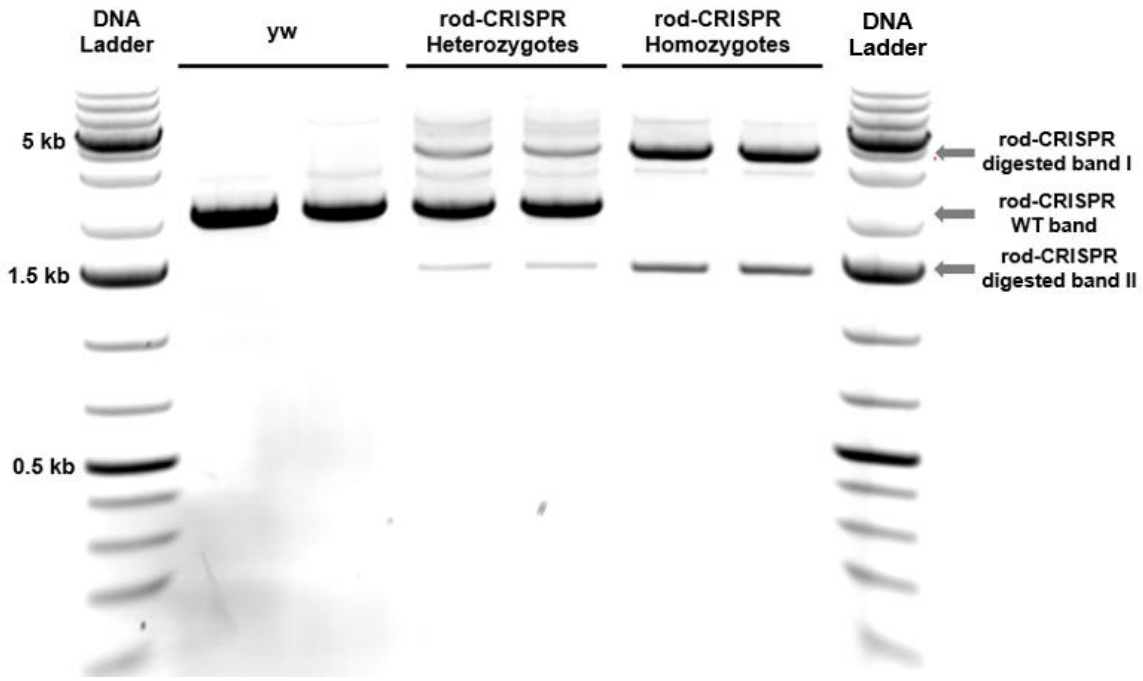

Figure 3-7. Restriction digestion of PCR products of 3' sequence in *rod* locus.

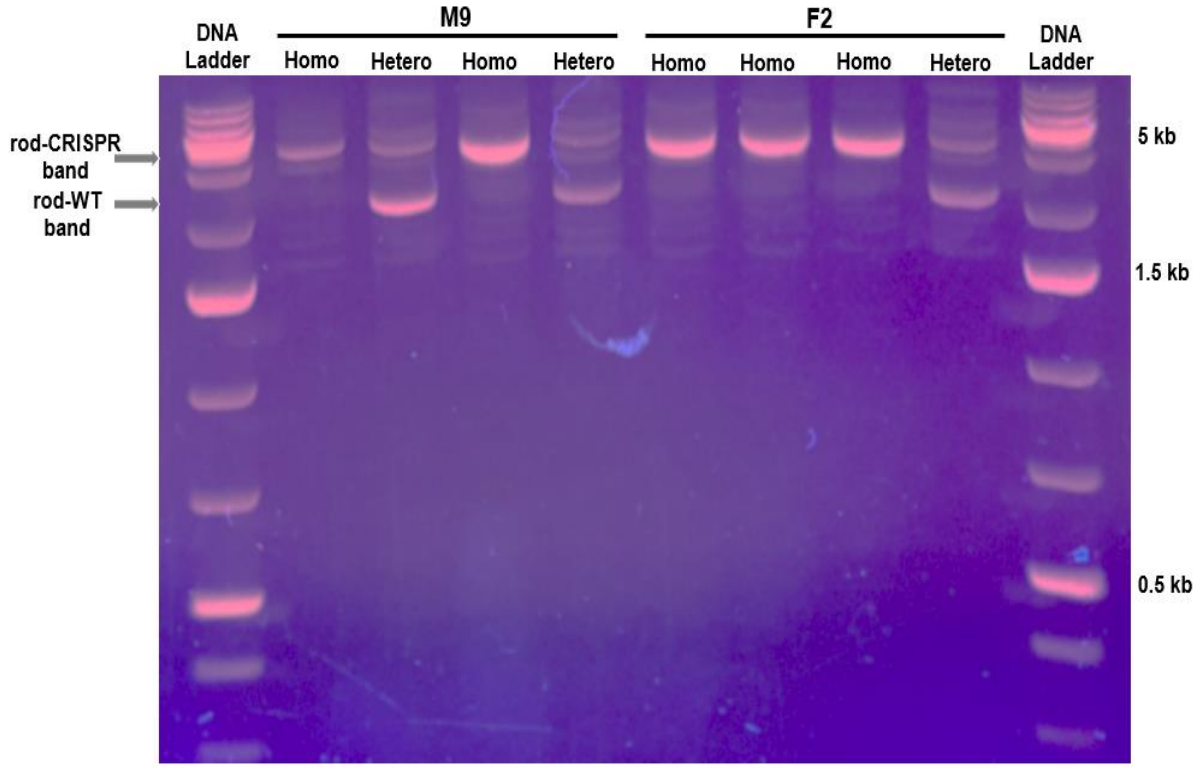

Figure 3-8. Detection of 3' sequence in rod locus in transformed flies without dsRed gene.

implicated by the position of rod CRISPR band that located below 5 kb after the depletion of DsRed sequence, but it was above 5kb originally when DsRed was present. The bands of rod-CRISPR appeared in both of the tested adult flies in M9 and F2, no matter heterozygous or homozygous.

To further confirm the identity of the rod-CRISPR band in these DsRed-negative transformants, restriction enzyme NotI-HF was utilized again to digest the PCR products derived from *yw* flies and M9 homozygotes. Before digestion, only one band showed in both groups but represent rod-WT in *yw* and rod-CRISPR in M9. After enzyme digestion, the rod-WT band in *yw* was unaffected, whereas the rod-CRISPR band disappeared in M9 and two digested bands showed up on the gel since there was solely one NotI-HF cut site in the rod-CRISPR sequence (Figure 3-9). Notably, although the 1.5 kb digested band remained the same, the other band resided at around 2 kb reflecting a shrunken fragment due to the loss of DsRed in the 3' end of rod locus. Therefore, the systematic PCR-based verifications confirmed the success of CRISPR-mediated genome integration by using long homology arms and the constructs we designed were accurately inserted into the 3' end of endogenous rod locus.

Verification of phage phiC31 integrase-mediated genome integration of TIR1

Similar to the microinjection for CRISPR lines, a total number of 200 embryos were injected with the TIR1 destination vector and 100 survival larvae were maintained in a 25 °C incubator. Then, the hatched adults with the phenotype of P{nos-phiC31.NLS}X; P{attP40} were crossed to males or virgins from double-

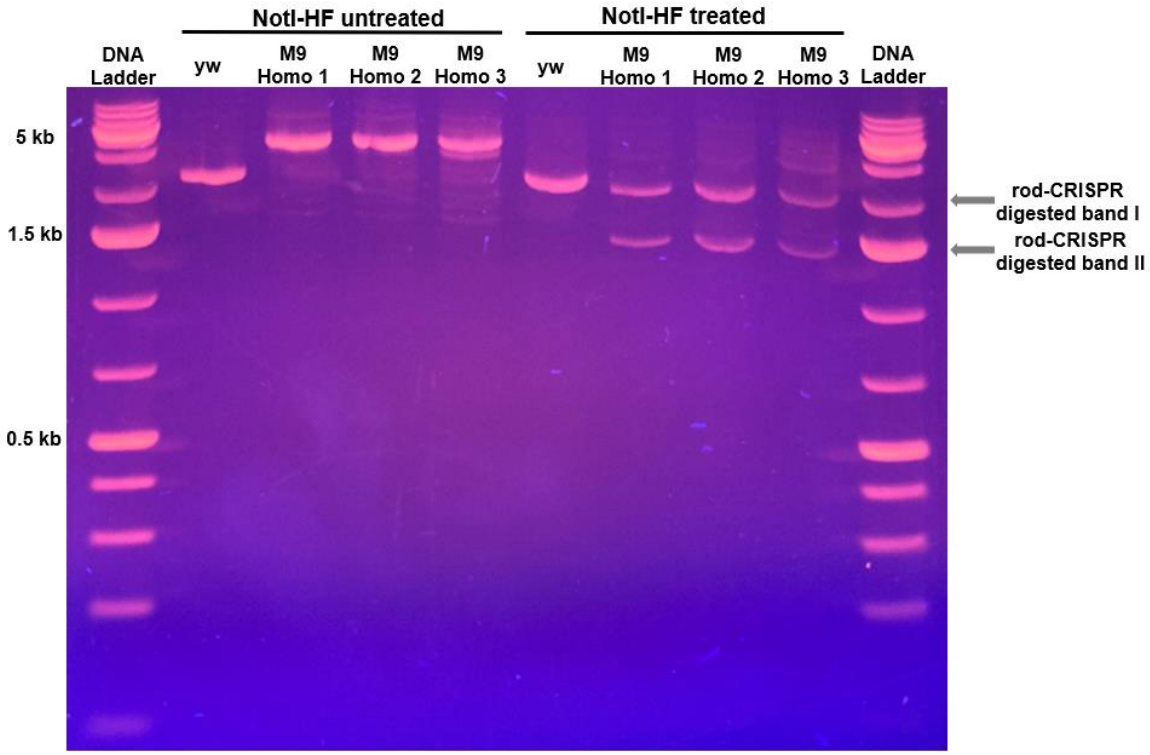

Figure 3-9. Restriction digestion of PCR products of 3' sequence in rod locus of transformants.

balancer stock (*w*; *CyO*/*Sco*; *MKRS*/*TM6B*) for two purposes. On the one hand, the gene of phiC31 integrase on X chromosome could be replaced and removed from the genome, creating a homozygous *w* background, while on the other hand, the introduction of the balancer chromosome protected the integrated TIR1 constructs from the recombination in female flies.

Owing to the mini-white marker in a *w* background, the offspring who were successfully transformed showed orange eyes and each individual, males and virgins, again mated to double-balancer flies to achieve a fully balanced state on 2nd and 3rd chromosomes. Besides the selection of eye marker, three PCRs were carried out by using two TIR1-specific primers (TIR1 forward and reverse) targeted to bam promoter and P10 terminator, respectively, and the templates were gDNAs extracted from three transformed stocks (*yw* fly was used as negative control). The result showed a clear band above 4 kb in all TIR1-transformed stocks, but not seen in *yw* control, suggest a successful integration of TIR1 in the genome (Figure 3-10).

However, the remaining question was whether the TIR1 construct had been precisely landed on att40 site as expected. To address this question, we deployed Sanger sequencing to confirm the position of the integrated construct with a pair of sequencing primers, one designed based on backbone sequence on M8079delta (LMPseqF) and the other targeted to attP40 site (PL-R). The sequencing result confirmed the happening of attB-mediated recombination on att40 landing-site and also detected the partial sequence of M8079delta vector. Unfortunately, due to the limitation of the length in sequencing, the obtained result did not cover any TIR

construct. But, considering the presence of mini-white marker, we reasoned that TIR1 has been precisely integrated into the attP40 site on chromosome 2.

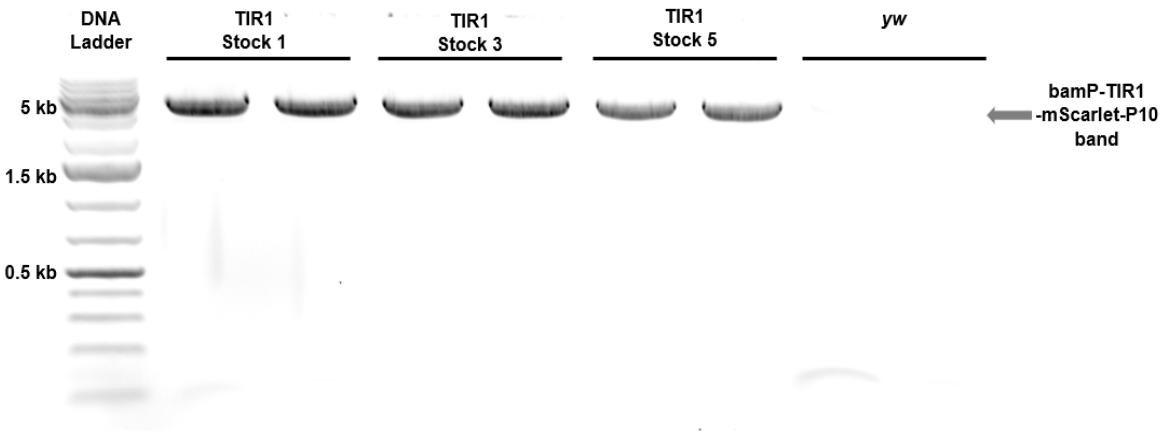

Figure 3-10. Detection of integrated TIR1 construct in transformed stocks.

DISCUSSIONS

CRISPR-mediated genomic integration in the 3' sequence of rod locus showed different results by using three types of homology arms. Surprisingly, no transformant was identified in the injection by using microhomology (23 bp) and short homology arms (600 bp), which implicates that short homology arms on donor DNA are not favorable to mediate the genome integration, particularly for a large donor DNA. Indeed, many studies on HDR-mediated gene knock-in reported that increased homology enhanced the efficiency of genome integration. In human ESCs, longer homology arms greatly increase the knock-in efficiency [Song et al 2010]. It was also the case in mice since the extension of homology arm length, from 50 bp to 200 bp, led to a more than 9-fold increase in the efficiency of genome targeting [Li et al 2014]. Similar tendencies have also been reported in human culture cells that the success rates of gene knock-in increased from 0.2% to 25.8% as the length of homology arm extends from 300 to 900 bp in 239 T cells which were consistent in iPSCs, but the highest efficiency dopped to 12.6% when 1500 bp homology arm was employed [Zhang et al 2017]. In *Drosophila*, the standard protocol of HDR-based CRISPR commonly uses 1 kb homology arm flanking the donor DNA to succeed in gene knock-in [Port et al 2014; Yu et al 2014; Xue et al 2014]. Therefore, our result confirmed that longer homology arms enhance the efficiency of CRISPR-based genome integration through an HDR-dependent pathway.

We failed not isolated transformants from the CRISPR-mediated integration by MMEJ, so we asked why a short homology was not able to mediate DNA integration.

It has been shown that the expression of Pol θ was conserved in *Drosophila* and the absence of Pol θ polymerase activity significantly reduced the frequency of MMEJ events [Beagan et al 2017]. MMEJ-mediated gene knock-in has been applied along with the PITCh system in both invertebrate and vertebrate species, with the variation of the knock-in efficiency from 25 -100% depending on the types of the gene, cell type and species as well as microhomology length. However, in our experiment, the PITCh-CRISPR system by using 23 bp homology arms failed to generate any transformant. It might be due to the length of microhomology since the genome integration rate in Zebrafish dramatically increased by approximately 30% as the length of the homology arm extended from 10 bp to 40 bp [Hisano et al 2015]. Therefore, an increased microhomology in donor DNA may enhance the opportunity of the searching between double-strand break site and donor DNA strand to promote junction formation between each other. In addition, current studies in PITCh-CRISPR were all based on the integration of a small piece of exogenous DNA, like GFP, but the donor DNA used in our experiment combined four different components and, despite the other three tags were small, the piggBacDsRed marker was around 2 kb. Thus, we speculated that a large-size DNA donor made MMEJ-based repair challenging to mediate the knock-in process and gave rise to a negative result in our experiment.

Besides the comparison of CRISPR-mediated genome integration between HDR and MMEJ, the other aim was to create a *rod*-depletion background conditionally for interrogating the potential role of ROD in the regulation of sister-orientation during meiosis. So far, we isolated a successful transformed line and verified the integrated

sequence by several rounds of PCRs by using either heterozygous and homozygous adults, suggesting the insertion constructs might not cause severe issues and lethality in the development. However, insertion of exogenous DNA in a native gene locus could bring unexpected effects on the viability or fertility in transgenic animals. Thus, a careful evaluation towards the potential effect by the insertion is necessary and can be conducted by additional crosses to the sibling in the same stock, wild type and compound flies, to evaluate viability, fertility and the incidence of chromosome NDJ. Moreover, a qRT-RCR would help to detect the transcription of integrated rod gene and fluorescence-microscopy can be performed to detect mVenus-tagged ROD protein in the spermatocytes of transformants. The transcription of TIR1 can also be detected by qRT-PCR by using gene-specific primers, but fluorescence-based detection may be challenging since lacking a natural binding partner in animal cells might cause a diffusible form of TIR1 in vivo and which make fluorescence signal faint or completely invisible. The problem can be addressed by western blotting which is capable of detecting the expression level of a protein with a specific antibody, suitable for both tagged ROD or TIR1.

Once the AID degron sequence and F-box protein TIR1 are expressed in the same cells, one additional step to trigger the protein degradation in vivo is the introduction of the plant hormone - auxin (usually indole-3-acetic acid, IAA). In *Drosophila*, the commonly used approach for auxin administration is to feed the flies by auxin-containing food sources. Recently, two studies in *Drosophila* embryos, ovaries and wing discs showed complete removal of the protein of interest from 12h

to 3 days after auxin treatment depending on different concentrations of auxin supplied in the foods [Bence et al 2017; Trost et al 2016]. However, the most efficient degradation in human cell culture appeared to completely remove proteins from the cells after one hour, indicating a high permeability of IAA in cultured cells [Li et al 2019]. Therefore, this provides the alternative for the application of IAA in cultured *Drosophila* testes, which could achieve higher efficiency than traditional drug administration.

For the future perspective, our interest will be focused on the function of ROD after obtaining *rod*-depleted spermatocytes. During the M-phase, ROD is initially recruited on the fibrous corona of kinetochores after nuclear envelop breakdown and exhibits a dynamic localization in a Dynein-dependent manner on spindle until all chromosomes arrive at opposite poles [reviewed in Chapter 1], which suggests the dual roles of ROD in microtubule-kinetochore attachment and poleward cargo transportation. Recently, many studies have attributed the microtubule end-on attachment to the interaction between RZZ complex and NDC80 complex. In the embryo of *C. elegans*, the depletion of RZZ subunits, either ROD or ZW10, affected the microtubule-kinetochore attachment and resulted in a slow congression of chromosomes to spindle equator. Even worse, the depletion of Spindly (adaptor between RZZ and Dynein) completely abolished the microtubule-loading on kinetochores, equivalent to the phenotype in NDC80 depleted-cell. Subsequently, a deeper study identified the interaction biochemically between the N-terminal β-propeller domain of ROD and the N-terminal tail of NDC80 and a binding assay revealed that reconstitution of N-terminus of ROD was capable of mediating the

interaction with ZW10 and NDC80, which suggests that ROD acts to prevent the premature or erroneous end-on microtubule-attachment through its interaction with NDC80 complex [Gassmann et al 2008; Cheerambathur et al 2013]. The inhibitory regulation of stable end-on attachment delays the stripping of kinetochore proteins and increases the interaction between kinetochore corona and lateral microtubule lattice. Different than the stable end-on attachment in the later stage, lateral attachment increases the chance of initial microtubule attachment on kinetochore and undergoes several conversion steps to form the finally end-on attachment. It has been proposed that RZZ and its partner Spindly can prevent premature stable attachment in a dynein-dependent manner since a phosphor-defective Spindly mutant accelerated the shedding of RZZ complex along the microtubule and led to a massive merotelic attachment caused by the premature formation of end-on attachments [Barbosa et al 2020]. Owing to the special docking position of ROD on kinetochore, it is involved in a joint of different microtubule attachments at the early and late stages. However, the role of ROD is still not fully understood. Therefore, we hope to use these conditional *rod*-depleted flies to interrogate how exactly ROD facilitates the communication between two forms of microtubule attachments and realize a smooth transition between each other to ensure proper chromosome orientation.

REFERENCES

Bae, S., Kweon, J., Kim, H. S., and Kim, J. S. (2014). Microhomology-based choice of Cas9 nuclease target sites. *Nature Methods*, *11*, 705-706.

Barbosa, J., Conde, C., and Sunkel, C. (2020). RZZ-SPINDLY-DYNEIN: you got to keep 'em separated. *Cell Cycle*, *19*, 1716-1726.

Bassett, A. R., and Liu, J. L. (2014). CRISPR/Cas9 and genome editing in Drosophila. *Journal of Genetics and Genomics*, *41*, 7-19.

Barišić-Jäger, E., Kręcioch, I., Hosiner, S., Antic, S., and Dorner, S. (2013). HPat a decapping activator interacting with the miRNA effector complex. *PLoS One*, *8*, e71860.

Beagan, K., Armstrong, R. L., Witsell, A., Roy, U., Renedo, N., Baker, A. E., and McVey, M. (2017). Drosophila DNA polymerase theta utilizes both helicase-like and polymerase domains during microhomology-mediated end joining and interstrand crosslink repair. *PLoS Genetics*, *13*, e1006813.

Bence, M., Jankovics, F., Lukácsovich, T., & Erdélyi, M. (2017). Combining the auxin-inducible degradation system with CRISPR/Cas9-based genome editing for the conditional depletion of endogenous Drosophila melanogaster proteins. *The FEBS journal*, *284*(7), 1056-1069.

Black, S. J., Ozdemir, A. Y., Kashkina, E., Kent, T., Rusanov, T., Ristic, D., and Pomerantz, R. T. (2019). Molecular basis of microhomology-mediated end-joining by purified full-length Polθ. *Nature Communications*, *10*, 1-16.

Carroll, D. (2011). Genome engineering with zinc-finger nucleases. *Genetics*, *188*, 773-782.

Cheerambathur, D. K., Gassmann, R., Cook, B., Oegema, K., and Desai, A. (2013). Crosstalk between microtubule attachment complexes ensures accurate chromosome segregation. *Science*, *342*, 1239-1242.

Engler, C., Kandzia, R., and Marillonnet, S. (2008). A one pot, one step, precision cloning method with high throughput capability. *PloS One*, *3*, e3647.

Engler, C., Gruetzner, R., Kandzia, R., and Marillonnet, S. (2009). Golden gate shuffling: a one-pot DNA shuffling method based on type IIs restriction enzymes. *PloS One*, *4*, e5553.

Findlay, G. M., Boyle, E. A., Hause, R. J., Klein, J. C., and Shendure, J. (2014). Saturation editing of genomic regions by multiplex homology-directed repair. *Nature*, *513*, 120-123.

Gaspar, H. B., Parsley, K. L., Howe, S., King, D., Gilmour, K. C., Sinclair, J., and Thrasher, A. J. et al. (2004). Gene therapy of X-linked severe combined immunodeficiency by use of a pseudotyped gammaretroviral vector. *The Lancet*, *364*, 2181-2187.

Gassmann, R., Essex, A., Hu, J. S., Maddox, P. S., Motegi, F., Sugimoto, A., and Desai, A. et al. (2008). A new mechanism controlling kinetochore–microtubule interactions revealed by comparison of two dynein-targeting components: SPDL-1 and the Rod/Zwilch/Zw10 complex. *Genes & Development*, *22*, 2385-2399.

Gratz, S. J., Cummings, A. M., Nguyen, J. N., Hamm, D. C., Donohue, L. K., Harrison, M. M., and O'Connor-Giles, K. M. et al. (2013). Genome engineering of Drosophila with the CRISPR RNA-guided Cas9 nuclease. *Genetics*, *194*, 1029-1035.

Gratz, S. J., Ukken, F. P., Rubinstein, C. D., Thiede, G., Donohue, L. K., Cummings, A. M., and O'Connor-Giles, K. M. (2014). Highly specific and efficient CRISPR/Cas9-catalyzed homology-directed repair in Drosophila. *Genetics*, *196*, 961-971.

Groth, A. C., Fish, M., Nusse, R., and Calos, M. P. (2004). Construction of transgenic Drosophila by using the site-specific integrase from phage φC31. *Genetics*, *166*, 1775-1782.

Hisano, Y., Sakuma, T., Nakade, S., Ohga, R., Ota, S., Okamoto, H., and Kawahara, A. et al. (2015). Precise in-frame integration of exogenous DNA mediated by CRISPR/Cas9 system in zebrafish. *Scientific Reports*, *5*, 1-7.

Huang, J., Zhou, W., Dong, W., and Hong, Y. (2009). Targeted engineering of the Drosophila genome. *Fly*, *3*, 274-277.

Joung, J. K., and Sander, J. D. (2013). TALENs: a widely applicable technology for targeted genome editing. *Nature reviews Molecular Cell Biology*, *14*, 49-55.

Karess, R. E., and Glover, D. M. (1989). rough deal: a gene required for proper mitotic segregation in Drosophila. *The Journal of Cell Biology*, *109*, 2951-2961.

Koole, W., Van Schendel, R., Karambelas, A. E., Van Heteren, J. T., Okihara, K. L., and Tijsterman, M. (2014). A Polymerase Theta-dependent repair pathway suppresses extensive genomic instability at endogenous G4 DNA sites. *Nature Communications*, *5*, 1-10.

Kremers, G. J., Goedhart, J., van Munster, E. B., and Gadella, T. W. (2006). Cyan and yellow super fluorescent proteins with improved brightness, protein folding, and FRET Förster radius. *Biochemistry*, *45*, 6570-6580.

Krishnan, B., Thomas, S. E., Yan, R., Yamada, H., Zhulin, I. B., and McKee, B. D. (2014). Sisters unbound is required for meiotic centromeric cohesion in Drosophila melanogaster. *Genetics*, *198*, 947-965.

Li, K., Wang, G., Andersen, T., Zhou, P., and Pu, W. T. (2014). Optimization of genome engineering approaches with the CRISPR/Cas9 system. *PloS One*, *9*, e105779.

Li, S., Prasanna, X., Salo, V. T., Vattulainen, I., and Ikonen, E. (2019). An efficient auxin-inducible degron system with low basal degradation in human cells. *Nature methods*, *16*, 866-869.

Meltzer, H., Marom, E., Alyagor, I., Mayseless, O., Berkun, V., Segal-Gilboa, N., and Schuldiner, O. (2019). Tissue-specific (ts) CRISPR as an efficient strategy for in vivo screening in Drosophila. *Nature Communications*, *10*, 1-9.

Mojica, F. J., García-Martínez, J., and Soria, E. (2005). Intervening sequences of regularly spaced prokaryotic repeats derive from foreign genetic elements. *Journal of Molecular Evolution*, *60*, 174-182.

Port, F., Chen, H. M., Lee, T., and Bullock, S. L. (2014). Optimized CRISPR/Cas tools for efficient germline and somatic genome engineering in Drosophila. *Proceedings of the National Academy of Sciences*, *111*, E2967-

E2976.
Port, F., and Bullock, S. L. (2016). Augmenting CRISPR applications in Drosophila with tRNA-flanked sgRNAs. *Nature Methods*, *13*, 852.
Rothkamm, K., Kruger, I., Thompson, L. H., and Löbrich, M. (2003). Pathways of DNA double-strand break repair during the mammalian cell cycle. *Molecular and cellular biology*, *23*, 5706-5715.
Salsman, J., and Dellaire, G. (2017). Precision genome editing in the CRISPR era. *Biochemistry and cell biology*, *95*, 187-201.
Song, H., Chung, S. K., and Xu, Y. (2010). Modeling disease in human ESCs using an efficient BAC-based homologous recombination system. *Cell stem cell*, *6*, 80-89.
Thyme, S. B., and Schier, A. F. (2016). Polq-mediated end joining is essential for surviving DNA double-strand breaks during early zebrafish development. *Cell Reports*, *15*, 707-714.
Trost, M., Blattner, A. C., & Lehner, C. F. (2016). Regulated protein depletion by the auxin-inducible degradation system in Drosophila melanogaster. *Fly*, *10*(1), 35-46.
Urnov, F. D., Rebar, E. J., Holmes, M. C., Zhang, H. S., and Gregory, P. D. (2010). Genome editing with engineered zinc finger nucleases. *Nature Reviews Genetics*, *11*, 636-646.
Van der Oost, J., Jore, M. M., Westra, E. R., Lundgren, M., and Brouns, S. J. (2009). CRISPR-based adaptive and heritable immunity in prokaryotes. *Trends in Biochemical Sciences*, *34*, 401-407.
Wang, H., Yang, H., Shivalila, C. S., Dawlaty, M. M., Cheng, A. W., Zhang, F., and Jaenisch, R. (2013). One-step generation of mice carrying mutations in multiple genes by CRISPR/Cas-mediated genome engineering. *Cell*, *153*, 910-918.
Wyman, C., and Kanaar, R. (2006). DNA double-strand break repair: all's well that ends well. *Annu. Rev. Genet.*, *40*, 363-383.
Xie, K., Minkenberg, B., and Yang, Y. (2015). Boosting CRISPR/Cas9 multiplex editing capability with the endogenous tRNA-processing system. *Proceedings of the National Academy of Sciences*, *112*, 3570-3575.
Xue, Z., Ren, M., Wu, M., Dai, J., Rong, Y. S., and Gao, G. (2014). Efficient gene knock-out and knock-in with transgenic Cas9 in Drosophila. *G3: Genes, Genomes, Genetics*, *4*, 925-929.
Yan, R., Thomas, S. E., Tsai, J. H., Yamada, Y., and McKee, B. D. (2010). SOLO: a meiotic protein required for centromere cohesion, coorientation, and SMC1 localization in Drosophila melanogaster. *The Journal of Cell Biology*, *188*, 335-349.
Yousefzadeh, M. J., Wyatt, D. W., Takata, K. I., Mu, Y., Hensley, S. C., Tomida, J., and Wood, R. D. (2014). Mechanism of suppression of chromosomal instability by DNA polymerase POLQ. *PLoS Genetics*, *10*, e1004654.
Yu, Z., Chen, H., Liu, J., Zhang, H., Yan, Y., Zhu, N., and Jiao, R. et al. (2014). Various applications of TALEN-and CRISPR/Cas9-mediated homologous recombination to modify the Drosophila genome. *Biology Open*, *3*, 271-280.
Zhang, J. P., Li, X. L., Li, G. H., Chen, W., Arakaki, C., Botimer, G. D., and Zhang, X.

B. et al. (2017). Efficient precise knockin with a double cut HDR donor after CRISPR/Cas9-mediated double-stranded DNA cleavage. *Genome Biology*, *18*, 1-18.

Zhang, Z., Zhang, S., Huang, X., Orwig, K. E., and Sheng, Y. (2013). Rapid assembly of customized TALENs into multiple delivery systems. *PloS One*, *8*, e80281.

VITA

Qiutao He was born in Nanjing City, Jiangsu Province, China in 1984. He graduated with a Bachelor's degree of Engineering in 2007 from the University of South China. Then, he pursued and graduated with a Master of Medicine from Wenzhou Medical University in 2011. He was enrolled in the graduate program at the University of Tennessee, Knoxville in 2013 and defended his dissertation in 2021.